

Electronic Theses and Dissertations, 2004-2019

2009

Sintering Additives For Nanocrystalline Titania And Processing Of Porous Bone Tissue Engineering Scaffolds

Arun Menon
University of Central Florida

 Part of the [Materials Science and Engineering Commons](#)
Find similar works at: <https://stars.library.ucf.edu/etd>
University of Central Florida Libraries <http://library.ucf.edu>

This Masters Thesis (Open Access) is brought to you for free and open access by STARS. It has been accepted for inclusion in Electronic Theses and Dissertations, 2004-2019 by an authorized administrator of STARS. For more information, please contact STARS@ucf.edu.

STARS Citation

Menon, Arun, "Sintering Additives For Nanocrystalline Titania And Processing Of Porous Bone Tissue Engineering Scaffolds" (2009). *Electronic Theses and Dissertations, 2004-2019*. 4097.
<https://stars.library.ucf.edu/etd/4097>

SINTERING ADDITIVES FOR NANOCRYSTALLINE TITANIA AND PROCESSING OF
POROUS BONE TISSUE ENGINEERING SCAFFOLDS

by

ARUN MENON

B.Tech. Jawaharlal Nehru Technological University, 2006

A thesis submitted in partial fulfillment of the requirements
for the degree of Master of Science
in the Department of Mechanical, Materials and Aerospace Engineering
in the College of Engineering and Computer Science
at the University of Central Florida
Orlando, Florida

Spring Term
2009

© 2009 Arun Menon

ABSTRACT

Titania (Titanium dioxide, TiO_2) has been researched as a promising biomaterial due to its excellent biocompatibility. However, the main limitation of titania is its poor mechanical properties which limit its use in many load-bearing applications. In this thesis report, the properties of titania were improved by doping with small quantities of MgO, ZnO and SiO_2 as sintering additives. Nanocrystalline powder was selected, as it possesses outstanding properties over conventional coarse-grained powders due to reduced grain size. Nanocrystalline anatase powder of size 5-15 nm was synthesized via a simple sol-gel technique. Small quantities of dopants were introduced into pure titania powder, through homogeneous mixing. The doped powder compositions were compacted uniaxially and sintered at 1300°C and 1500°C , separately, in air. The effects of sintering cycle and temperature on the microstructure, densification and mechanical properties of the sintered structures were studied. Mg doped structures recorded maximum sintered density of 3.87 g.cm^{-3} . Phase analysis was carried out using powder XRD technique using Cu $K\alpha$ radiation. Microstructural analysis was performed using Scanning electron microscopy. The mechanical properties were assessed by evaluating hardness and biaxial flexural strength (ASTM F-394) of the structures. Results showed 12% increase in hardness and 18% increase in biaxial flexural strength in structures doped with ZnO and SiO_2 , respectively. Further, simulated body fluid maintained at 36.5°C was used to study the bioactivity and degradation behavior of the structures.

The second part of the work aimed in the processing of porous titania scaffolds using polyethylene glycol as the pore-former. The green structures were sintered at 1400°C and 1500°C , separately in air and their properties have been studied. Microstructural analysis was carried out using Scanning electron microscope (SEM). Porosity was evaluated using the

immersion technique. Vickers hardness and biaxial flexural tests were used to carry out the mechanical characterization. Further, the biomechanical/biodegradation behavior of the structures was assessed in simulated body fluid (SBF). Biodegradation and change in biomechanical properties as a function of time were studied in terms of weight change, change in Vickers hardness and biaxial flexural strength.

The mechanical properties of porous titania scaffolds doped separately with MgO and ZnO have also been studied to investigate the influence of these additives on the properties of porous structures. The Vickers hardness and biaxial flexural strength were seen to improve with the addition of these sintering additives.

Dedicated to my family and friends

ACKNOWLEDGMENTS

I would like to express gratitude to my adviser Dr. Samar J. Kalita for his support, guidance and motivation throughout my thesis work. I would also like to thank Dr. Linan An and Dr. Yongho Sohn for serving as my thesis committee members and evaluating my thesis. I would also like to extend my thanks to the Mechanical, Materials and Aerospace Engineering (MMAE), Advanced Material Processing and Analysis Centre (AMPAC) and Materials Characterization Facility (MCF) of University of Central Florida for the financial and experimental support.

Special thanks to Mr. Abdulbaset Benwali of MMAE who helped me a lot in getting many laboratory aids like chemicals, spare parts of machinery and equipments needed, etc. I would also like to thank Ms. Cindy Harle of AMPAC, Ms. Jeanine Clements and Mr. Rodney Baker of MMAE for their timely assistance and help.

I would like to thank all my friends too. Finally, sincere thanks to my dear parents and my loving brother for their continuous encouragement and support throughout my studies at UCF.

TABLE OF CONTENTS

LIST OF FIGURES	xi
LIST OF TABLES	xv
LIST OF ACRONYMS/ ABBREVIATIONS	xvi
1. INTRODUCTION	1
1.1 Motivation.....	1
1.2 Research Objectives.....	3
1.3 Research Plan.....	4
2. LITERATURE REVIEW	9
2.1 Introduction to Bioceramics.....	9
2.2 Titania as Bioceramic	12
2.3 Porous ceramics as bone scaffolds.....	13
2.4 Sintering additives for nanocrystalline titania	16
2.5 Polyethylene glycol for processing of porous ceramic scaffolds.....	20
3. METHODOLOGY	22
3.1 Raw materials used	22
3.2 Synthesis and characterization of nanocrystalline titania powder	23
3.3 Processing of metal-ion doped titania structures	25
3.4 Processing of phase-pure porous scaffolds.....	28
3.5 Processing of metal-ion doped porous scaffolds	30
3.6 Characterization of metal-ion doped titania structures	32

3.6.1 Phase characterization using X-Ray diffraction technique	32
3.6.2 Porosity measurements	32
3.6.3 Microstructural Analysis.....	33
3.6.4 Mechanical Characterization	33
3.6.4.1 Vickers hardness testing	33
3.6.4.2 Biaxial flexural testing.....	35
3.7 Bioactivity and biodegradation study	37
3.8 Characterization of Phase-pure porous scaffolds.....	40
3.8.1 Porosity measurements	40
3.8.2 Microstructural Analysis.....	40
3.8.3 Mechanical Characterization	40
3.8.3.1 Vickers hardness testing	40
3.8.3.2 Biaxial flexural testing.....	41
3.9 Bioactivity and biodegradation study	41
3.10 Characterization of metal-ion doped porous scaffolds	42
3.10.1 Porosity measurements	42
3.10.2 Mechanical Characterization	42
3.10.2.1 Vickers hardness testing	42
3.10.2.2 Biaxial flexural testing.....	42
3.11 Bioactivity studies.....	43
4. RESULTS AND DISCUSSIONS.....	44
4.1 Sintering and densification study.....	44
4.1.1 Metal-ion doped titania structures	44

4.1.2 Phase-pure porous scaffolds	47
4.1.3 Metal-ion doped porous scaffolds.....	49
4.2 Porosity measurements	50
4.2.1 Metal-ion doped titania structures	50
4.2.2 Phase-pure porous scaffolds	51
4.2.3 Metal-ion doped porous scaffolds.....	52
4.3 Phase analysis of metal-ion doped titania structures	53
4.4 Microstructural analysis.....	55
4.4.1 Metal-ion doped titania structures	55
4.4.2 Phase-pure porous scaffolds	59
4.5 Mechanical Characterization	63
4.5.1 Vickers hardness testing	63
4.5.1.1 Metal-ion doped titania structures	63
4.5.1.2 Phase-pure porous scaffolds	67
4.5.1.3 Metal-ion doped porous scaffolds.....	68
4.5.2 Biaxial flexural testing.....	70
4.5.2.1 Metal-ion doped titania structures	70
4.5.2.2 Phase- pure porous scaffolds	75
4.5.2.3 Metal-ion doped porous scaffolds.....	76
4.6 Biodegradation Studies	80
4.6.1 Metal-ion doped titania structures	80
4.6.2 Phase-pure porous scaffolds	83
4.6.3 Metal-ion doped porous scaffolds.....	88

5. CONCLUSIONS..... 91

6. FUTURE DIRECTIONS AND SUGGESTIONS 93

LIST OF REFERENCES 95

LIST OF FIGURES

Figure 1: Schematic of Research plan for processing and characterization of metal-ion doped titania structures	5
Figure 2 : Schematic of Research plan for processing and characterization of phase - pure porous scaffolds	7
Figure 3 : Schematic of Research plan for processing and characterization of metal-ion doped porous scaffolds	8
Figure 4: MgO – TiO ₂ phase diagram [77].	17
Figure 5: ZnO – TiO ₂ phase diagram [80].	18
Figure 6: SiO ₂ – TiO ₂ phase diagram [77].	19
Figure 7: Flowchart showing steps involved in sol-gel processing of nanocrystalline titania	24
Figure 8: Setup showing the Sol-gel synthesis of nanocrystalline titania	24
Figure 9 : High temperature furnace used for the sintering of titania structures	27
Figure 10: Vickers hardness tester	34
Figure 11: Setup showing the biaxial flexural testing	36
Figure 12: Incubator used for biodegradation study	39
Figure 13: Setup showing titania samples placed in SBF solution.....	39
Figure 14: Effects of doping on sintered density of TiO ₂ structures sintered at 1500oC for 3 h. 45	
Figure 15: Comparison of sintering cycles on densification - Cycle A: sintering at 1500oC for 3 h; Cycle B: sintering at 1500oC for 0.5 h and hold at 1300oC for 3 h.	46
Figure 16 : Variation in sintered density for the pure titania and porous scaffolds with temperature.	48

Figure 17: Variation of sintered density with composition for pure, porous and porous scaffolds doped with sintering additives. (A – 2 wt% MgO, B – 2 wt% ZnO).....	49
Figure 18: % Porosity vs. Composition for all the sintered structures. - Cycle A: sintering at 1500oC for 3 h; Cycle B: sintering at 1500oC for 0.5 h and hold at 1300oC for 3 h.....	50
Figure 19 : % Porosity Vs Composition for pure titania and porous scaffolds.	51
Figure 20: Variation of % porosity with composition for pure, porous and porous scaffolds doped with sintering additives. (A – 2 wt% MgO, B – 2 wt% ZnO).	52
Figure 21: X-ray powder diffraction pattern of synthesized nanocrystalline TiO ₂ (Anatase) powder.....	53
Figure 22: X-ray powder diffraction patterns of (i) Pure TiO ₂ , (ii) A2, (iii) B2 (iv) C3 sintered at 1500oC for 3 h.	54
Figure 23: XRD patterns of titania showing peak shifts due to dopant addition.....	54
Figure 24: EDS spectrum and SEM micrographs of TiO ₂ ceramics sintered at 1500oC for 3 h (Cycle A). a - Pure TiO ₂ , b -A2, c - B2, d – C3. Microcracks are shown by arrows.....	56
Figure 25: EDS Spectrum and SEM micrographs of TiO ₂ ceramics sintered at 1500oC for 0.5 h and hold at 1300oC for 3 h. a- Pure TiO ₂ , b- A2, c- B2, d- C3.....	58
Figure 26: SEM micrographs of porous scaffolds sintered at 1500oC for 3 h. a – P5, b – P10, c – P15, d – P20, e – P25.....	61
Figure 27: SEM micrographs of porous scaffolds sintered at 1500oC for 3 h. a – Pure TiO ₂ , b – P5, c – P10, d – P15, e – P20, f – P25.....	62
Figure 28: Effects of doping on hardness of TiO ₂ structures sintered using Cycle A	64
Figure 29: Indent on the surface of titania captured from the Vickers hardness tester	64

Figure 30: Effect of sintering parameters on hardness of pure and doped nanocrystalline titania. Cycle A represents sintering at 1500oC for 3 h. Cycle B represents sintering at 1500oC for 0.5 h and 1300oC for 3 h.	65
Figure 31 : Variation of hardness with density for all the sintered structures	66
Figure 32: Variation in hardness of pure and porous scaffolds	67
Figure 33 : Variation of hardness with sintered density for phase-pure porous scaffolds.....	68
Figure 34: Variation of hardness with composition for pure, porous and porous scaffolds doped with sintering additives. (A – 2 wt% MgO, B – 2 wt% ZnO).	69
Figure 35: Variation of hardness with sintered density for metal-ion doped porous scaffolds. ...	70
Figure 36: Effect of doping on biaxial flexural strength of nanocrystalline TiO ₂ structures sintered using Cycle A.	72
Figure 37: Effect of sintering parameters on biaxial flexural strength of pure and doped nanocrystalline titania. Cycle A represents sintering at 1500oC for 3 h and Cycle B represents sintering at 1500oC for 0.5 h and 1300oC for 3 h.	73
Figure 38 : Variation of density with biaxial strength for metal-ion doped structures.....	74
Figure 39: Variation of biaxial flexural strength for the pure and porous scaffolds.....	75
Figure 40: Variation of biaxial flexural with sintered density for phase-pure porous scaffolds ..	76
Figure 41: Variation of biaxial flexural strength with composition for pure, porous and porous scaffolds doped with sintering additives. (A – 2 wt% MgO, B – 2 wt% ZnO).	77
Figure 42: Variation of biaxial strength with sintered density for all metal-ion doped porous scaffolds.	78
Figure 43: Variation in the density of the TiO ₂ structures placed in SBF with time.	80
Figure 44: Variation in the hardness of the TiO ₂ structures placed in SBF with time.	81

Figure 45: Variation in the biaxial flexural strength of the TiO ₂ structures placed in SBF with time.	82
Figure 46: % Weight change Vs. time (days) for all the compositions.	83
Figure 47: XRD pattern of porous scaffold placed in SBF for 42 days.....	84
Figure 48: SEM micrographs showing formation of apatite crystals on the surface of titania	85
Figure 49: Variation in hardness of pure and porous scaffolds placed in SBF with time	86
Figure 50 : Variation in biaxial flexural strength of pure and porous scaffolds placed in SBF with time	87
Figure 51: % Weight change Vs Composition for all metal-ion doped porous scaffolds	88
Figure 52: Variation in surface hardness for metal-ion doped porous scaffolds	89
Figure 53: Variation in biaxial flexural strength for the metal-ion doped porous scaffolds.....	90

LIST OF TABLES

Table 1: Properties of PEG:	21
Table 2: Chemicals used for the synthesis of nanocrystalline titania	22
Table 3: Properties of additives used.....	26
Table 4 : Compositions of TiO ₂ ceramics studied.....	27
Table 5 : Compositions of TiO ₂ porous scaffolds	29
Table 6 : Compositions of metal-ion doped porous scaffolds	31
Table 7 : Ionic concentrations of human blood plasma and SBF	38
Table 8 : Grain size analysis of pure titania and porous scaffolds.....	60

LIST OF ACRONYMS/ ABBREVIATIONS

TiO ₂	Titanium Dioxide, Titania
TTIP	Titanium Tetraisopropoxide
CAS	Chemical Abstracts Service
XRD	X-ray Diffraction
SEM	Scanning Electron Microscopy
SBF	Simulated Body Fluid
PEG	Polyethylene Glycol
PTFE	Poly Tetra Fluoro Ethylene
TEM	Transmission Electron Microscopy
HAP	Hydroxyapatite

1. INTRODUCTION

1.1 Motivation

Nanocrystalline TiO₂ possesses a wide range of attractive properties including excellent photocatalytic activities [1], high refractive index [2], good chemical stability [3], and enhanced biocompatibility and bioactivity [4-7]. It has found many applications in photocatalytic purification [8, 9], gas sensors and solar cells [10, 11], electro-chromic devices and capacitors [12]. Nanophase TiO₂ also exhibits good biocompatibility and functions as a good biomaterial for orthopedic applications [13]

During recent years, many processes have been developed to synthesize nanocrystalline TiO₂ powder, *viz.*, solvothermal [14], hydrothermal [15], mechanochemical [16], mechanical alloying [17], thermal decomposition [18], chemical vapor deposition [19] and sol-gel technique [20]. Among all the processing routes, the sol-gel process possesses advantages such as good process control, improved homogeneity and yield of highly pure powder. This technique produces nanocrystalline powder possessing remarkably improved mechanical, catalytic, optical, chemical and electrical properties. In this work, the simple sol-gel technique was used to synthesize nanocrystalline titania with particle size of 5-15 nm.

Poor mechanical performance of TiO₂ ceramic has been a concern to the scientific community and ceramicists, which limits its applications to non-load bearing applications. Nevertheless, recent research showed that ceramic structures processed from nanocrystalline TiO₂ powder have shown promising results (improved densification, hardness and compression strength). There is no doubt that a good sintering process is the key to achieving improved densification and mechanical properties. Similarly, selection and incorporation of appropriate

sintering additives is another proven method of enhancing mechanical performance of ceramic structures. Various sintering techniques, viz., spark plasma sintering [21, 22], hot pressing [23], high pressure low temperature sintering [24], two-step pressure-less sintering [25] have been explored in the recent years to sinter the TiO₂ structures with variable results. Of these, the pressure-less sintering is a relatively low cost process, which is employed in this study.

Though remarkable success has been made on photocatalytic, sensor and chemical behavior of nanocrystalline TiO₂ through common metal ion/oxide doping [26-30], little is reported on studies attempting to enhance the mechanical properties of TiO₂ ceramics. After extensive literature review, I found that there is very little available describing studies the influence of sintering additives on the mechanical properties of bulk TiO₂ structures as a function of sintering and processing parameters. Hence, this research effort doped nanocrystalline TiO₂ with selective oxides as sintering additives and studied their effects on the densification, mechanical properties, biodegradation and bioactivity.

TiO₂ possesses excellent biocompatibility [4-7], therefore, nanocrystalline TiO₂ coatings can be used to substitute mechanically weak hydroxyapatite coatings on prosthetic devices including nails and screws [31]. Although excellent biocompatibility nano-phase TiO₂ is established, not much is reported on biodegradation behavior of TiO₂ structures doped with metal ions. Metal ions, such as Mg²⁺, Na⁺, Zn²⁺ and Si⁴⁺ are very well known to be prevalent in the inorganic part of the bone [32], and they play a vital role in bone repair and regeneration. I hypothesized that the oxides of these metals can be safely used to integrate with nanocrystalline TiO₂ as sintering additives, without altering bioactivity and biocompatibility. Objective of this thesis work was to study the effect of MgO, ZnO and SiO₂ as sintering additives for TiO₂ structures and study their physical, mechanical and biodegradation behavior.

The need for a better scaffold to treat large bone-defects resulting from skeletal condition still prevails, and it has been a challenge to meet all the biomedical requirements. It is established that an ideal bone scaffold should be osteogenic, resorbable, have porous structure, possess good mechanical strength and suitable surface chemistry. It is hypothesized that that these requirements can be fulfilled by creating porous scaffolds using nanocrystalline titania. Nano-TiO₂ has shown improved mechanical strength and osteoblast functions, and proved to be a promising orthopedic biomaterial.

1.2 Research Objectives

The primary objective of this research was to develop doped and porous titania structures in biomedical industry for bone-graft applications. The specific objectives of this work are:

- To improve the mechanical properties of titania (TiO₂) ceramics and to control its rate of resorption by introducing MgO, SiO₂ and ZnO as sintering additives in small quantities.
- To study the effect of additives on densification and microstructural characteristics of TiO₂ ceramics.
- Phase characterization of metal-ion doped TiO₂ structures using XRD analysis.
- Assessment of mechanical properties of all the sintered structures.
- To investigate the bioactivity and mechanical property degradation of pure and doped TiO₂ structures placed in simulated body fluid (SBF) for a period of 42 days.
- To develop phase-pure porous titania structures by the addition of polyethylene glycol (PEG) as the pore-former.

- To investigate the effect of PEG addition on the microstructure and mechanical properties of titania ceramics.
- Evaluation of porosity changes with change in quantity of pore-former added.
- Understanding the correlation between microstructure evolution and mechanical property changes.
- Assessment of biomechanical properties of porous titania structures.
- To study the influence of MgO and ZnO as sintering additives on the mechanical properties of porous titania structures.

1.3 Research Plan

The following research plan was adapted for metal-ion doped titania structures to achieve the research objectives:

- Sintering and densification of green structures.
- Porosity measurement using simple immersion technique.
- Phase characterization of sintered structures by powder X-ray diffraction (XRD).
- Microstructure evolution as a function of sintering temperature using Scanning Electron Microscopy (SEM).
- Characterization of mechanical properties of the sintered structures through Vickers hardness testing and biaxial flexural testing.
- Study of biodegradation and biomechanical properties of all sintered titania structures in SBF.

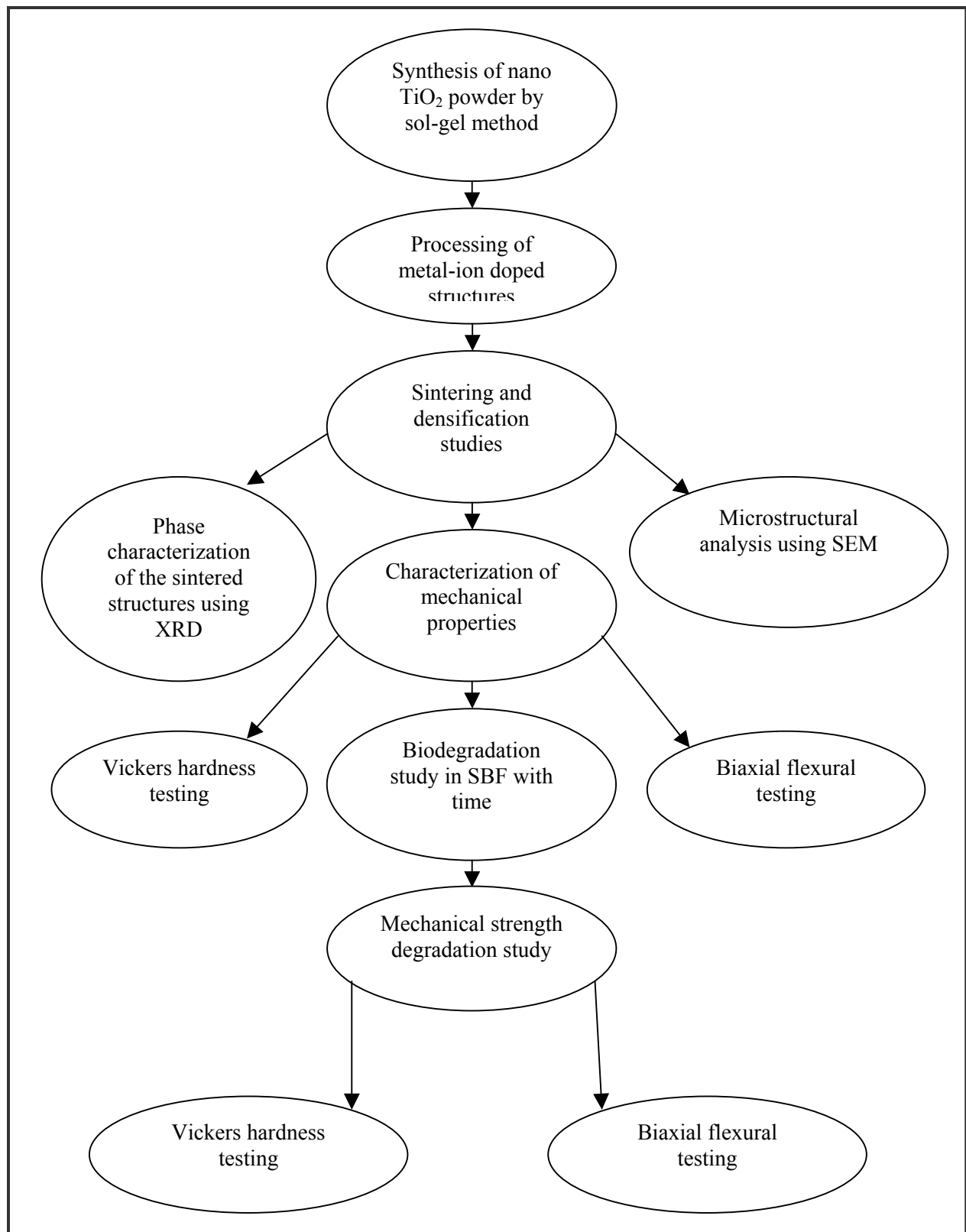


Figure 1: Schematic of Research plan for processing and characterization of metal-ion doped titania structures

The following research plan was adapted for the porous titania scaffolds to achieve the research objectives:

- Sintering and densification of green structures.
- Porosity measurement using simple immersion technique.
- Microstructure evolution as a function of sintering temperature using Scanning Electron Microscopy (SEM).
- Characterization of mechanical properties of the sintered structures through Vickers hardness testing and biaxial flexural testing.
- Study of bioactivity of all sintered porous titania structures in SBF.
- Phase analysis of the structures placed in SBF using XRD
- Microstructural analysis of the structures placed in SBF using SEM
- Study of biomechanical degradation of the structures using Vickers hardness testing and biaxial flexural testing.

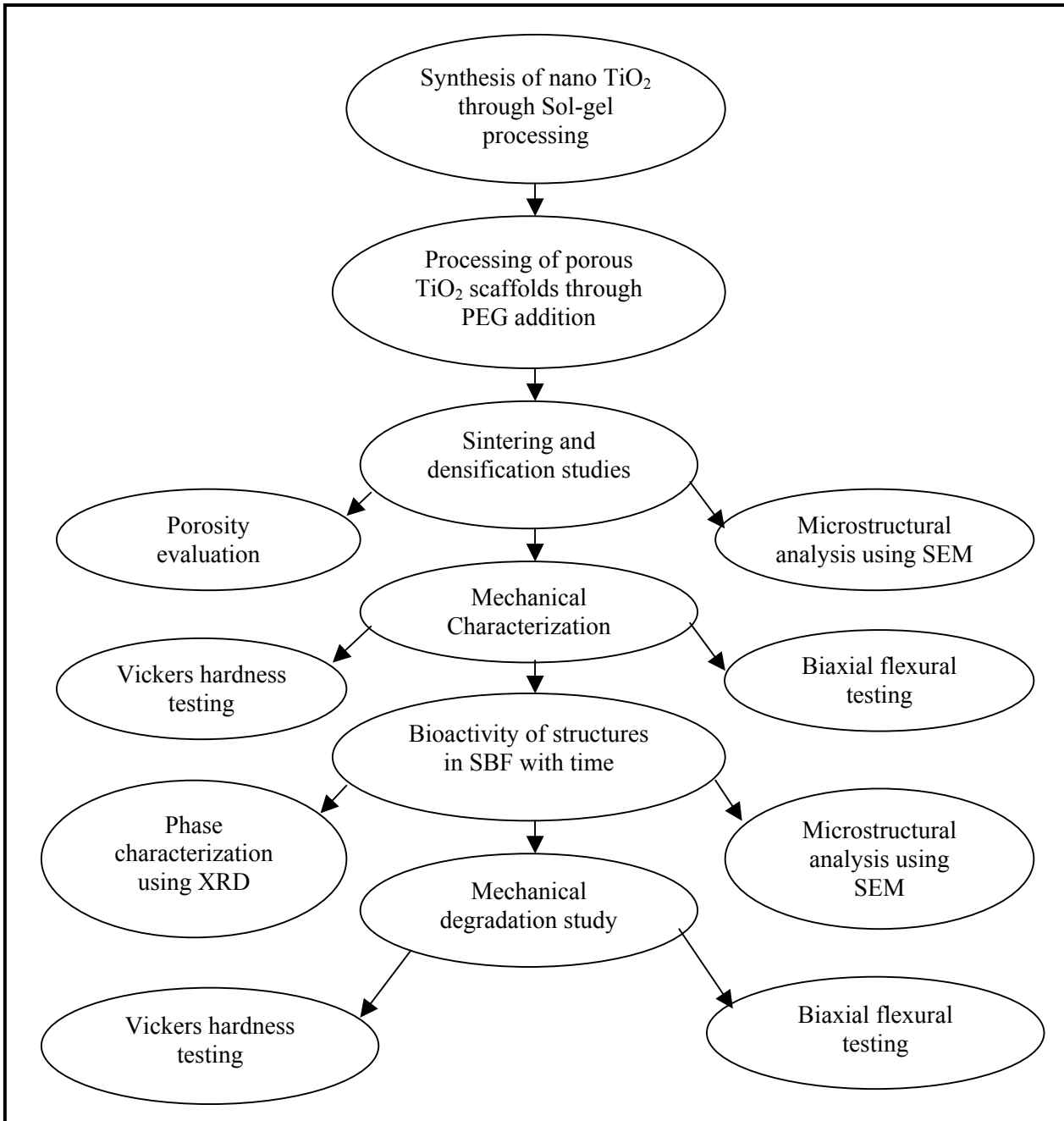


Figure 2 : Schematic of Research plan for processing and characterization of phase - pure porous scaffolds

The following research plan was adapted for doped porous titania scaffolds to achieve the research objectives:

- Sintering and densification of green structures.
- Porosity measurement using simple immersion technique.
- Characterization of mechanical properties of the sintered structures through Vickers hardness testing and biaxial flexural testing.

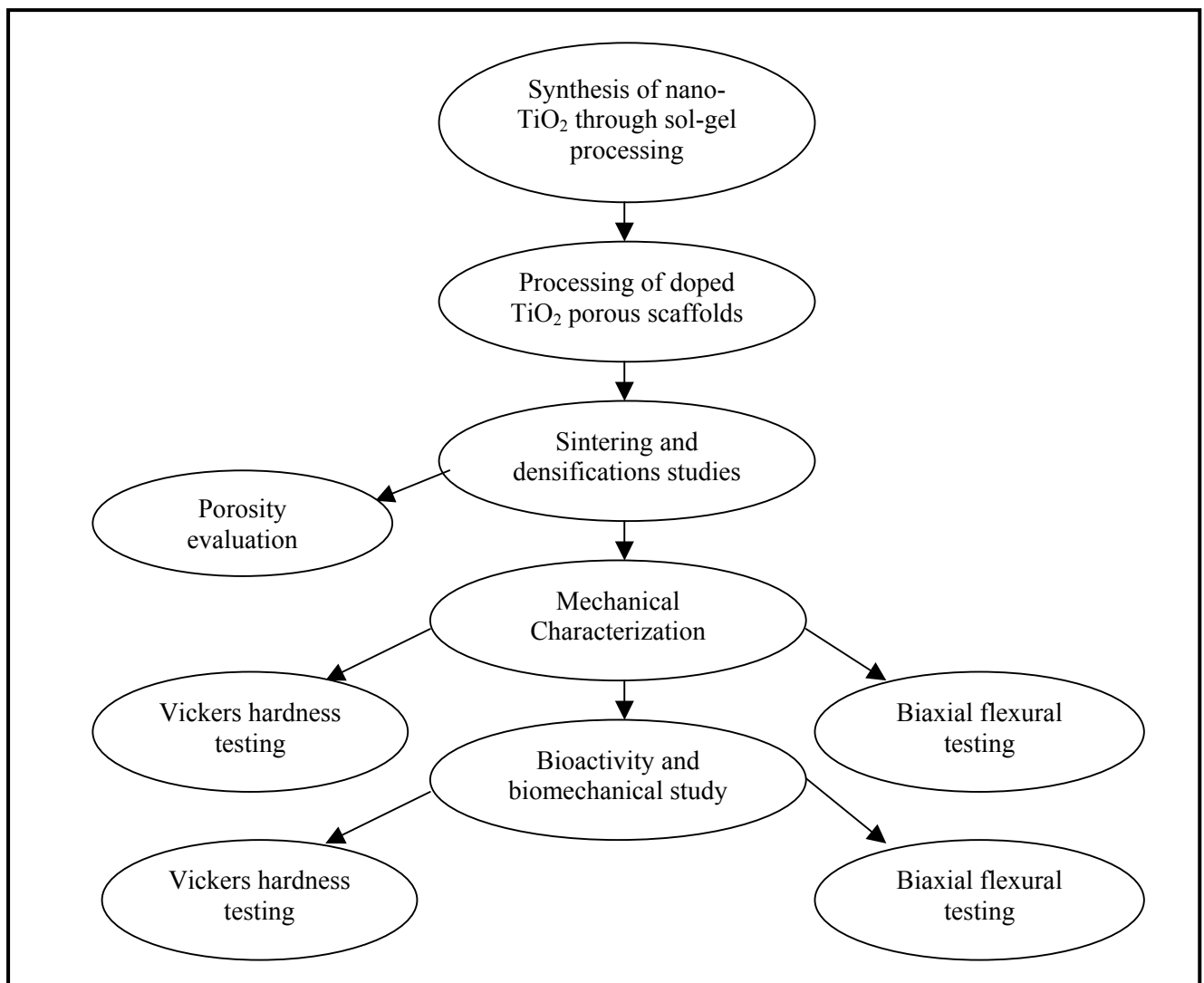


Figure 3 : Schematic of Research plan for processing and characterization of metal-ion doped porous scaffolds

2. LITERATURE REVIEW

2.1 Introduction to Bioceramics

Bioceramics are the novel ceramics which are used to replace bone defects without eliciting any toxic response inside the body. Many bioceramics developed during the recent years, such as hydroxyapatite, alumina, zirconia, tricalcium phosphate, etc have been a benefit to millions of people. These bioceramics possess several advantages such as high hardness, good compression strength, low density, good wear resistance, good biocompatibility and above all these possess compositional similarity with bone. Bioceramics are grouped into three classes:

- Bioinert ceramics
- Bioresorbable ceramics
- Bioactive ceramics

Bioinert ceramics belong to the class of materials which do not interact with the physiological systems like surrounding tissues inside the body and are always treated as foreign materials by the body. These are mostly used in structural support implants such as bone plates, bone screws, femoral heads, etc. Other applications of these materials include dental implants and hip prostheses. These materials possess many advantages such as excellent corrosion resistance, good biocompatibility, high strength, high wear resistance and low friction. Examples of these materials are alumina, zirconia, titania.

Bioresorbable ceramics are the materials which are designed to degrade gradually with time and be replaced with natural tissues. Applications of these materials include drug delivery devices, for repairing damaged bone, herniated discs, maxillofacial and dental defects. Although

these classes of materials are biocompatible, there is no control over the rate of resorption and the rate at which the strength degrades. Examples include tricalcium phosphate, aluminium calcium phosphate, biocoral, plaster of paris, etc.

Bioactive ceramics are the materials which undergo chemical reactions at the interface and lead to bonding of tissues at the interface. These materials possess a wide range of bonding rates and thickness of interfacial bonding layers. These materials should have good mechanical strength, fracture toughness and good interfacial bond strength. These materials are used as coating for metallic prostheses, in the reconstruction of dental defects, as replacements of middle ear ossicles. Examples include bioactive glasses such as bioglass, bioactive glass ceramics and synthetic hydroxyapatite. A very common characteristic of all bioactive implants is the formation of hydroxyl carbonate apatite (HCA) layer on their surface when implanted. This phase is equivalent in composition and structure to the mineral phase of bone.

Bioceramics are being used in many health care industries for developing eye glasses, thermometers, diagnostic instruments, chemical ware, etc [33]. Bioceramics are used for structural applications such as repair and re-construction of damaged bones and tissues, as a coating for metallic implants to improve their biocompatibility. Bioactive glasses have been used as enzyme carriers since they possess many advantages like good resistance to microbial attack, temperature, pH changes, high pressure [34]. Any biomaterial placed within a living tissue cannot be considered completely inert, but any ceramic having molecular structure completely different from that of a living tissue are generally stable inside inside the body. Various materials have been tried and tested for their applications as bone graft materials in the recent years. These classes of materials degrade *invivo* while natural tissues regenerate and take over the physiological and structural functions of the prostheses. Bioresorbable materials belong to this

class of materials. Calcium phosphate is a good example of this type. It also possesses excellent biocompatibility and compositional similarity to that of bone [35, 36]. However, these materials possess poor mechanical properties, which restrict their use in many applications [32, 34, 37]. Common applications of calcium phosphate ceramics include hip replacements and dental implants. Corals are bioresorbable ceramics which provide excellent structure for the ingrowth of bone, and its main component calcium carbonate, is gradually resorbed by the body.

Hydroxyapatite is a recently developed bioactive bioceramic that is extensively researched for use as a promising biomaterial. Synthetic hydroxyapatite shows promotion of new bone growth on its surface, however, the rate of bone growth is slower compared to other bioactive materials [38]. During the recent years, lot of research work has been done to improve the properties of many of these bioceramics. Zirconia-alumina nanocomposite was developed, which possesses improved biocompatibility by hydroxyapatite addition [39]. The mechanical and biological properties of calcium phosphate ceramics have been improved by controlling the particle size, shape and morphology, distribution and agglomeration of particles [40]. Trace metal ions that are present in the bone mineral were used to improve the bioactivity of synthetic Hap [41-43]. The toughness of Hap nanocomposite was improved by the addition of 3 wt.% zirconia [44]. Also it has been shown that mechanical properties of Hap can be improved through the addition of glass [43, 45-48].

Many attempts have been made during the recent years to develop nanoscale bioceramics. This is because properties of nanostructured materials is superior to the fine grained materials as the surface to volume ratio increases for the nanoscale materials which provides more surface for the cell adhesion and proliferation of calcium containing minerals on the surface of these materials [49]. The other advantage is, lower sintering temperature can be employed to sinter

these materials. These nanostructured bioceramics are useful for orthopedic and dental implants. Plastic strain up to 100% could be permitted in nanograined brittle ceramics [50]. Properties of nanocrystalline hydroxyapatite, titania, zinc phosphate, etc are being studied by various researchers for use as bioceramics in future.

2.2 Titania as Bioceramic

Nanocrystalline titania is a potential material for many biomedical applications. Titania belongs to the class of bioinert ceramics. Many studies have been carried out during the recent years proved that titania exhibits excellent biocompatibility and bioactivity [4-7]. Titania in the form of films has been used for studying the bioactivity. The films exhibit various interesting characteristics such as ease of fabrication, non-toxicity, optical transparency and good chemical stability [51]. The films are deposited onto a solid substrate and have been employed to immobilize biomolecules, enzymes and proteins [52, 53].

Apatite is known to be an excellent biomaterial which is used in many biomedical implants and bone repairs. It has been proved by many researchers that apatite precipitates can be formed biomimetically on the surface of titania in simulated body fluid (SBF) [54-57]. The apatite formation on the surface of the titania is governed by the heterogeneous nucleation and growth. During the deposition process, the calcium ions are attracted to the negatively charged interface between titania coating and the SBF solution. In this process, CaTiO_3 forms at the interface which combines with the phosphate ions in the solution giving rise to apatite nuclei. This process continues and leads to the deposition of more apatite crystals on the surface of titania as the time progresses [58]. Once the apatite has formed, the osteoblasts adhere to the apatite layer and produce a network of collagen fibres, which constitutes the organic part of the

bone. This collagen network is mineralized by apatite and the new bone is formed [59]. It has also been shown in some studies that titanates generally show good chemical durability and higher elastic modulus than silicates and phosphates [60]. Hence, titania is considered as a novel bioceramic for all biomedical applications.

Several techniques like chemical treatment [61, 62], anodic oxidation [56, 63, 64], ion beam enhanced deposition [65] have been carried out for the preparation of titania films. In some recent studies titania has also been suggested as an alternative to hydroxyapatite coatings. The hydroxyapatite coatings possess poor adhesion strength. Using anodic oxidation, titania is formed with a chemical bond between the oxide and the Ti substrate that results in enhanced bond strength. A bone like apatite layer is formed on titania in simulated body fluid (SBF). Much of the research work carried out during the recent years aimed at studying the bioactivity and biocompatibility of titania films processed through various techniques, however, to our knowledge not much was reported in studying the biocompatibility and biodegradation study of bulk titania structures, so this work was undertaken to study the properties of bulk titania structures immersed in simulated body fluid for a period of six weeks.

2.3 Porous ceramics as bone scaffolds

Porous ceramic materials for biomedical applications are the materials with open porosity whose structure closely resembles that of a cancellous bone. These materials can be used as scaffolds inside the body. There are many requirements for materials to be used as tissue engineering scaffolds [66]:

- Excellent biocompatibility: The scaffold should be either biodegradable or bioactive or both.

- Interconnected porosity: An ideal scaffold should be a three dimensionally interconnected porous structure with pore sizes in the range of 40-400 μm for richer blood supply, nutrient delivery and gas exchanges to help the bone cells to grow steadily inside the scaffold.
- Optimal surface chemistry and suitable bioactivity to exploit body's natural repair process by suitable cell attachment, proliferation and differentiation
- Compatible mechanical properties: An ideal scaffold should have compatible mechanical strength and toughness to withstand complex stress states at the site of application and avoid problems like *stress shielding*. The strength degradation due to bioresorption of an ideal scaffold should be such that it retains sufficient strength to support the structure for atleast 6-8 months while allowing the bone cells to grow inside.
- The material should be easy to process into 3D complex shapes in a controllable and reproducible manner.

Various processing techniques have been utilized to fabricate porous ceramic scaffolds to enhance tissue regeneration and bone repair. Some methods involve the use of pore-formers, which get fired off during the pyrolysis leaving voids in the ceramic material. Porous alumina and calcium aluminates can be produced by this technique wherein calcium carbonate is used as a pore-former. Porous structures with 33-48% porosity were produced by this technique [67, 68]. Porous Hap ceramic blocks were fabricated using Hap slurry mixed with foaming agent followed by sintering at elevated temperature. However, the drawback of this technique is that there is no control over pore size distribution and interconnectivity in the final structure. Second method involves the addition of a low melting point agent which is mixed with the ceramic. This

material melts and get removed consecutively giving rise to pores in the ceramic structure. Porous ceramic surfaces can also be prepared by mixing metal or salt particles into the surface. These particles can then be removed with a suitable etchant which produces porous surface layer[67, 68]. The third approach is called replamineform process which is used to fabricate inert, bioactive, ceramic and polymeric implants that duplicate the macroporous microstructures of corals that have interconnected pores [69]. The natural corals are initially machined to the desired shapes. The machined coral is fired to drive off the carbon dioxide from the limestone leaving behind a calcia structure to be used as an investment material to form a porous structure. The desired material is then cast into pores and the calcia mold is removed from the structure by dissolving in dilute hydrochloric acid. Porous hydroxyapatite implants fabricated by replamineform process, have been used for craniofacial reconstruction and have showed rapid bone in-growth. Their corresponding forms are called HA200 and HA500 respectively. The method produces porous implants with pore size varying from 140 μm to 1000 μm . The disadvantage with this process is that there is no control over the pore sizes, their sizes and interconnectivity. Rapid prototyping (RP) or Solid Freeform fabrication (SFF) techniques have been explored to fabricate controlled porosity ceramic scaffolds with varying pore size, shape, volume and three dimensional interconnectivity. Other techniques used for the fabrication of porous ceramics for orthopedic applications are Selective Laser Sintering (SLS) and stereolithography.

The advantage of these materials is inertness combined with mechanical stability with highly convoluted interface when bone grows through the pores of the ceramic[34]. Hulbert [68], and Schors and Holmes [70] have shown that these materials can be used as a functional implant when load-bearing is not a primary requirement. The disadvantages of these materials is the

aging with time which leads to decrease in mechanical strength, hence these materials cannot be used for long-term applications unless they are resorbable [33]. A highly porous scaffold just provides a temporary mechanical support for the cells and to resist the forces of wound contraction without damage to the pore structure. The applications of these materials are as bone-filling materials for critically sized defects [66].

2.4 Sintering additives for nanocrystalline titania

Sintering additives or dopants are the material(s) added to the ceramic powder before the sintering process. Titania structures processed in many cases possess poor mechanical properties which limit its application in many load-bearing applications. Lot of research was carried out during the recent years to improve the photocatalytic, optical and dielectric behavior of titania through metal ion doping. It has been shown that addition of nickel, zinc and chromium enhanced the photovoltaic characteristics of titania when used in solar cells [71]. Many doping techniques like flame fusion [72], reactive r.f. sputtering [73], etc have been used. Doping plays a very important role in determining many functional properties of titania. Properties of Al-doped titania was studied by Gesenhues [74]. High resolution transmission electron microscopy of Nb-doped titania powder was studied by Akiyama *et al* [75]. After extensive literature review, I found very little available describing the influence of sintering additives on the mechanical properties of bulk titania structures as a function of sintering and processing parameters. Hence, this work aimed at studying the same.

For this work MgO, ZnO and SiO₂ were selected as sintering additives. Metal ions, such as Mg²⁺, Na⁺, Zn²⁺ and Si⁴⁺ are very well known to be prevalent in the inorganic part of the bone [76], and they play a vital role in bone repair and regeneration. Further, it is believed that the

bioactivity of titania is inferior due the absence of these ions. I used these oxides to integrate with nanocrystalline TiO_2 as sintering additives, without altering bioactivity and biocompatibility. Objective of this work was to study the influence of MgO , ZnO and SiO_2 as sintering additives for titania structures and study their physical, mechanical and biodegradation behavior.

The $\text{MgO} - \text{TiO}_2$ phase diagram is shown in Figure 4. In this system, there are about four different eutectic reactions occurring at 1583°C , 1592°C , 1606°C , 1707°C , respectively. When the liquid composition is cooled down to the eutectic temperatures, a eutectic microstructure consisting of alternate lamellar structure is obtained. However, temperatures close to 1600°C are essential for such reactions to start up.

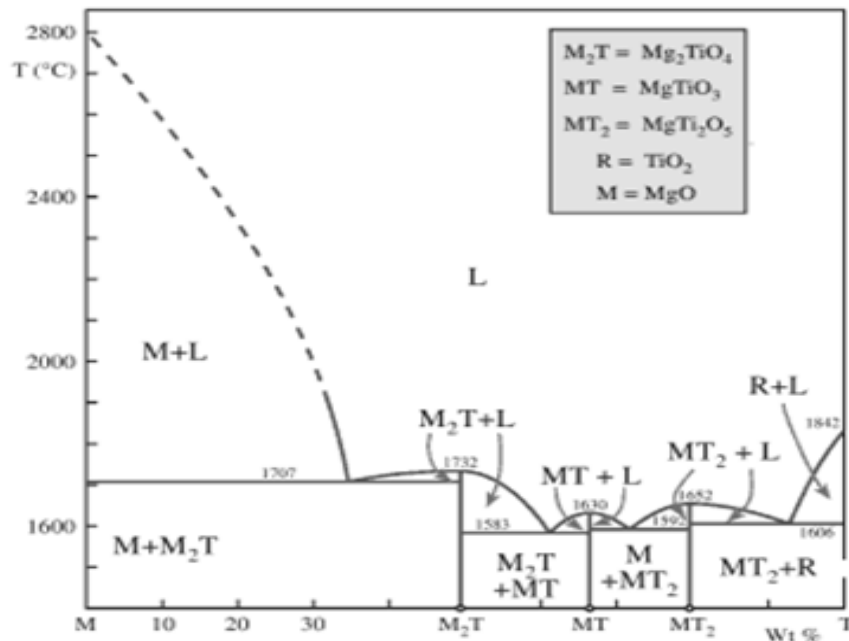


Figure 4: $\text{MgO} - \text{TiO}_2$ phase diagram [77]. (adapted from book: Cer.Mater.Sci.Engg. by C.Barry Carter, M. Grant Norton, Springer, 2007)

The ZnO-TiO₂ phase diagram is as shown in Figure 5. In this system, there is a eutectic reaction taking place at 1418°C where liquid gives rise to Zn₂TiO₄ and rutile phase. The other eutectic reaction takes place at 1537°C where liquid gives rise to Zn₂TiO₄ and ZnO. It was shown that Zn₂Ti₃O₈ formed when the anatase phase was present and ZnTiO₃ formed when the rutile phase was present [78]. The low temperature portion of the ZnO – TiO₂ phase diagram is not easy to be studied because of the sluggishness of reactions and similarities in diffraction patterns [79].

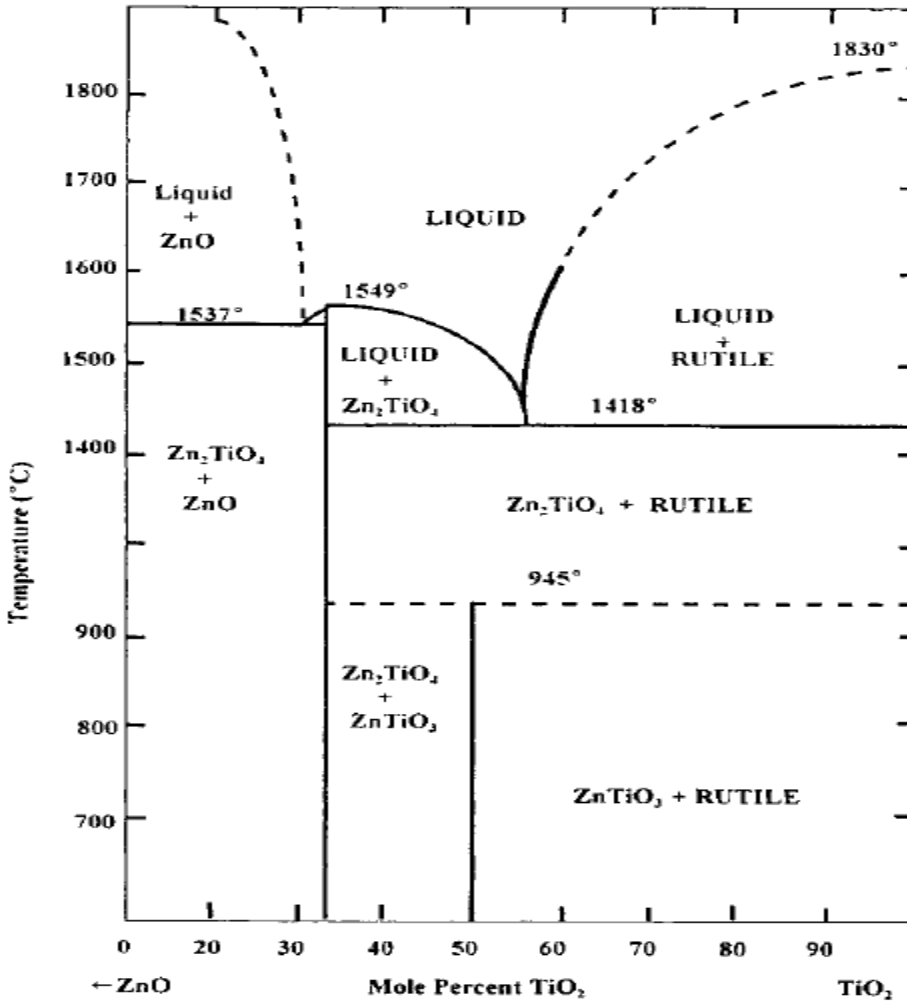


Figure 5: ZnO – TiO₂ phase diagram [80].(adapted from Phase equilibria in the system ZnO—TiO₂ by F.H.Dulin and D.E. Rase, J.Am.Cer.Soc,43: 125-131, (1960))

The SiO_2 — TiO_2 phase diagram is shown in Figure 6. This system undergoes a eutectic reaction at 1550°C , where liquid transforms into rutile and cristobalite (a polymorph of SiO_2). At temperatures below 1550°C there is no solubility between the two phases.

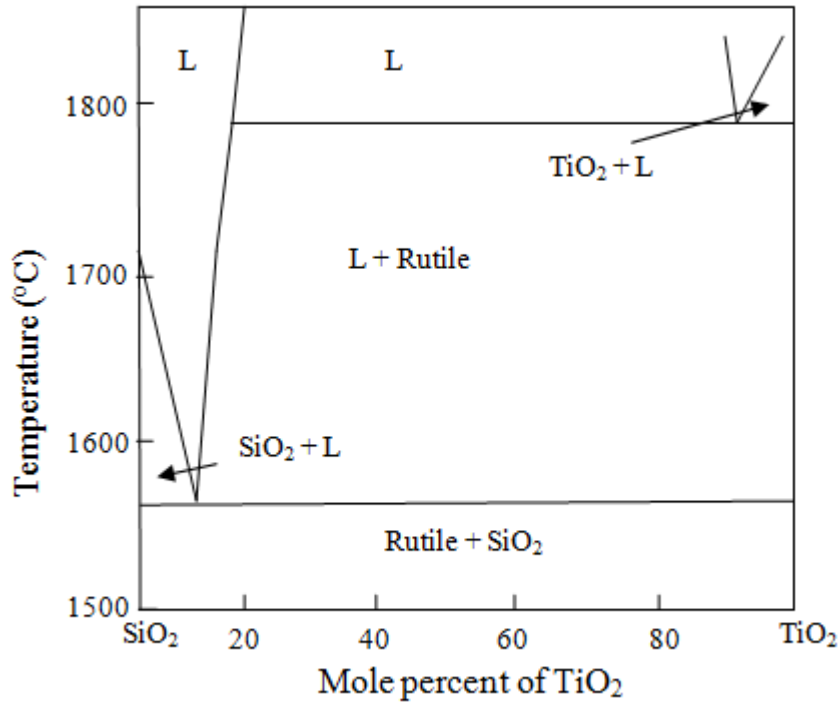


Figure 6: SiO_2 – TiO_2 phase diagram [77]. (adapted from book: Cer.Mater.Sci.Engg. by C.Barry Carter, M. Grant Norton, Springer, 2007)

2.5 Polyethylene glycol for processing of porous ceramic scaffolds

Polyethylene glycol (PEG) was used as a pore-former for the processing of porous titania structures due to the following advantages:

- Possesses a low melting point, hence melts easily.
- Possesses low flash point.
- It acts as an excellent binder to bind the particles hence providing good strength to the green structures.
- It is non-toxic and possesses no interaction with biological chemicals.
- It is cheap and is easily available as biology grade material.

Lot of research work has been carried out to process porous titania structures using polyethylene glycol as the template. J.Jiao [81] prepared mesoporous titania-silica composite using polyethylene glycol (PEG) 20,000 as the template direction reagent with the assistance of supercritical carbon-dioxide. M. Takeshi [82] synthesized porous titania films by dip-coating technique using polyethylene glycol as the template material. B.Shaojing [83] prepared nanocrystalline porous titania films on titanium substrates by sol-gel method with polyethylene glycol as a template. Porous titania films on glass substrates have been fabricated by using a sol-gel dip coating method with polyethylene glycol as the template [84]. A novel inorganic–organic composite solid electrolyte was prepared by using TiO₂ nanotubes (TiNTs) as filler in polyethylene glycol (PEG) and this was used for the fabrication of solid-state dye-sensitized solar cells (DSSCs) [85]. Some important properties of PEG used are tabulated in Table 1.

Table 1: Properties of PEG:

Chemical formula	(C₂H₄O)_n.H₂O
CAS #	25322-68-3
Physical appearance	White solid
Odor	Mild odor
Purity (%)	99.5
Molecular mass	8000
Particle Size (µm)	63
Density (g/cc)	1.03
Melting point (°C)	60
Boiling point (°C)	184
Flash point (°C)	270
Solubility in water	Soluble
Toxicology	May act as an irritant

3. METHODOLOGY

This section describes in detailed experimental procedure starting from raw materials used, synthesis of nanocrystalline titania, processing of bulk titania structures with sintering additives, processing of porous and doped porous titania structures, followed by the characterization of the sintered structures. The Sol-gel technique was used to synthesize nanocrystalline titania powder. This technique was established by Mr. Shipeng Qiu in our laboratory.

3.1 Raw materials used

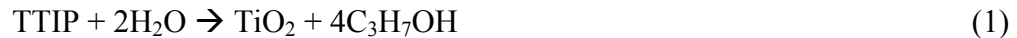
Table 2: Chemicals used for the synthesis of nanocrystalline titania

Chemical Name	Molecular Formula	Purity	Company
Titanium (IV) tetraisopropoxide	$\text{Ti}[\text{OCH}(\text{CH}_3)_2]_4$	98+%	Fisher Scientific, USA
Deionized water	H_2O	—	Fisher Scientific, USA
Isopropanol	$\text{CH}_3\text{CH}(\text{OH})\text{CH}_3$	70%	Fisher Scientific, USA
Nitric acid	HNO_3	6 M	Fisher Scientific, USA

Table 2. gives the list of various chemicals used in the Sol-gel synthesis of nanocrystalline titania powder. The same technique was used throughout the entire study to synthesize nano-powder which was the starting material for the processing of bulk and porous titania structures.

3.2 Synthesis and characterization of nanocrystalline titania powder

Nanocrystalline Titanium dioxide powder with particle size of 5-15 nm was prepared by a simple Sol-gel technique. This technique was initially established by Mr. Shipeng Qiu in our laboratory. The technique uses titanium isopropoxide, isopropanol and deionized water as the starting materials. For the synthesis process initially TTIP solution was titrated into a solution containing homogeneously mixed deionized water and isopropanol. Homogeneous mixing during the titration process was carried out by a magnetic stirrer. After the titration process few drops of nitric acid were added to maintain the pH of the solution at 2. The titration process was carried out for about an hour and the obtained solution was allowed to peptize overnight. The peptized solution contained two distinct layers: The top layer is the by-product formed during hydrolysis process and bottom layer consists of gel composed of titanic acid, which was dried in a table-top muffle furnace at a temperature of 110°C for about 15 h, which led to the formation of yellow block crystals of titania. These crystals were crushed and grounded into a fine powder in mortar and pestle. Following this process the powder was finally calcined at 400°C for 3 h [20]. The hydrolysis reaction involving the formation of Titanium dioxide is represented by the equation:



The various steps involved in the synthesis of nanocrystalline titania via sol-gel technique is shown in Figure 7. The experimental setup for this technique is shown in Figure 8.

The obtained powder was characterized using X-Ray diffraction to confirm the nanocrystalline nature of the powder. Details of the same are mentioned in section 3.6.1.

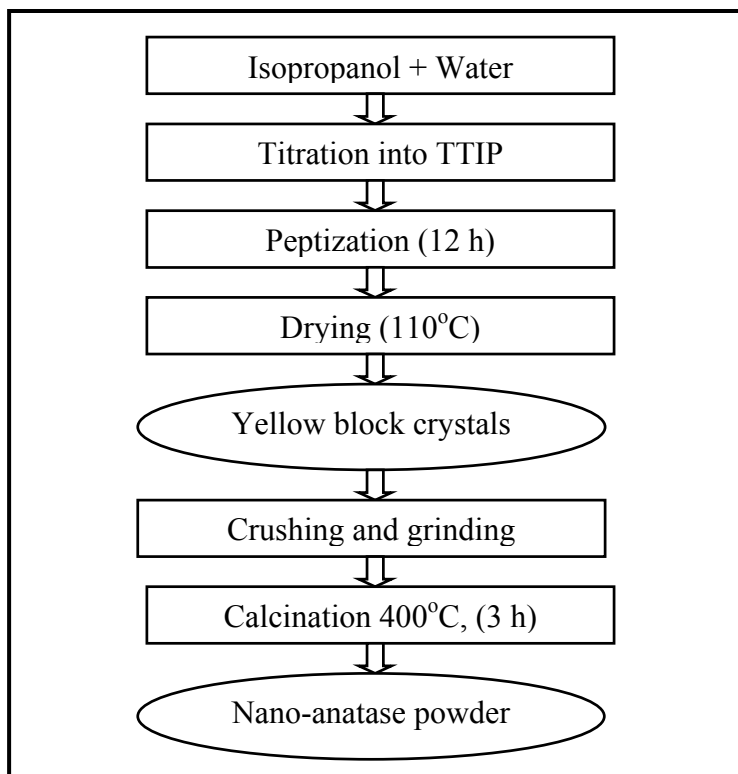


Figure 7: Flowchart showing steps involved in sol-gel processing of nanocrystalline titania



Figure 8: Setup showing the Sol-gel synthesis of nanocrystalline titania

3.3 Processing of metal-ion doped titania structures

The nanocrystalline powder obtained in the above process was separately mixed with various sintering additives at different wt. % ratios. The sintering additives selected were magnesium oxide (MgO, 98% pure, Alfa Aesar), zinc oxide (ZnO, 99% pure, Alfa Aesar), silicon (IV) oxide (SiO₂, 99.5% pure, Alfa Aesar). These additives were selected as these are known to be prevalent in the bone mineral as well. The additives so selected were into TiO₂ powder separately at differing wt. % (1.0 wt. %, 2.0 wt%, 3.0 wt %). The mixing was thoroughly and homogeneously carried out for 15 minutes using mortar and pestle. The pure as well as the doped powder compositions were uniaxially compacted in a steel mold using cold die compaction technique using 31 MPa pressure. The powder was densified during the compaction process producing green samples with minimum porosity which is due to the powder rearrangement by sliding and rolling. Uniaxial hydraulic press from Carver, inc. (Webash, IN) was used to prepare the green samples. Dry P.T.F.E. film was sprayed into the inner surface of the mold during the compaction process in order to minimize the friction. Some important properties of the additives used are summarized in Table 3. Compositions of the powder mixture of TiO₂ with different sintering additives are presented in Table 4.

The green density of the processed structures were measured and the sintering of these structures were carried out in a high temperature programmable muffle furnace (Model 46100, Dubuque, IA, Barnstead International Co) (as shown in Figure 9) in air. I employed two different sintering cycles for all the samples to study the effect of sintering temperature on the densification and other mechanical properties of TiO₂. Both the sintering cycles employed were such that the sintered samples developed good densification and contain no visible cracks. The

first cycle (Cycle A) employed consisted of several steps: initial holding at 150°C in order for the furnace to stabilize.

Table 3: Properties of additives used

Property	MgO	ZnO	SiO₂
Other name	Periclase	Zincite	Quartz
CAS #	1309-48-4	1314-13-2	7631-86-9
Purity (%)	98	99	99.5
Particle size (µm)	45	45	38
Molar mass (g/mole)	40.3	81.41	60.08
Crystal Structure	Cubic	Hexagonal	Tetrahedral
Density (g/cm³)	3.58	5.606	2.2
Melting point (°C)	2800	1975	1710
Boiling point (°C)	3600	Sublimes	2230
Solubility in water (per 100ml)	0.0086	Insoluble	0.012
pH	10.3	6.95	~2
Vapor Density	1.39	2.26	2.8
Refractive Index	1.72	1.9	1.46
Hardness (GPa)	58	45	7
Tensile Strength (MPa)	125	137	100
Young's Modulus (MPa)	300	380	70.5
Compression Strength (MPa)	1250	1260	1350
Dielectric Constant	9.7	2.1	3.9

Table 4 : Compositions of TiO₂ ceramics studied

Abbreviation	Amount of Additives	Composition of Additives
Pure TiO ₂	—	—
A1	1.0 wt%	MgO
A2	2.0 wt%	MgO
A3	3.0 wt%	MgO
B1	1.0 wt%	ZnO
B2	2.0 wt%	ZnO
B3	3.0 wt%	ZnO
C1	1.0 wt%	SiO ₂
C2	2.0 wt%	SiO ₂
C3	3.0 wt%	SiO ₂



Figure 9 : High temperature furnace used for the sintering of titania structures

Second holding at 400°C for 0.5 h to remove residual stresses; finally holding at 1500°C for 3 h for attaining good densification, followed by cooling down to room temperature. The second cycle (Cycle B) was a two step process consisting of the following steps: initially holding at 250°C for 1 h, second holding at 400°C for 0.5 h to remove residual stresses; then holding at 1500°C for 0.5 h and then stepping down to 1300°C and maintained for 3 h followed by slow cooling to room temperature. Heating rate of 3°C min⁻¹ and a cooling rate of 5°C min⁻¹ was employed to reduce cracking due to thermal stress gradients. The density of the sintered ceramic structures produced using both the cycles was separately measured and mechanical testing was carried out on these specimens. However, the structures produced using Cycle A were selected for carrying out the biodegradation analysis.

3.4 Processing of phase-pure porous scaffolds

TiO₂ porous ceramic scaffolds were prepared using polyethylene glycol (PEG) as the pore-former. Nanocrystalline titanium dioxide for this purpose was synthesized by the Sol-gel technique as discussed in section 3.1.1. The obtained nanocrystalline powder was mixed with measured quantity (i.e. 5 wt.%, 10 wt.%, 15 wt.%, 20 wt.%, 25 wt.%) of polyethylene glycol (PEG, Molecular biology grade, Fisher Scientific, NJ) separately and grounded into fine powder using mortar and pestle. The powder compositions were compacted uniaxially in a steel mold, using cold die compaction technique using 31 MPa pressure. The powder was densified during the compaction process producing green samples with minimum porosity due to the powder rearrangement by sliding and rolling. Uniaxial hydraulic press from Carver, inc. (Webash, IN) was used to prepare the green samples. Dry P.T.F.E. film was sprayed into the inner surface of the mold during the compaction process in order to minimize the friction. Compositions of the powder mixture of TiO₂ with varying quantity of polyethylene glycol are presented in Table 5.

Table 5 : Compositions of TiO₂ porous scaffolds

Abbreviation	Amount of PEG
Pure TiO₂	—
P5	5 wt%
P10	10 wt%
P15	15 wt%
P20	20 wt%
P25	25 wt%

The green densities of structures were measured and sintering was carried out in a high temperature muffle furnace (Model 46100, Dubuque, IA, Barnstead International Co.) in air. I employed two different sintering temperatures for the samples to study the effect of sintering temperature on densification and other mechanical properties of TiO₂. Both the sintering temperatures (1400°C and 1500°C) employed were such that the sintered samples developed good densification and contained no visible cracks. The selection of sintering temperature was based on previous research done [20, 86] where best mechanical properties were obtained for all the sintered structures. In this study, for the first set of samples, the sintering cycle employed consisted of different steps: initial holding at 150°C for furnace stabilization; then removing residual stresses through holding at 400°C; finally holding at 1500°C for 3 h for achieving desired densification. Heating rate of 3°C min⁻¹ and a cooling rate of 5°C min⁻¹ were used to minimize cracking due to thermal stresses. For the second set of samples, the program remained the same; however the final holding temperature was reduced to 1400°C. The sintered densities

of the all structures were measured and later the mechanical characterization was performed. The structures sintered at 1500°C were selected for carrying out the biodegradation analysis.

3.5 Processing of metal-ion doped porous scaffolds

Metal ion doped TiO₂ porous scaffolds were prepared using polyethylene glycol (PEG) as the pore-former with 2 wt. % MgO and 2 wt. % ZnO added separately as the sintering additives. Nanocrystalline titanium dioxide for this purpose was synthesized by the Sol-gel technique as discussed in section 3.1.1. The obtained nanocrystalline powder was mixed with measured quantity (i.e. 10 wt.%, 15 wt.%) of polyethylene glycol (PEG, Molecular biology grade, Fisher Scientific, NJ) and 2 wt.% magnesium oxide (MgO, 98% pure, Alfa Aesar), 2 wt.% zinc oxide (ZnO, 99% pure, Alfa Aesar) separately and uniform mixing was carried out using mortar and pestle. The respective powder compositions were then uniaxially compacted in a steel mold, using cold die compaction technique at a pressure of 31 MPa. The powder densified into green structures during the process of compaction, with minimum porosity due to the powder rearrangement by sliding and rolling. Uniaxial hydraulic press from Carver, inc. (Webash, IN) was used to press all the green structures. Dry layer of P.T.F.E. film was sprayed into the inner surface of the die so that the friction can be reduced considerably. Table 6 presents the abbreviation used in representing different compositions of TiO₂ with the pore-formers as well as sintering additives.

Table 6 : Compositions of metal-ion doped porous scaffolds

Abbreviation	Amount of Additives	Composition of Additives	Amount of PEG
Pure TiO₂	—	—	—
A10	2.0 wt%	MgO	10 wt%
A15	2.0 wt%	MgO	15 wt%
B10	2.0 wt%	ZnO	10 wt%
B15	2.0 wt%	ZnO	15 wt%

The green density of the structures was measured and the sintering was carried out in a high temperature programmable furnace (Model 46100, Dubuque, IA, Barnstead International Co.) in air. I employed 1500°C as the sintering temperature for our samples in order to study the densification and other mechanical properties of all the sintered structures. With this sintering temperature, all the sintered samples developed good densification and contain no visible cracks. The sintering cycle employed consisted of different steps: initial holding at 150°C for the furnace to stabilize; then holding at 400°C to get rid of stresses in the structures; finally holding at 1500°C for 3 h. Heating rate of 3°C min⁻¹ and cooling rate of 5°C min⁻¹ were used in order to minimize cracking due to thermal stresses. The sintered density of the ceramic structures was measured and mechanical characterization was then done to evaluate the mechanical properties. But, the microstructural study was not done for these structures. The bioactivity study of these structures was carried out for a period of 21 days in simulated body fluid.

3.6 Characterization of metal-ion doped titania structures

3.6.1 Phase characterization using X-Ray diffraction technique

The phase evolution/ transformation in pure and doped TiO₂ structures sintered at 1500°C (Cycle A) was carried out using Powder X-ray diffraction (XRD) technique. For carrying out this analysis, the sintered ceramic structures of various compositions were ground to fine powder separately using pestle and mortar. These powders of various compositions were then subjected to XRD analysis in a Rigaku diffractometer (Model D/MAX-B, Rigaku.Co., Japan) supplied with Ni filtered Cu K α radiation ($\lambda = 0.154059$ nm) at a voltage of 40 kV and at a current of 30 mA. The XRD patterns were recorded in 2θ range of 20° to 70°, with a step size of 0.02° and a scanning rate of 1.5 degree/min. The crystallite size was further verified from the XRD patterns using Scherrer's equation:

$$\beta = k\lambda / (L\cos\theta) \quad (2)$$

Where β is the full width at half maximum, k is a constant (usually taken as 0.9), θ is the Bragg angle, λ is the wavelength of the X-rays and L is the average crystallite size.

3.6.2 Porosity measurements

The percentage of porosity in the sintered samples was evaluated using a simple immersion technique. The following equation was used to calculate the apparent porosity in the samples [87]:

$$\xi_a = [(m_s - m_d) / (m_s - m_w)] * 100 \quad (3)$$

Where m_s , m_d and m_w represent the saturated mass, dry mass and mass in water.

In this technique, the sintered structures were cleaned thoroughly to remove dust particles. The samples were then soaked in distilled water for a day. The excess water was drained off the surface and the sample was rolled in cotton and then the saturated mass of the sample was measured using Acculab analytical balance (Model DI-300, Inotek Instruments, NY), accurate to 0.001g. For measuring the mass of the structures in water a wire basket which was previously weighed in water was employed. The mass of basket together with the sample in water was then recorded. Therefore by subtracting the weight of the basket in water from the total mass of the sample together with the basket, the mass of the sample in water was calculated. The sample was then heated in the oven at 100°C and the dry mass (m_d) was measured.

3.6.3 Microstructural Analysis

The influence of sintering additives on the grain size of all the sintered ceramic structures was observed and analyzed using Scanning electron microscopy (SEM). The surface porosity of the structures after sintering can also be observed. A magnetron sputter coater from Emitech. Inc. was used to coat the surface of the sintered structures. The total coating time was one minute for each of the specimens used in the study. The gold coated specimens were observed in a JEOL SEM (JEOL, Model 6400F, Japan).

3.6.4 Mechanical Characterization

3.6.4.1 Vickers hardness testing

The mechanical properties of all the pure as well as the doped TiO₂ structures sintered at 1500°C (Cycle A) and 1300°C (Cycle B) were evaluated by conducting hardness measurements. The hardness was measured using Vickers hardness tester (LECO Co., Model

LV-700, MI) as shown in Figure 10. Sintered structures of all compositions were indented at several locations to evaluate their hardness. During the test, a load of 1kgf with a total loading time of 5 s was applied in order to make sure that no cracks are observed on specimen surface. The pellets used were 1.6 mm thick and were 9.9 mm in diameter. One sample corresponding to each composition was tested for the hardness at various locations and the average hardness was then calculated. The results were then compared and analyzed.



Figure 10: Vickers hardness tester

3.6.4.2 Biaxial flexural testing

Biaxial flexural strength tests were performed according to the ASTM F-394 standard specifications with a slight alteration in fixture dimension so that the specimen size could be accommodated. Flexural strength properties of pure and doped TiO₂ structures sintered at 1500°C (Cycle A) and 1300°C (Cycle B) were studied. The testing was carried out at a constant crosshead speed of 0.05 mm/min in a tensile tester (Instron Co., Model 3369). ASTM F394 standard specification supports the use of piston on three ball test. Here, the TiO₂ disc pellet is supported by three ball bearings near its periphery, at the same time equal distance from load piston is maintained. To ensure that uniform loading is attained a layer of polythene sheet was placed between the piston and test specimens.

A hardened steel ball 0.75 mm in diameter was placed at end of the piston. This system presses against the three balls (1.98 mm in diameter) system. This test was specially designed for carrying out biaxial flexural testing of disc shaped specimens. To meet the ASTM standard specifications the 3-ball test system was made using hardened steel balls. The dimensions of the steel balls and specimens used in the test were smaller than the specified ASTM standards. This arrangement was specially done to accommodate the smaller dimensions of the specimens.

The sintered titania structures were centered and supported on the three steel balls which are 120° apart on a circle of 7.5 mm diameter. The setup is shown in Figure 11. To distribute the load evenly a polyethylene sheet was placed between the specimen and moving piston setup system, which was done according to the ASTM standards. Instron tensile testing machine with a crosshead speed of 0.05 mm/min was used to carry out the testing. The fracture load was used to calculate the flexural strength. The following equations were used [86]:

$$S = -0.2387 P (X-Y)/d^2 \quad (4)$$

Where **S** is maximum central tensile stress in MPa and **P** is the total load causing fracture in N.

$$X = (1+\nu) \ln (B/C)^2 + [(1-\nu)/2] (B/C)^2 \quad (5)$$

$$Y = (1+\nu) [1 + \ln (A/C)^2] + [(1-\nu)] (A/C)^2 \quad (6)$$

where, ν is Poisson's ratio (taken as 0.27), **A** is radius of support circle in mm, **B** is the radius of loaded area or ram tip in mm, **C** is the radius of specimen in mm and, **d** is specimen thickness at fracture origin in mm.

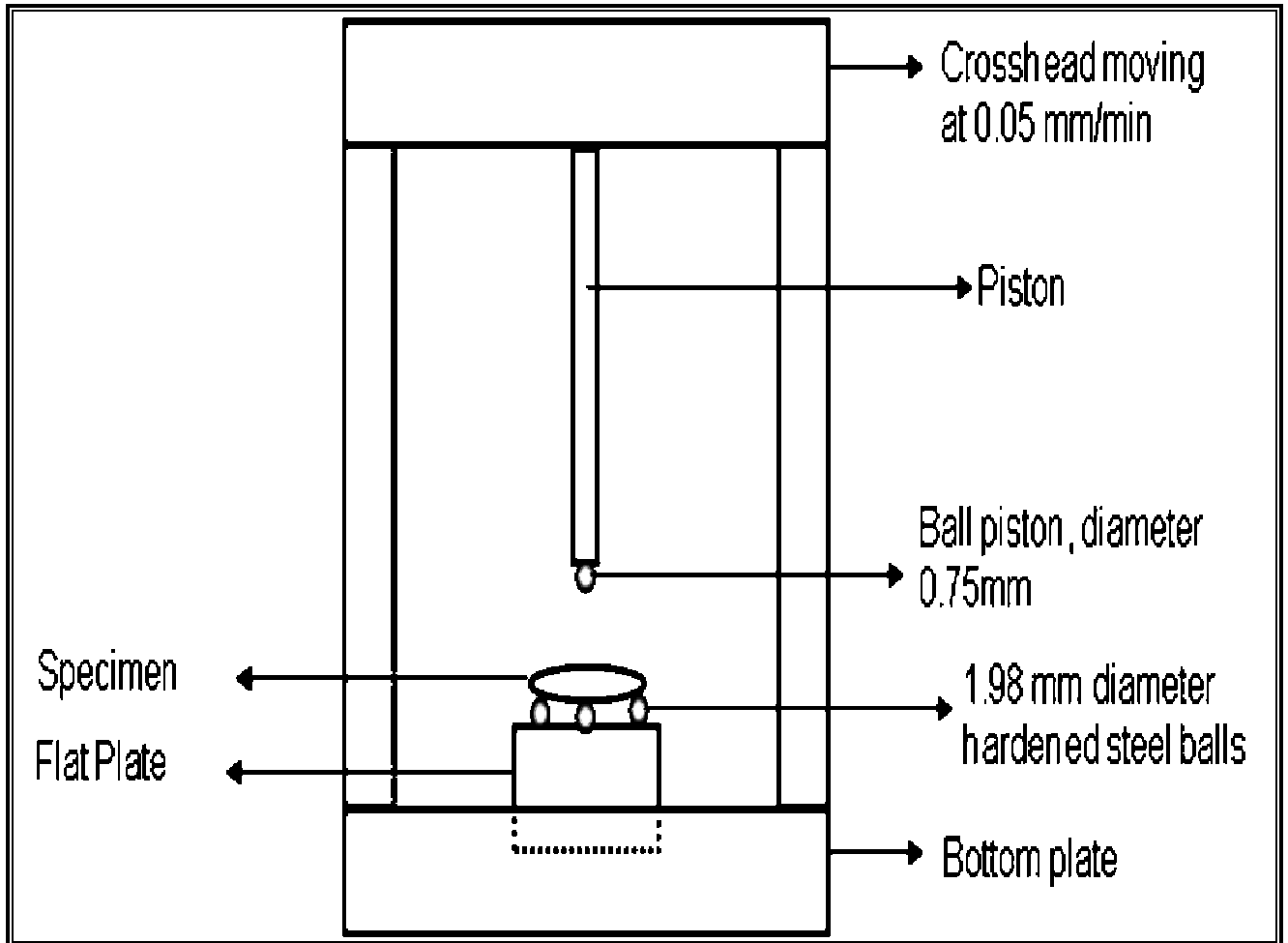


Figure 11: Setup showing the biaxial flexural testing

The advantages of this testing is since central loading area is exposed to the maximum tensile stress the failure of the material due to defects are eliminated completely. Also this testing technique is more conservative than other experimental techniques which use uniaxial stress.

3.7 Bioactivity and biodegradation study

The biodegradation rate of pure and doped TiO₂ structures sintered at 1500°C (Cycle A) was determined on the basis of their weight-loss and change in density with time, simulated body fluid (SBF). Strength-loss was evaluated by performing biaxial flexural strength test and hardness testing. The bioactivity of various bioceramics and other biomaterials have been assessed using SBF which eventually leads to apatite layer formation on the surface of materials used for study. Simulated body fluid (SBF) has an ion concentration nearly equal to that of human blood plasma (Na⁺ 142.0, K⁺ 5.0, Ca²⁺ 2.5, Mg²⁺ 1.5, Cl⁻ 147.8, HCO₃⁻ 4.2, HPO₄²⁻ 1.0, and SO₄²⁻ 0.5 mM, and a pH of 7.3), as shown in Table 7 [88, 89].

In this work, SBF was used to determine the effect of dopants on biodegradation behavior of nanostructured TiO₂ ceramics. Pure TiO₂, A2, B2 and C3 structures sintered at 1500°C for 3 h were prepared for the biodegradation study. These compositions were selected as these possessed better mechanical properties. These selected samples were immersed in SBF solution, maintained inside an incubator at a constant temperature of 36.5°C. An incubator having compartments was used for this study. Three samples of each composition namely, pure TiO₂, A2, B2, C3 were placed in perforated plastic trays filled with freshly prepared SBF. These trays were placed inside the incubator which is maintained at 36.5°C. The setup is as shown in Figure 12 & 13. The samples were left in the plastic trays and the SBF was refilled with a newly prepared solution of SBF every three days, so that the pH and ionic concentration is maintained throughout the study. One tray containing samples of each of these compositions were taken out

at the end of each week, and the samples were dried at 110°C in a table-top furnace and weight loss was measured. The dimensions of the dried samples were recorded and the change in the weight was determined and hence the density was calculated.

Table 7 : Ionic concentrations of human blood plasma and SBF

Ions	Human blood plasma (mM)	SBF (mM)
Na⁺	142.0	142.0
K⁺	5.0	5.0
Ca²⁺	1.5	1.5
Mg²⁺	2.5	2.5
Cl⁻	103.0	148.8
HCO₃⁻	27.0	4.2
HPO₄²⁻	1.0	1.0
SO₄²⁻	0.5	0.5

Dried specimens after each point of time (Day 14, 21, 28 , 35, 42) were measured for hardness change on Vickers hardness tester, to study the change in biomechanical properties. One specimen of every composition was taken out from SBF at different points of time. The hardness was taken at five different locations on each specimen. The average hardness value was recorded. The biaxial testing was also carried out on these structures in order to determine the change in the biaxial flexural strength with time.



Figure 12: Incubator used for biodegradation study



Figure 13: Setup showing titania samples placed in SBF solution

3.8 Characterization of Phase-pure porous scaffolds

3.8.1 Porosity measurements

The porosity measurements were carried out in the same way as discussed in section 3.6.2. The same procedure was adopted.

3.8.2 Microstructural Analysis

The microstructure of the sintered porous ceramics was observed using a Scanning Electron Microscope (SEM) to observe and analyze the influence of pore former on the grain size and surface porosity of all the processed structures. The specimens sintered at 1500°C (Cycle A) were selected for microstructural examination. The structures used for this examination were 1.6 mm thick and had average diameter of 9.8 mm. A magnetron sputter coater from Emitech. Inc. was used to coat the surface of the sintered structures. The total coating time was one minute for each of the specimens used in the study. JOEL SEM (Model 6400F, Japan) was used to observe the microstructures.

3.8.3 Mechanical Characterization

3.8.3.1 Vickers hardness testing

The surface hardness of all the porous TiO₂ structures sintered at 1500°C and 1400°C were evaluated. Automated Vickers hardness tester was used to carry out hardness testing. All the sintered structures were indented at several locations to evaluate their hardness. During the test, a load of 1kgf with a total loading time of 5 s was applied in order to make sure that no cracks are observed on specimen surface. The pellets used were 1.6 mm thick and were

9.9 mm in diameter. One sample corresponding to each composition was tested for the hardness at various locations and the average hardness was then calculated. The results were then compared and analyzed.

3.8.3.2 Biaxial flexural testing

Biaxial flexural testing was carried out for the structures sintered at 1500°C and 1400°C respectively. This testing was carried out in a tensile tester (Instron Co., Model 3369). The crosshead speed during the test operation was 0.05 mm/min. The test description and procedure is the same as discussed in section 3.6.4.2. The results of this test were then analyzed to see the effect of changing sintering temperature and varying pore former addition on the mechanical strength of all the sintered structures.

3.9 Bioactivity and biodegradation study

The biodegradation rate of the structures (P10, P15, P20) sintered at 1500°C were studied. The change in weight, degradation of hardness and biaxial flexural strength in simulated body fluid (SBF) was studied. Specimens taken out of the SBF solution were dried in a table-top furnace at 110°C for about 3 h and finally the change in the weight was recorded. Vickers hardness tester was used to measure the surface hardness of the structures at the end of day 14 and 42 to study the surface mechanical property deterioration. One specimen of each composition was taken out from SBF and tested for hardness at many different locations. The average hardness value was finally calculated for each of these compositions. The biaxial testing was also carried out on these structures in order to determine the change in the flexural strength with time.

3.10 Characterization of metal-ion doped porous scaffolds

3.10.1 Porosity measurements

The porosity measurements were carried out in the same way as discussed in section 3.6.2. The same procedure was adopted.

3.10.2 Mechanical Characterization

3.10.2.1 Vickers hardness testing

The mechanical properties of all the metal ion doped porous TiO₂ structures sintered at 1500°C were evaluated by conducting hardness measurements. Automated Vickers hardness tester was used to carry out hardness testing. All the sintered structures were indented at several locations to evaluate their hardness. During the test, a load of 1kgf with a total loading time of 5 s was applied in order to make sure that no cracks are observed on specimen surface. The pellets used were 1.6 mm thick and were 9.9 mm in diameter. One sample corresponding to each composition was tested for the hardness at various locations and the average hardness was then calculated. The results were then compared and studied.

3.10.2.2 Biaxial flexural testing

Biaxial flexural testing was carried out for all the sintered structures. The flexural testing was carried out on a tensile tester (Instron Co., Model 3369) at a constant crosshead speed of 0.05 mm/min. The test description and procedure is the same as discussed in section 3.1.3.2. The results of this test were then analyzed to study the effect of dopant and pore former addition on the mechanical strength of all the sintered structures.

The microstructural analysis using Scanning electron microscopy was however not done on these samples.

3.11 Bioactivity studies

The rate of biodegradation of structures (A10, A15, B10, B15) sintered at 1500°C were studied. The weight change, degradation of hardness and biaxial flexural strength of the samples was done as discussed in section 3.7 and 3.9. Specimens taken out of the SBF solution were dried in a table-top furnace at 110°C for about 3 h and the change in weight was calculated. These structures were also tested for their hardness in a Vickers hardness tester, at the end of day 21 to study the surface mechanical property deterioration. One specimen of each composition was removed from SBF and hardness at five different locations was taken from which the average hardness were calculated. The biaxial flexural testing was also carried out on these structures in order to determine the change in the flexural strength with time.

4. RESULTS AND DISCUSSIONS

4.1 Sintering and densification study

4.1.1 Metal-ion doped titania structures

The green ceramic structures prepared by uniaxial pressing were measured for the density which was finally subjected to sintering. The average bulk density of 1.85 g.cm^{-3} was recorded for the green samples. About ten green samples of each of the compositions were selected for the sintering process. The sintering was done at 1500°C for 3 h (Cycle A). Figure 14 shows the average sintered densities plotted as a function of composition. The pure TiO_2 structures recorded a sintered density of 3.79 g.cm^{-3} . Whereas, for compositions A1, B1 and C1 sintered density of 3.81 g.cm^{-3} , 3.82 g.cm^{-3} and 3.81 g.cm^{-3} were recorded. The increase in quantity of additives led to improved densification. For B2 and C3 structures a sintered density was 3.85 g.cm^{-3} was recorded. The maximum sintered density of 3.87 g.cm^{-3} was recorded for A2 structures. Based on these results, the three compositions (A2, B2 and C3) were studied extensively in this work and were selected for sintering using Cycle B.

These results can be better explained with the help of SEM microstructures. Figure 24 shows the micrographs of the structures sintered using Cycle A. The results showed that the grain size of the sintered ceramics increased with the increase in presence of sintering additives. As seen from Figure 24c, grain growth was significant for composition B2; even then these structures possessed better density than pure TiO_2 structures as the porosity (8%) was lesser than the porosity (9.25%) which was recorded for pure TiO_2 structures. Also, the presence of micro cracks along the grain (Fig 24a), led to a decrease in densification. In contrast, composition A2 and C3 (Figure 24 b, d) showed significantly improved sintered density although their grain sizes

were much higher than that of pure TiO₂. This is due to the fact that sintering additives possibly improved grain boundary properties, thereby improving sintered density.

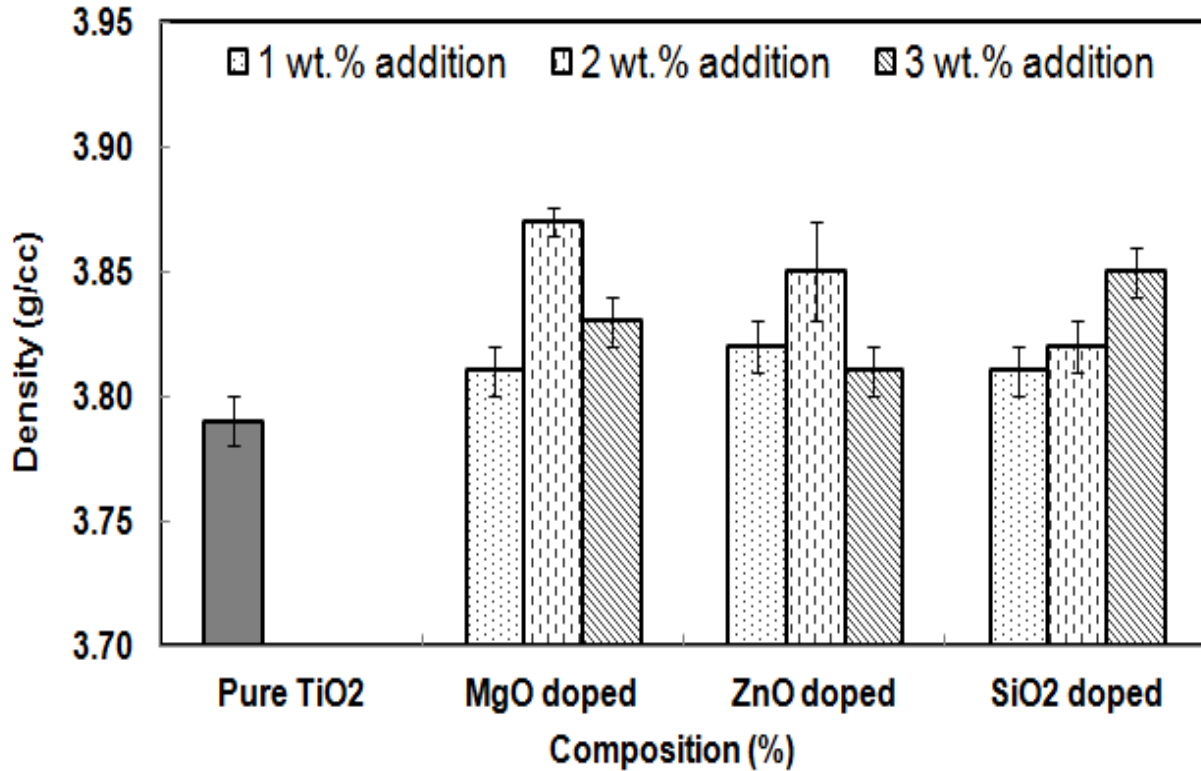


Figure 14: Effects of doping on sintered density of TiO₂ structures sintered at 1500°C for 3 h.

Compositions A2, B2, C3 and pure TiO₂ structures were selected for sintering using Cycle B (1500°C for 0.5 h and 1300°C for 3 h). The green structures possessed green density of 1.85 g.cm⁻³. Five green samples of each of the compositions were sintered and average sintered density of all the structures was recorded. Pure TiO₂ structures possessed a sintered density of 3.74 g.cm⁻³. Whereas compositions A2, B2 and C3 possessed sintered densities of 3.82 g.cm⁻³, 3.80 g.cm⁻³ and 3.79 g.cm⁻³, respectively. Average sintered densities obtained in both sintering cycles (A and B) were then plotted as a function of compositions as shown in Figure 15.

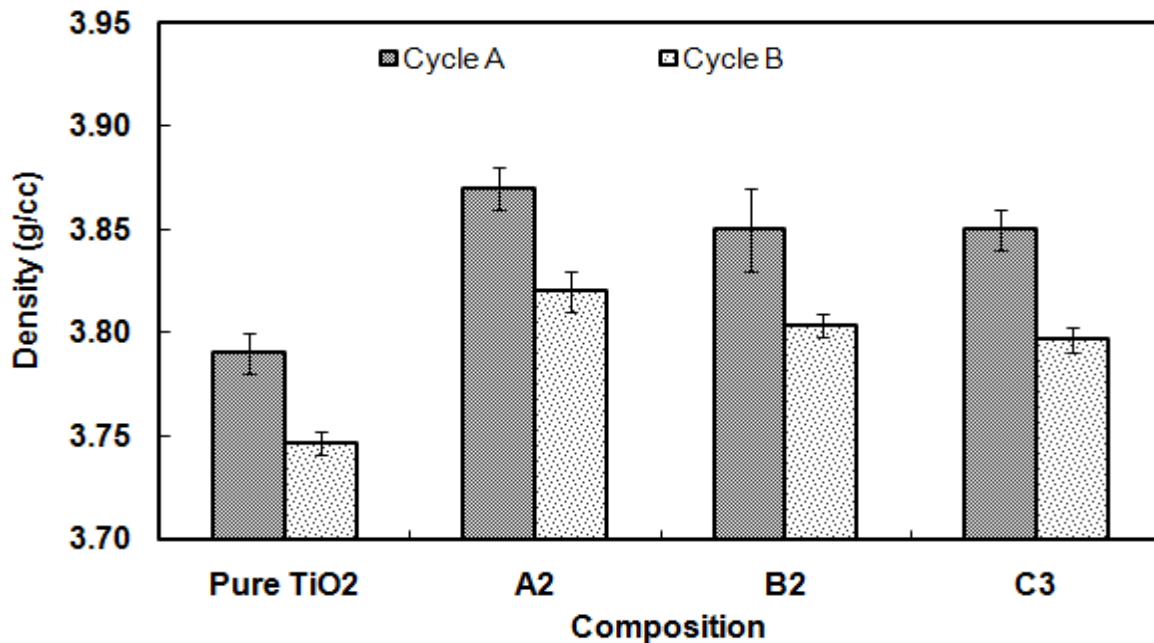


Figure 15: Comparison of sintering cycles on densification - Cycle A: sintering at 1500°C for 3 h; Cycle B: sintering at 1500°C for 0.5 h and hold at 1300°C for 3 h.

Figure 25 shows the micrographs of structures sintered using Cycle B. The micrographs of doped structures clearly show the influence of dopants on particle size of sintered powder. Figure 25a shows that even though the grains are smaller and visible, the grain boundary is less distinct. The porosity of pure TiO₂ structures, as seen from micrographs was higher than the structures of other compositions. This is also in line with porosity calculations where 12.3% porosity was recorded for pure TiO₂ and about 11% was recorded for the other compositions. All structures sintered using Cycle B had higher porosity with interconnected pores. The presence of surface porosity in these structures hindered proper densification when compared to structures sintered using Cycle A. Hence lower densification was obtained for these structures.

4.1.2 Phase-pure porous scaffolds

The bulk density of the green structures were measured. All the green structures had an average green density of 1.79 g cm^{-3} . About five to eight structures of each of the different compositions were prepared. The prepared samples were sintered at two different temperatures separately; namely 1500°C for 3 h and 1400°C for 3 h. After sintering, the density of all the samples was calculated separately and the effect of sintering temperature and quantity of pore-former added on the densification of the structures were studied. Figure 16 shows the plot between average sintered densities and composition. The structures sintered at 1500°C for 3 h were initially studied. The highest sintered density of 3.8 g.cm^{-3} was recorded for the pure titania structures. The increased sintered density is due to the absence of pore former. Whereas, for the porous TiO_2 structures the density decreased as the amount of pore former increased. For the porous structures sintered at this temperature the highest sintered density of 3.36 g.cm^{-3} was obtained for P5 structures and a minimum density of 2.71 g.cm^{-3} was obtained for P25 structures.

Some of the green structures were sintered at 1400°C for 3 h. Sintering at this temperature led to lower densification of all the samples used in this study. For pure TiO_2 structures a maximum sintered density of 3.77 g.cm^{-3} was recorded. For the porous structures, highest sintered density of 3.32 g.cm^{-3} was recorded for the P5 structures, whereas the minimum sintered density of 2.63 g.cm^{-3} was recorded for P25 structures. The variation in the sintered density with the amount of pore-former added and sintering temperature is shown in Figure 16.

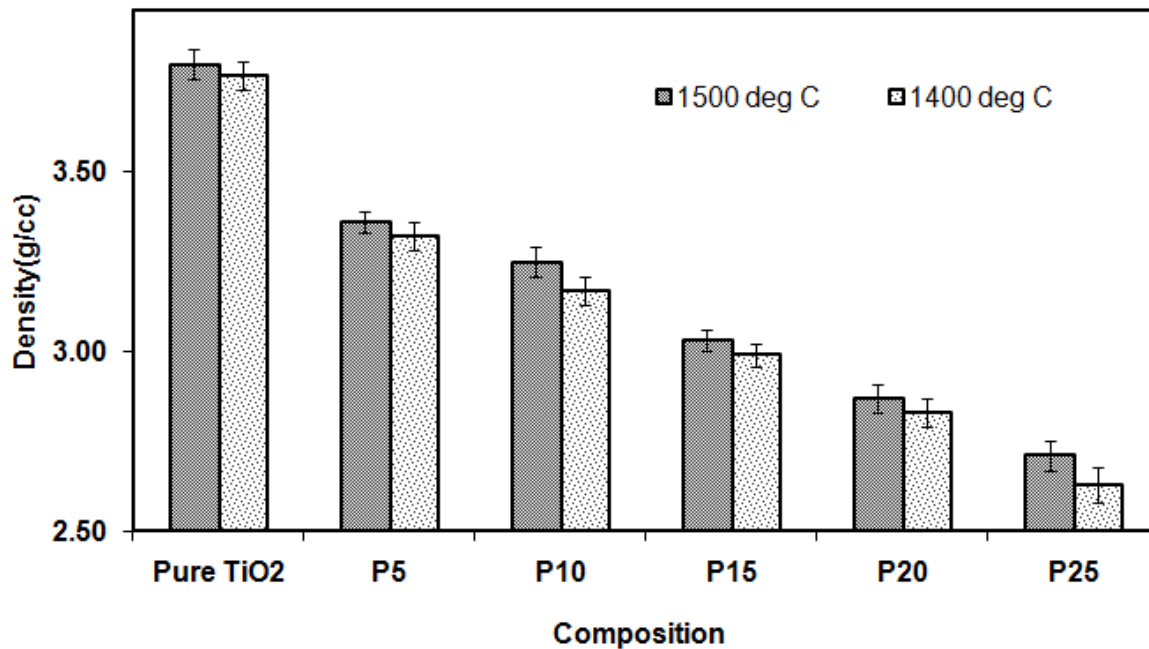


Figure 16 : Variation in sintered density for the pure titania and porous scaffolds with temperature.

The results of densification study can be better explained with the help of SEM micrographs as shown in Figure 26 & 27. From the micrographs it is clear that the surface porosity increased with the increase in quantity of pore-former added. For pure TiO₂ the surface porosity was minimum, hence these structures possessed increased density. For all the other structures, the total porosity and pore volume increased as the % of pore-former increased which led to the decrease in the densification.

4.1.3 Metal-ion doped porous scaffolds

Structures of doped porous ceramics were measured for their green density. The average green density of 1.79 g.cm^{-3} was recorded. To study the effect of sintering additives (A – 2 wt% MgO, B – 2 wt% ZnO) on the densification of TiO_2 porous ceramics, about five samples of each composition types (A10, B10, A15, B15) were sintered at 1500°C for 3 h. The average sintered density of structures of each of the different compositions was recorded. The data was then compared with pure TiO_2 and compositions (P10 and P15—which do not contain sintering additives). Figure 17 shows a plot between the average sintered densities vs the composition. Among the doped porous structures, highest densification of 3.5 g.cm^{-3} was obtained for A10 structures and minimum densification of 3.23 g.cm^{-3} was obtained for B15 structures. The results show that the addition of sintering additives to porous TiO_2 structures improved the densification.

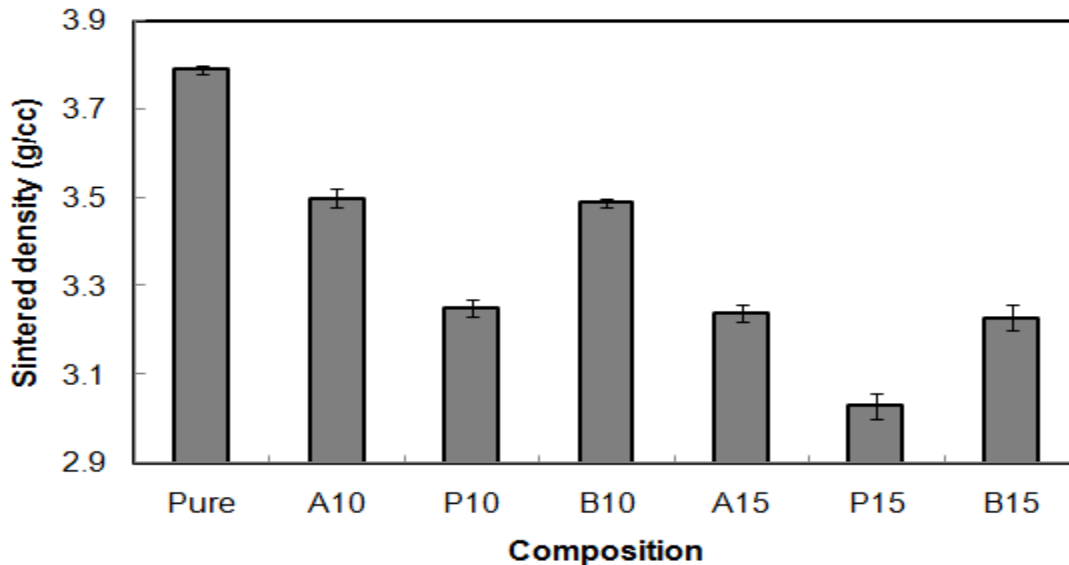


Figure 17: Variation of sintered density with composition for pure, porous and porous scaffolds doped with sintering additives. (A – 2 wt% MgO, B – 2 wt% ZnO)

4.2 Porosity measurements

4.2.1 Metal-ion doped titania structures

The bulk porosity in sintered samples was evaluated using equation (3). It was observed that % porosity increased with a decrease in sintering temperature. For pure TiO₂ structures, a porosity of 12.5% (± 0.21) was recorded. In case of A2, B2 and C3 porosity of 10% (± 0.3), 11.2% (± 0.24) and 11% (± 0.27) were recorded respectively. The variation in the porosity of all the structures with sintering temperature is shown in Figure 18.

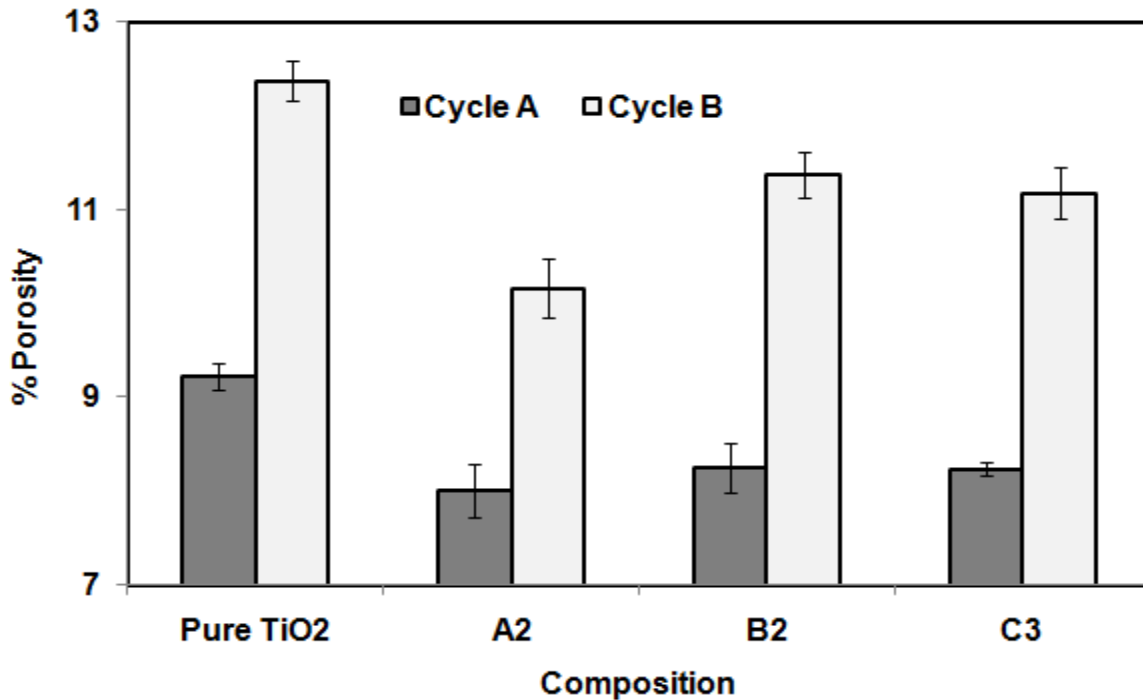


Figure 18: % Porosity vs. Composition for all the sintered structures. - Cycle A: sintering at 1500°C for 3 h; Cycle B: sintering at 1500°C for 0.5 h and hold at 1300°C for 3 h.

From the SEM micrographs of the pure TiO₂ structures (Figure 26a), it can be clearly seen that increased surface porosity led to lower densification.

4.2.2 Phase-pure porous scaffolds

The percentage of porosity in all the phase-pure porous titania structures was calculated using the immersion technique as mentioned earlier. Minimum porosity of 14.98% (± 0.6) was obtained for P5 structures sintered at 1500°C for 3 h and maximum porosity of 48.31% (± 0.19) was obtained for P25 structures sintered at 1400°C for 3 h. The variation of % porosity with composition is shown in Figure 19. It was observed that higher porosity was obtained for the structures sintered at 1400°C.

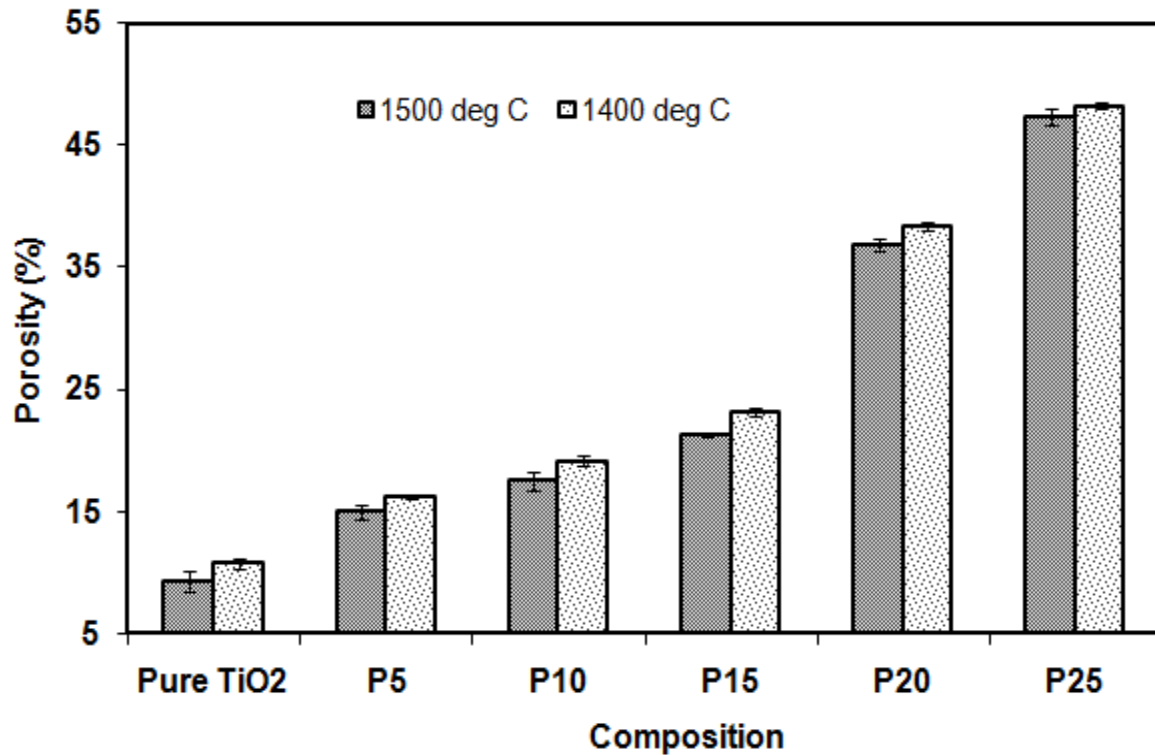


Figure 19 : % Porosity Vs Composition for pure titania and porous scaffolds.

4.2.3 Metal-ion doped porous scaffolds

The percentage of porosity in all the metal ion doped porous structures were calculated using the immersion technique as mentioned earlier. Minimum porosity of 13.17% (± 0.6) was obtained for A10 structures and maximum porosity of 17.95% (± 0.39) was obtained for B15 structures sintered at sintered at 1500°C for 3 h . The variation of % porosity with composition is shown in Figure 20. It was observed that porosity of the porous structures decreased with the addition of sintering additives.

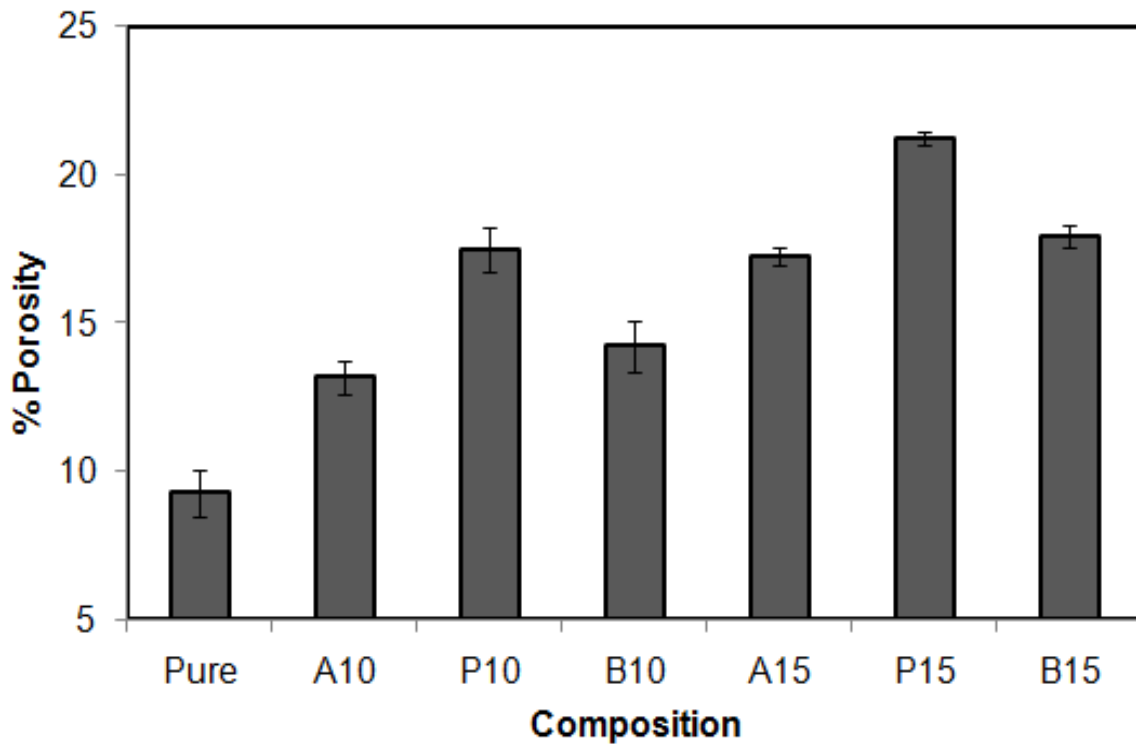


Figure 20: Variation of % porosity with composition for pure, porous and porous scaffolds doped with sintering additives. (A – 2 wt% MgO, B – 2 wt% ZnO).

The microstructural analysis of these structures using scanning electron microscopy was however not done.

4.3 Phase analysis of metal-ion doped titania structures

The XRD pattern of as-calcined nanocrystalline TiO₂ powder is as shown in Figure 21. Scherrer's equation, Eq. (1), at $2\theta = 25.36^\circ$, $\lambda = 1.54059 \text{ \AA}$, $\beta = 0.726^\circ$, gives the crystallite size of the calcined TiO₂ powder, which was found to be 11.2 nm. The nanocrystalline nature of the as calcined powder is indicated by the broadening of the diffraction peaks, which shows that the powder is highly crystalline. The XRD patterns of the pure, A2, B2, C3 compositions sintered at 1500°C (Cycle A) are shown in Figure 22. It is evident from these diffraction patterns that majority of the phase is rutile. Two minor peaks of the anatase were also observed. JCPDS standard files #21-1272 and #21-1276 were used to confirm the presence of anatase phase. Almost identical patterns were recorded for all compositions. The results revealed that the phase purity of TiO₂ did not alter with the presence of these additives. All the other compositions including the ones sintered using Cycle B were not analyzed for their phases.

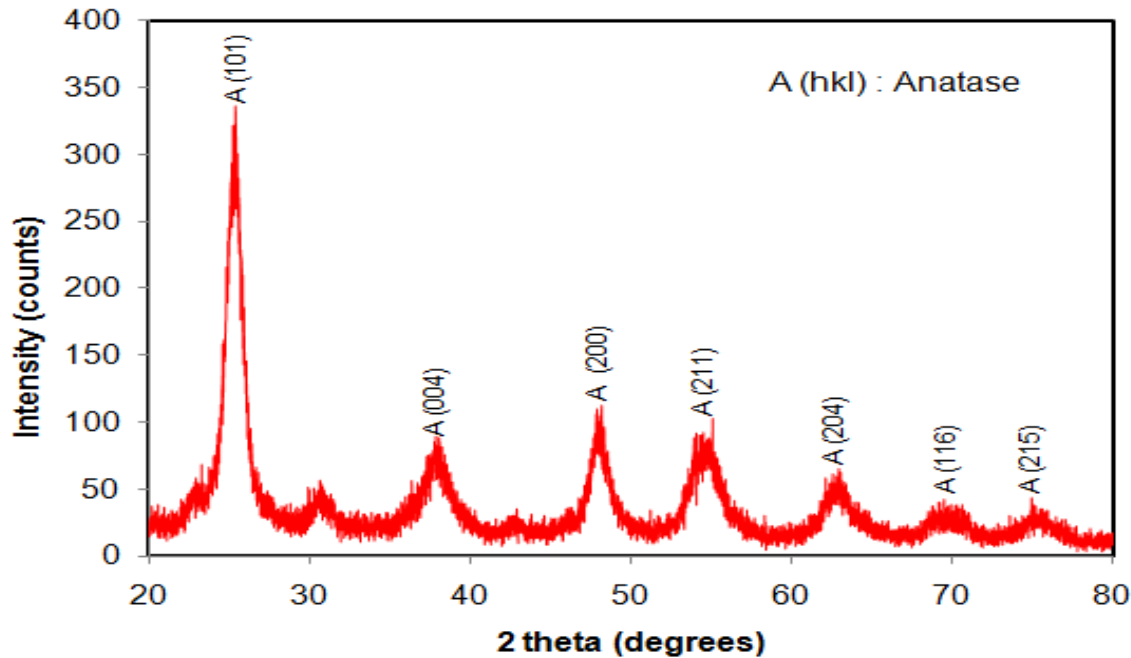


Figure 21: X-ray powder diffraction pattern of synthesized nanocrystalline TiO₂ (Anatase) powder.

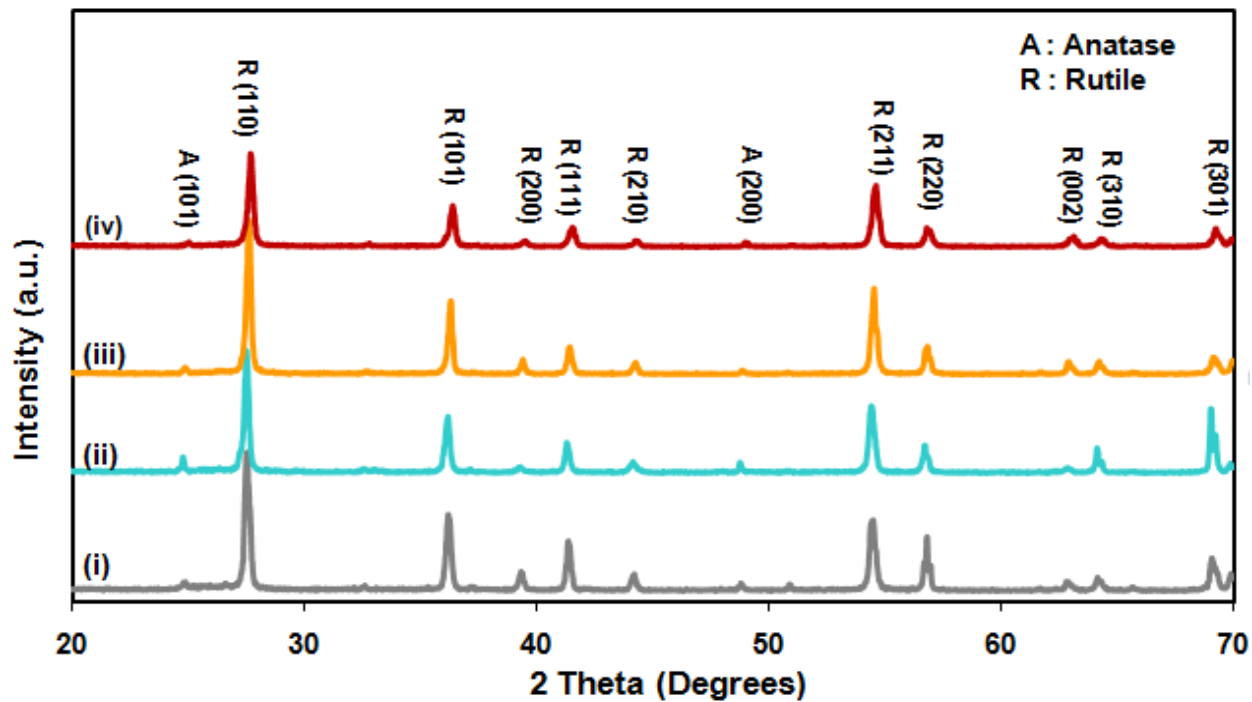


Figure 22: X-ray powder diffraction patterns of (i) Pure TiO₂, (ii) A2, (iii) B2 (iv) C3 sintered at 1500°C for 3 h.

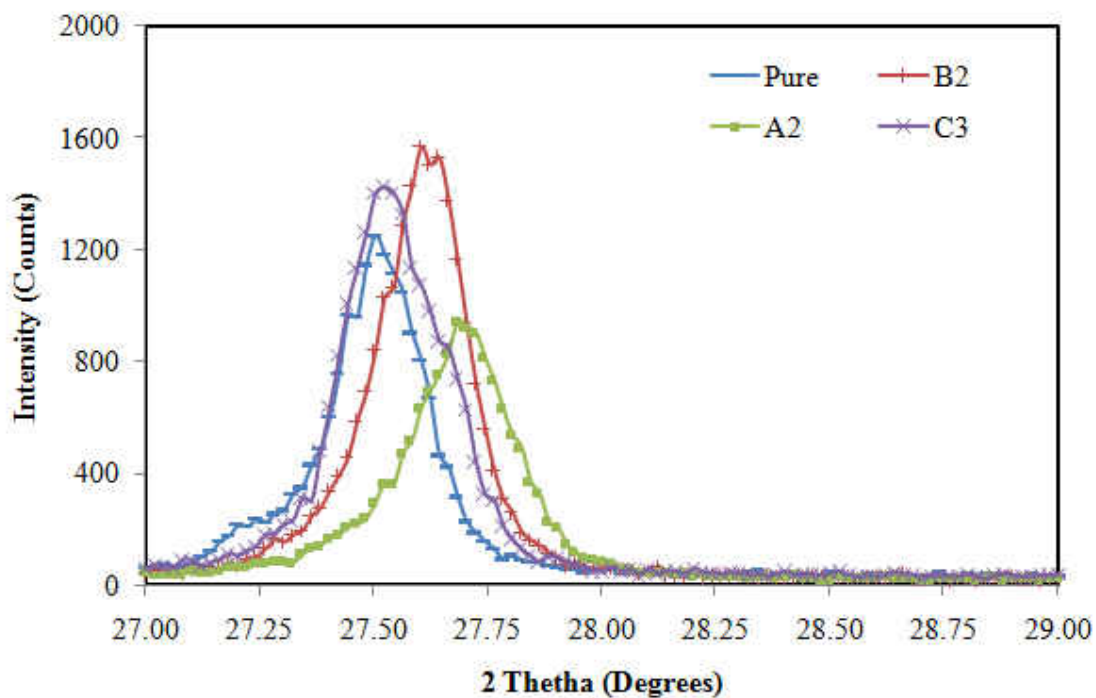


Figure 23: XRD patterns of titania showing peak shifts due to dopant addition.

Figure 23 shows the shift in the diffraction patterns of doped titania structures. It is seen that the addition of dopants created lattice distortions in titania lattice, which led to the shift of the peaks to the right side. The titanium atoms possess atomic radii of 2 Å. The peak shift was maximum in case of magnesium doped structures, as magnesium atoms possess higher atomic radius (1.72 Å). Hence, the lattice strains were more leading to the higher peak shift towards the right. In case of ZnO addition, there was a slight shift too, but this was not as high as in MgO addition. The zinc atoms possess an atomic radii of 1.53 Å, which is smaller than the size of the magnesium atoms. Hence the lattice strains were comparatively smaller, thus the peak shift was minimum. However, in case of SiO₂ addition, the lattice distortion was the least owing to the smaller size of silicon atoms (1.46 Å) in comparison to titanium atoms. Therefore, the peak shift in this case was the least due to lower strains in the lattice.

4.4 Microstructural analysis

4.4.1 Metal-ion doped titania structures

SEM was used to study, compare and analyze the effect of sintering additives on microstructure and mechanical properties of titania ceramics. Initially, all the structures sintered using Cycle A were analyzed. SEM micrographs of pure, A2, B2 and C3 structures are shown in Figure 24 a, b, c, d, respectively. In all micrographs, the grain boundaries are clearly visible confirming the crystallinity of the ceramics. The micrographs also showed no secondary phase or precipitate formation at the grain boundaries, which also correlates well with the XRD results, where no secondary phases were recorded in the diffraction patterns. It is clear that there was considerable grain growth with the increase in sintering temperature. The grain size was determined by linear intercept method.

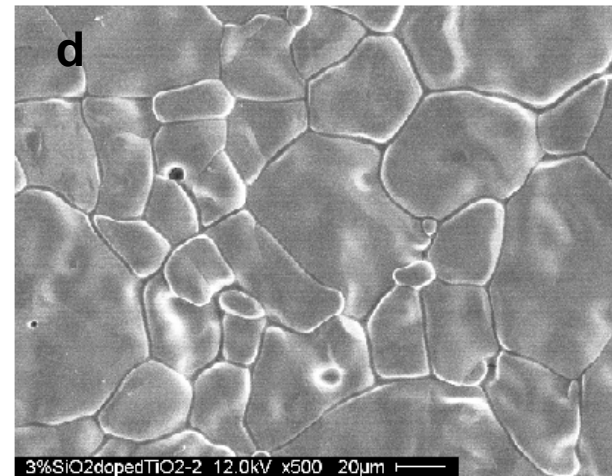
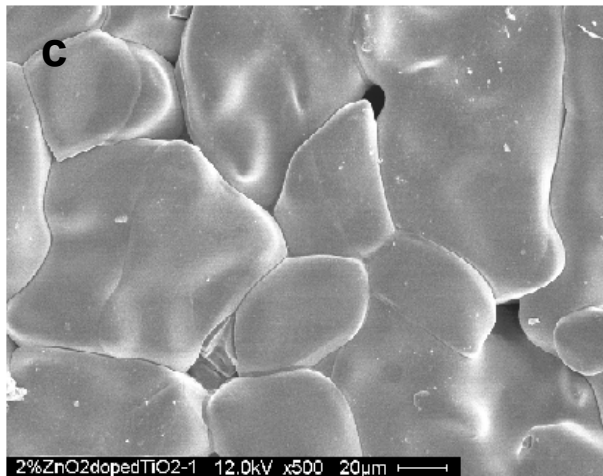
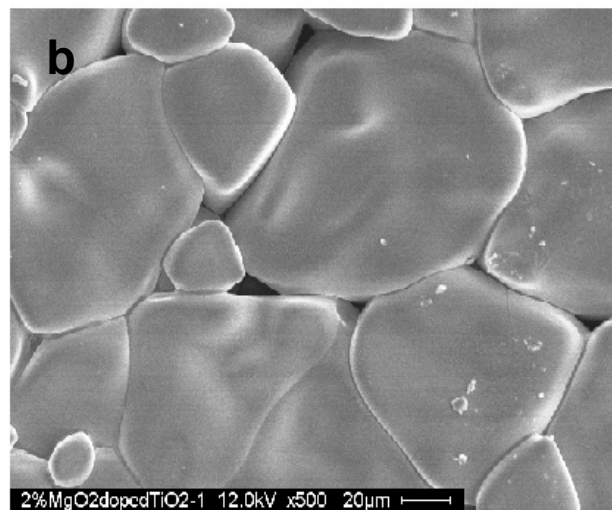
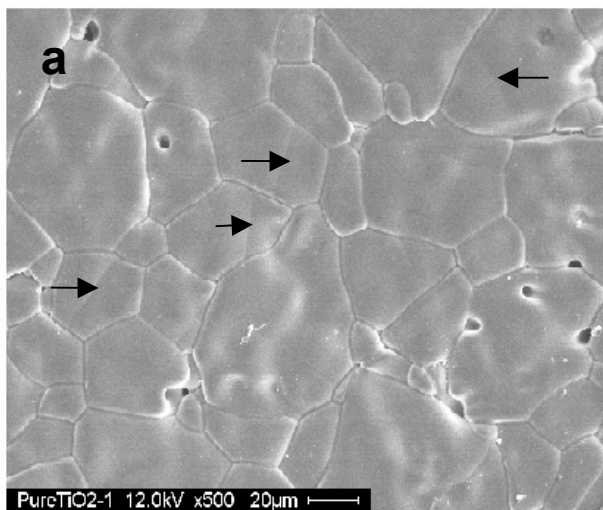
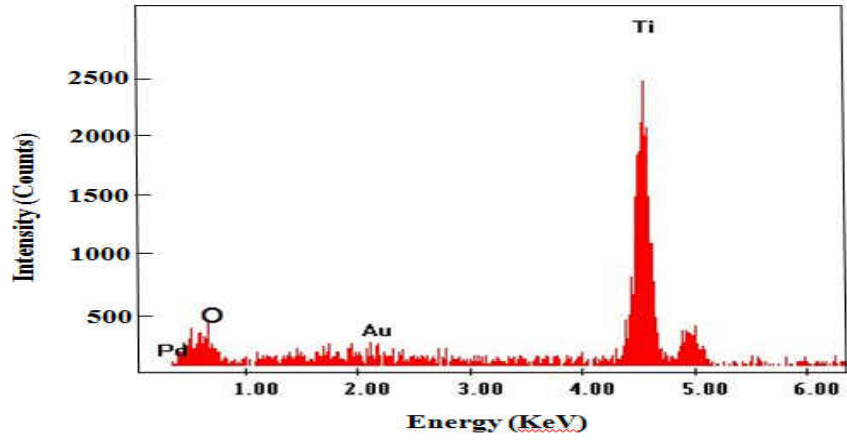


Figure 24: EDS spectrum and SEM micrographs of TiO₂ ceramics sintered at 1500°C for 3 h (Cycle A). **a** - Pure TiO₂, **b** - A2, **c** - B2, **d** - C3. Microcracks are shown by arrows.

It was found that for pure TiO₂ structures, average grain size of 24.4 μm was recorded. In case of A2 and B2 structures the maximum average grain size of 52.4 μm and 43.5 μm were recorded. For C3 structures there was limited grain growth and average grain size of 27 μm was recorded. The SEM results showed that the grain size of the sintered ceramics increased with the increase in presence of sintering additives. Also, it is clear from the micrographs that the pure TiO₂ structures had surface porosity, which contributed to poor densification during sintering. Also, the presence of micro cracks along the grain (Figure 24 a), led to a decrease in densification. Compositions pure TiO₂ and C3 showed very small difference in their grain sizes when sintered using this cycle. On the contrary, the compositions A2 and B2, had higher grain sizes, but still possessed improved sintered density; this is possibly because the sintering additive present in the structure possibly improved the grain boundary properties thereby improving the sintered density. For these structures, grain boundary networking formed are continuous. The porosity in sintered structures was also evaluated using Eq. (3). From the calculations, percentage of porosity was found out to be about 9% (± 0.19), for pure TiO₂ structures. Whereas, for compositions A2, B2 and C3, calculated value of porosity was about 8 vol%.

The compositions pure, A2, B2, C3 sintered using Cycle B were also observed using SEM. Microstructures of this sintering cycle are shown in Figure 25 a, b, c, d. Since sintering temperature was lesser in this cycle, grain growth was also less. The micrographs show that there is a clear distinction between the grain boundaries and the grains hence, linear intercept method can be conveniently applied to calculate the grain diameter. It was found that in case of pure TiO₂ structures average grain size of 7.8 μm was recorded. Even for the structures sintered using Cycle B, there was an increase in grain size for all the structures. For compositions A2 and C3, average grain size of 10 μm and 9.25 μm was recorded. In case of B2 structures, the grain

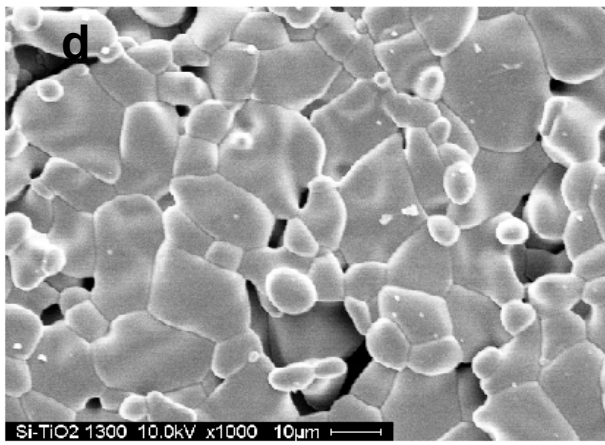
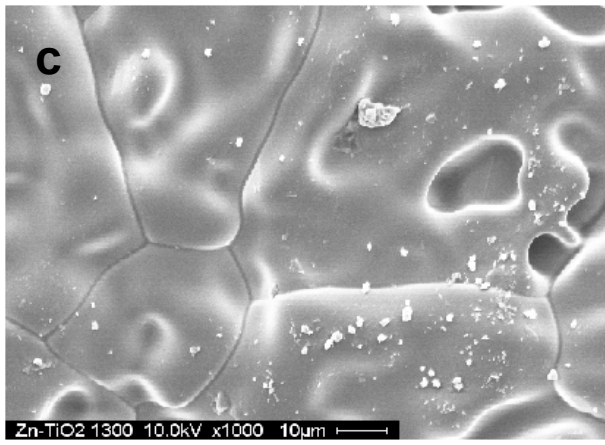
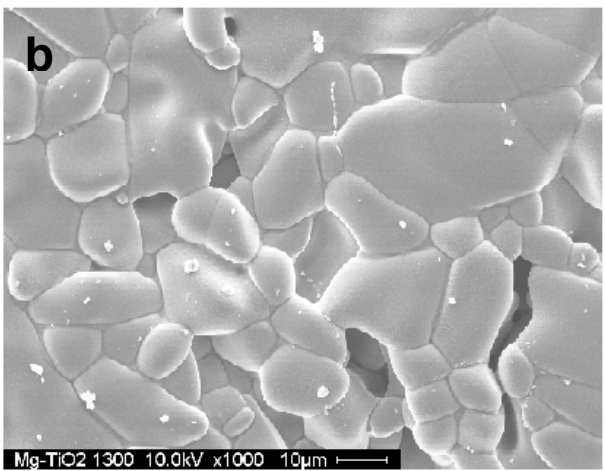
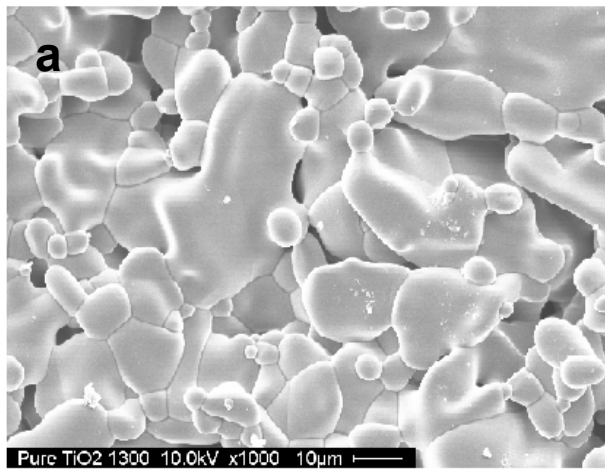
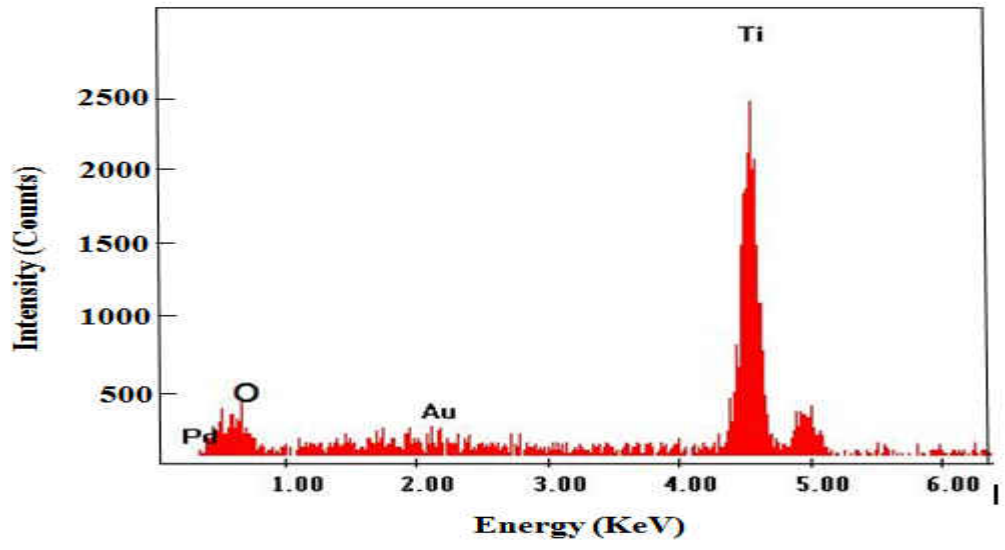


Figure 25: EDS Spectrum and SEM micrographs of TiO₂ ceramics sintered at 1500°C for 0.5 h and hold at 1300°C for 3 h. a- Pure TiO₂, b- A2, c- B2, d- C3.

growth was significant; the average grain size was calculated to be 38.9 μm . For B2 structures even though the grain size was large, the calculated bulk porosity was much lesser than the pure TiO_2 structures, which contributes to its increased sintered density. It is also believed that presence of the additive possibly improved the grain boundary properties of TiO_2 thereby improving its sintered density. All structures sintered using this cycle had higher porosity with interconnected pores.

The EDS spectrum was taken at the entire area on each SEM micrograph. Spectrums were taken on each of the micrographs shown in Figures 24 and 25. One such spectrum is shown in the figures. The spectrum showed the presence of titanium and oxygen. However, the presence of dopants could not be found from the EDS maps. This is probably because of the low concentration of these metal oxides. The collection time for each spectrum was one minute.

4.4.2 Phase-pure porous scaffolds

SEM was used to study the effects of pore-formers on the microstructural features of all the sintered structures. Only the structures sintered at 1500°C for 3 h were analyzed for the microstructures. The micrographs at a very low magnification are shown in Figure 26. It can be observed that the surface porosity of the structures increased with the increase in quantity of pore-former added. Micrographs at a still higher magnification are shown in Figure 27. The grain size in all the cases was calculated using the linear intercept method. The calculated grain size of all the porous structures is given in Table 8. From the micrographs it is also evident that addition of pore-former inhibited the grain growth in TiO_2 ceramics. It was observed that the grain size was reduced to one-half times with the addition of 25 % PEG to pure TiO_2 . From the micrographs of porous structures, it can be noted that grain boundary is less distinct and all the

pores formed are interconnected. The overall pore diameter varied from 50 μ m to 200 μ m for all porous structures.

Table 8 : Grain size analysis of pure titania and porous scaffolds

Composition	Grain size (microns)
Pure TiO₂	24.71
P5	18.53
P10	15.88
P15	15.22
P20	14.39
P25	11.90

The microstructures of the phase-pure porous scaffolds are shown in Figures 26 and 27. Figure 26 represents low magnification micrographs, whereas Figure 27 show the microstructures at a still higher magnification.

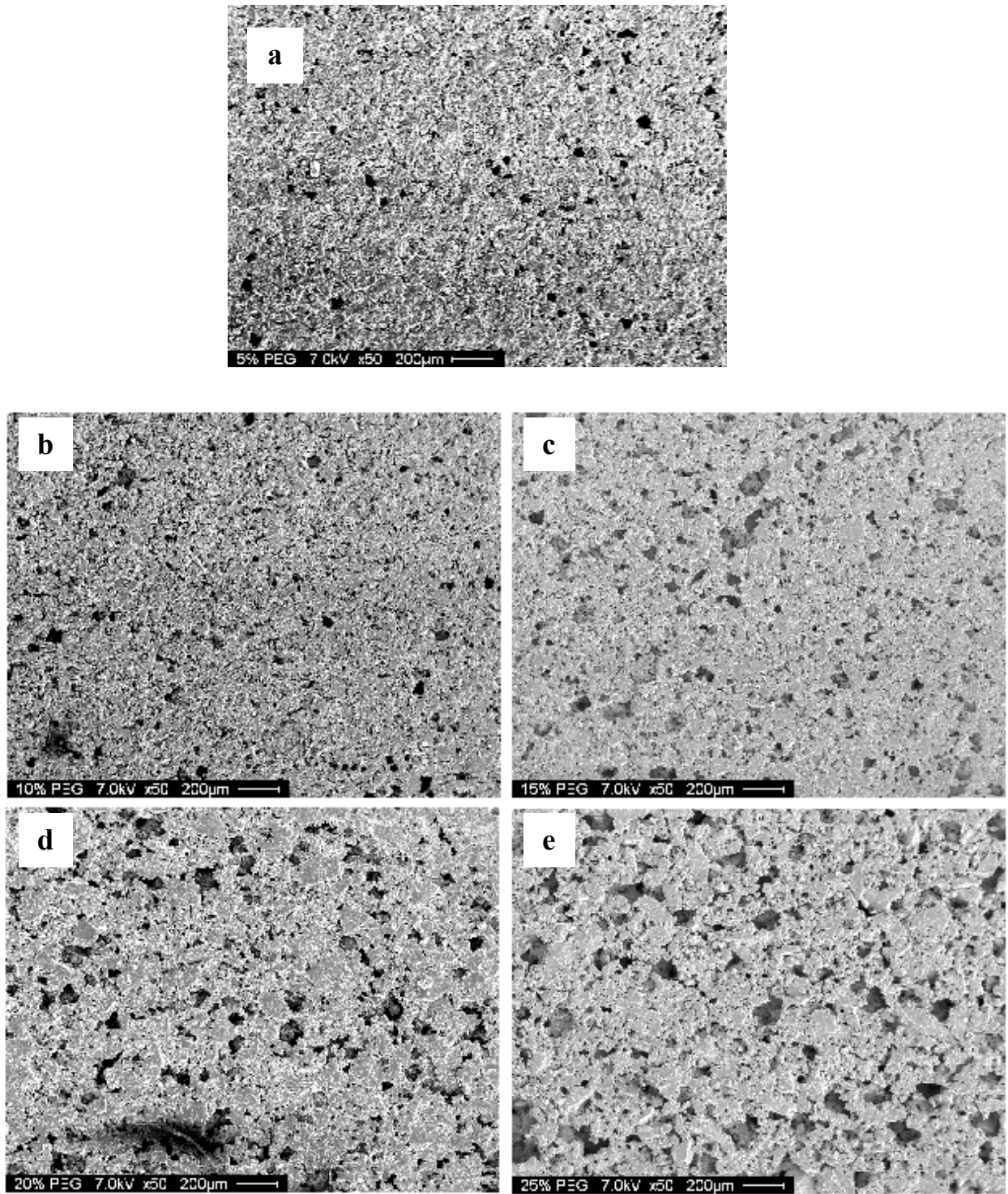


Figure 26: SEM micrographs of porous scaffolds sintered at 1500°C for 3 h. **a** – P5, **b** – P10, **c** – P15, **d** – P20, **e** – P25.

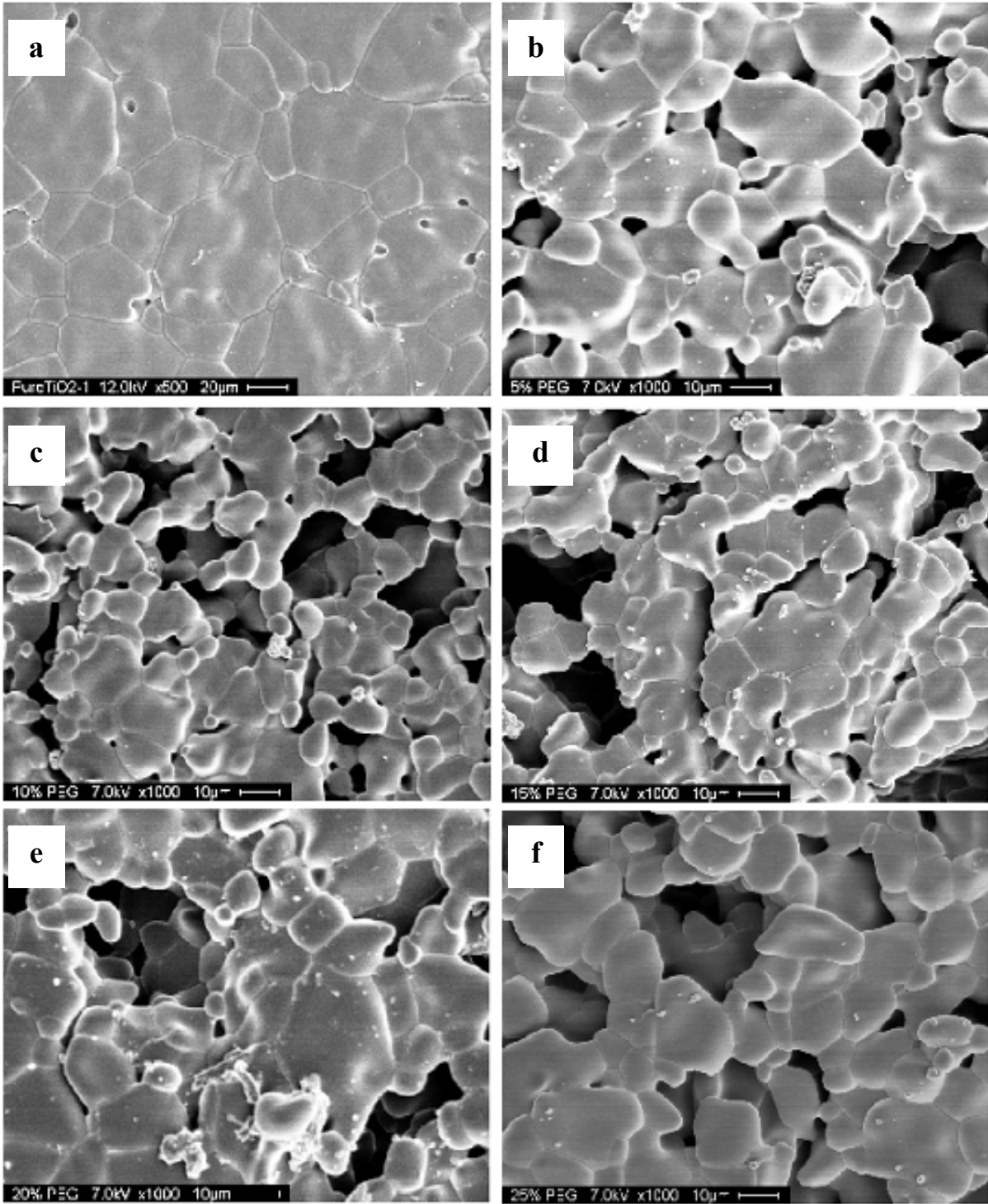


Figure 27: SEM micrographs of porous scaffolds sintered at 1500°C for 3 h. **a** – Pure TiO₂, **b** – P5, **c** – P10, **d** – P15, **e** – P20, **f** – P25.

4.5 Mechanical Characterization

4.5.1 Vickers hardness testing

4.5.1.1 Metal-ion doped titania structures

Results of Vickers hardness testing revealed that the surface hardness of TiO₂ ceramics increased with the presence of these sintering additives. Hardness testing was done on all the structures sintered using both the cycles. Figure 28 presents the average hardness as a function of composition, sintered using cycle A. It can be observed that presence of sintering additives enhanced the surface hardness of all the TiO₂ structures. Pure TiO₂ structures, showed a hardness of 449.0(± 8.9) HV, whereas composition B2 showed the highest hardness (501.0±9.3 HV). For MgO and SiO₂ additions, compositions A2 and C3 showed the best hardness of 495.1(±3.9) HV and 500.4(±7.5) HV, respectively. Minimum hardness of 452.7±(8.2) HV was recorded in composition C1. Overall, there was 12%, 11% and 8% increase in hardness for compositions B2, C3 and A2 respectively when compared to the pure TiO₂ structures. The presence of additives possibly improved the grain boundary properties of TiO₂ thereby improving the hardness of all the structures. The hardness could also be related to sintered density. It was found that hardness increased with the increase in sintered density. The structures (A2, B2, C3) for which highest sintered density was recorded, the hardness was also recorded to be high. For these structures, grain boundary networking formed was continuous. As seen from Figures 24 b & d, grain boundaries are distinct and each grain is clearly visible, hence these structures possessed better mechanical properties in terms of hardness.

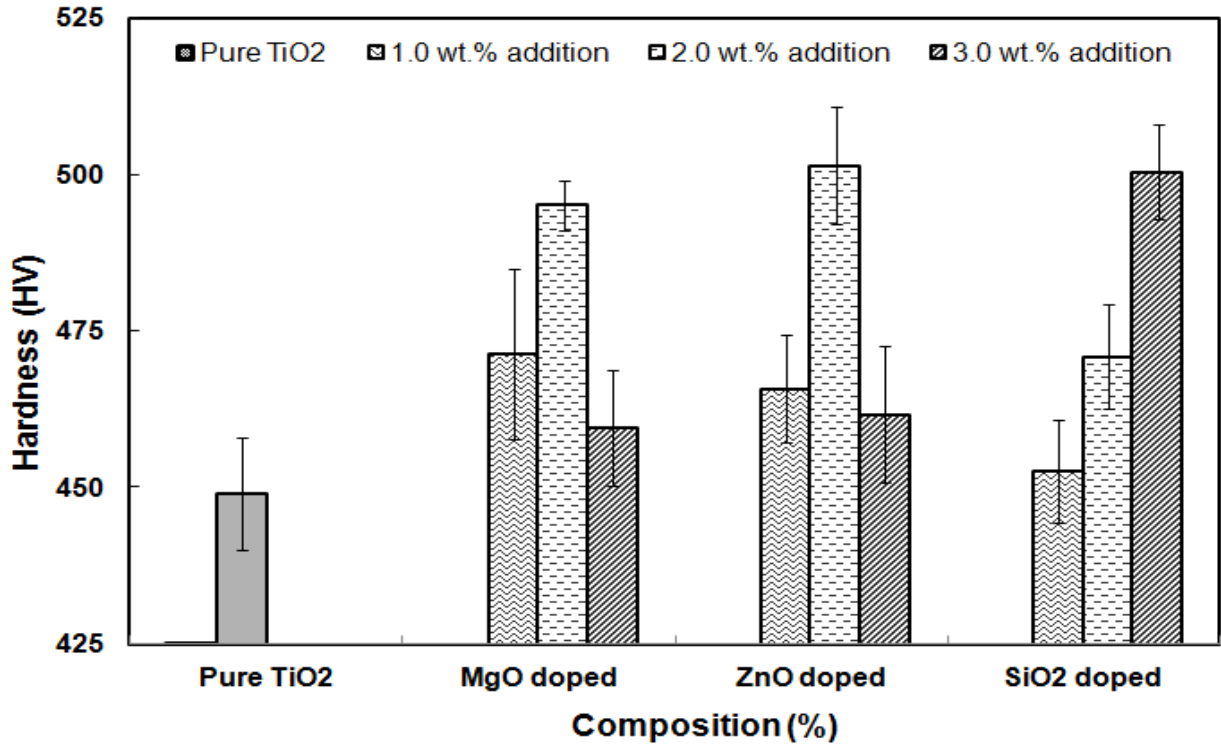


Figure 28: Effects of doping on hardness of TiO₂ structures sintered using Cycle A

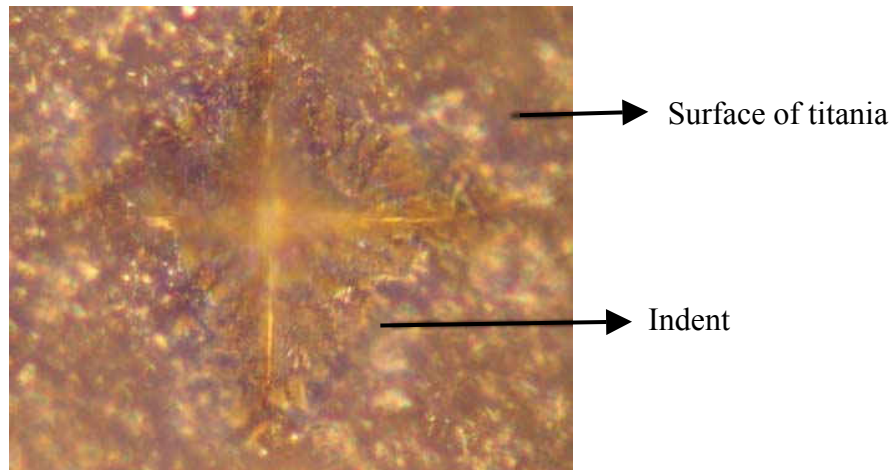


Figure 29: Indent on the surface of titania captured from the Vickers hardness tester

For sintering Cycle A, compositions A2, B2 and C3 showed significantly improved hardness. Accordingly, these compositions were selected to study the influence of sintering parameters using Cycle B. The sintered specimens were measured for their hardness, as well. It was observed that hardness is also dependent on sintering temperature. The structures sintered at higher temperature (Cycle A) had better hardness compared to structures sintered at lower temperature (Cycle B). This is due to low porosity in the structures sintered at higher temperature. A comparison of their hardness values for both the sintering cycles is shown in Figure 30. For cycle B, Pure TiO₂ exhibited an average hardness of 435.8(±6.5) HV, whereas a maximum hardness of 492.3(±8.4) HV was recorded in composition B2. Overall, doped TiO₂ structures showed better hardness than the pure form. It is also worth noting that the doped structures sintered using Cycle B had better hardness values when compared to the pure TiO₂

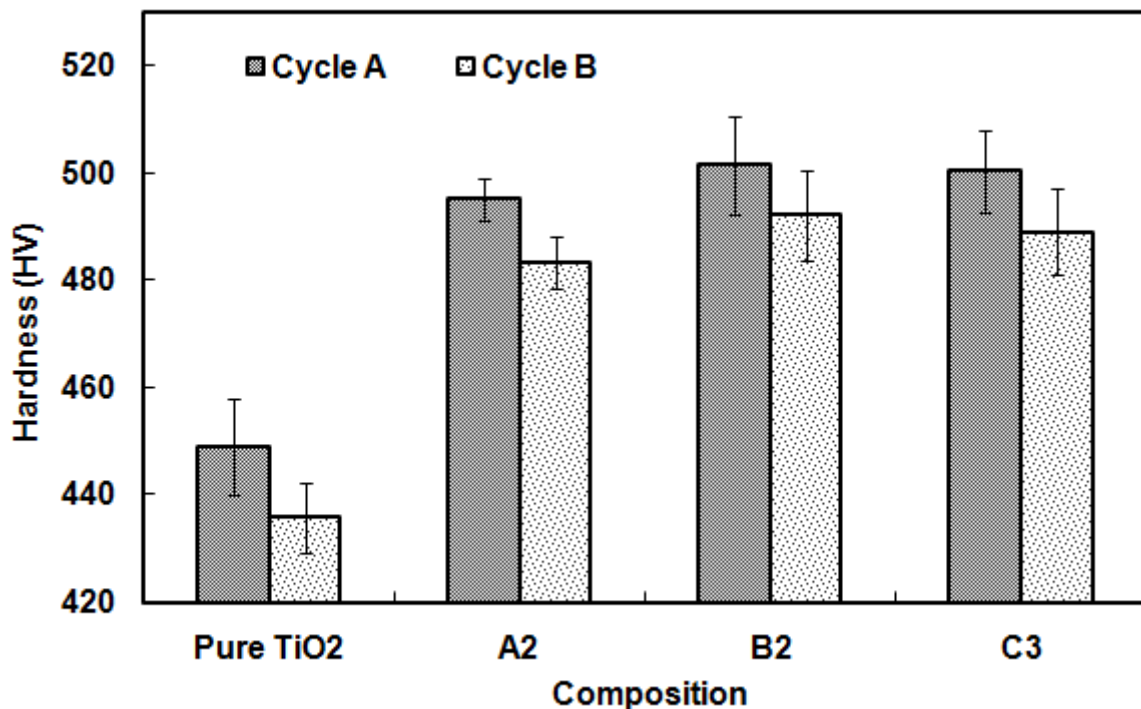


Figure 30: Effect of sintering parameters on hardness of pure and doped nanocrystalline titania. Cycle A represents sintering at 1500°C for 3 h. Cycle B represents sintering at 1500°C for 0.5 h and 1300°C for 3 h.

structures sintered using Cycle A. I believe that the grain boundary properties of TiO₂ was enhanced in presence of these additives thereby improving its hardness. The change in hardness with sintering temperature can also be explained with the help of SEM micrographs. Figure 25a shows that even though the grains are smaller and visible, the grain boundary is less distinct; hence these structures possessed poor hardness when compared to the structures sintered using Cycle A. Also, the increased surface porosity in these structures led to the decrease in hardness.

The variation of density with hardness is shown in Figure 31. It is evident from the plot that hardness increases with the increase in density. These results also conjugate with the porosity calculations.

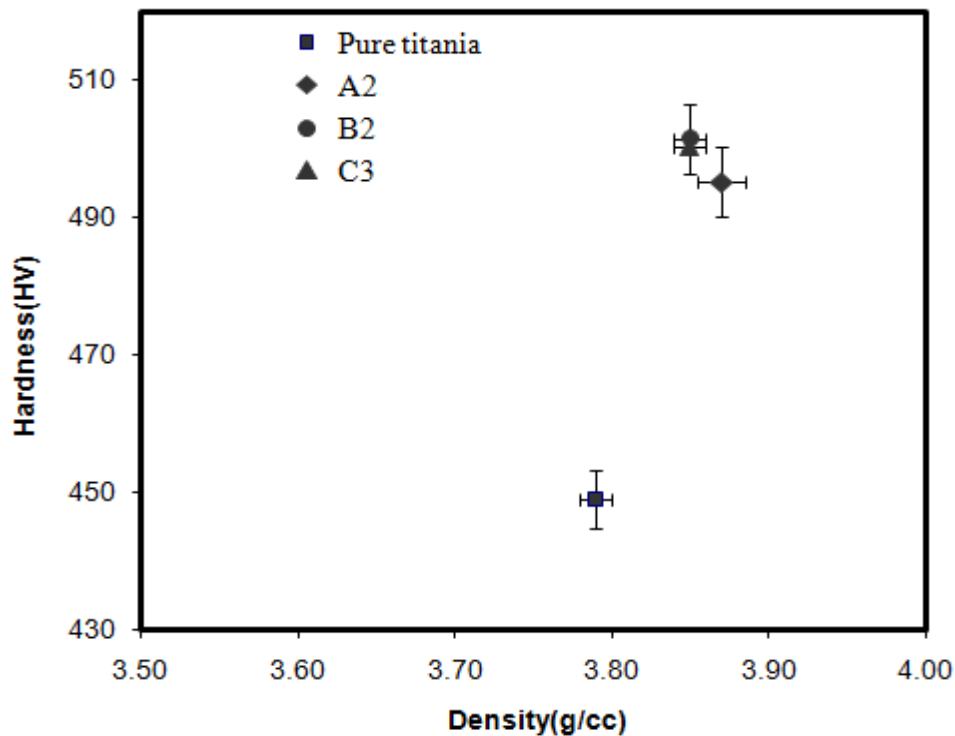


Figure 31 : Variation of hardness with density for all the sintered structures

4.5.1.2 Phase-pure porous scaffolds

Results of Vickers hardness test showed that presence of PEG decreased the surface hardness of TiO₂ structures. Hardness test was performed at five different locations on one sample corresponding to each composition and the average value was recorded. It was found that by increasing the quantity of pore-former, the hardness decreased. The average hardness of each of these composition types were calculated and plotted as a function of composition as shown in Figure 32 . A maximum hardness of 267.5(±3.46) HV was obtained for P5 sintered at 1500°C for 3 h and a minimum hardness of 122.9(±3.05) HV was obtained for P25 structures sintered at 1400°C for 3 h. The micrographs of the porous structures also indicate that the grain boundary is less distinct. Hence the hardness of the structures was also less when compared to the pure TiO₂ structures.

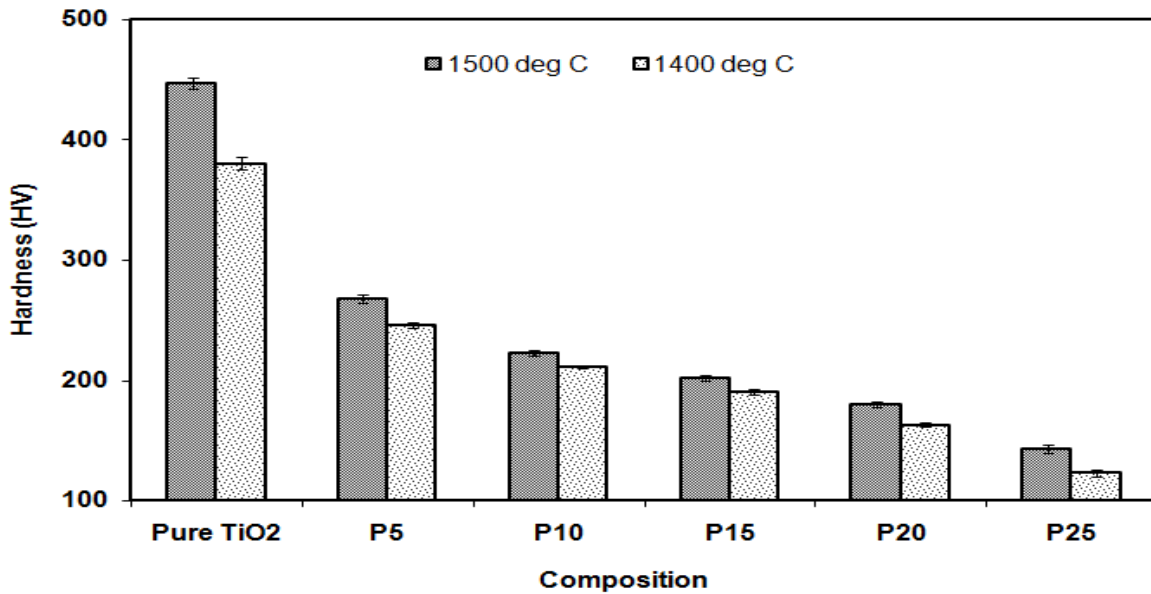


Figure 32: Variation in hardness of pure and porous scaffolds

The variation of hardness with density for all the phase-pure porous scaffolds is shown in Figure 33. It can be noted that hardness increases with an increase in the sintered density.

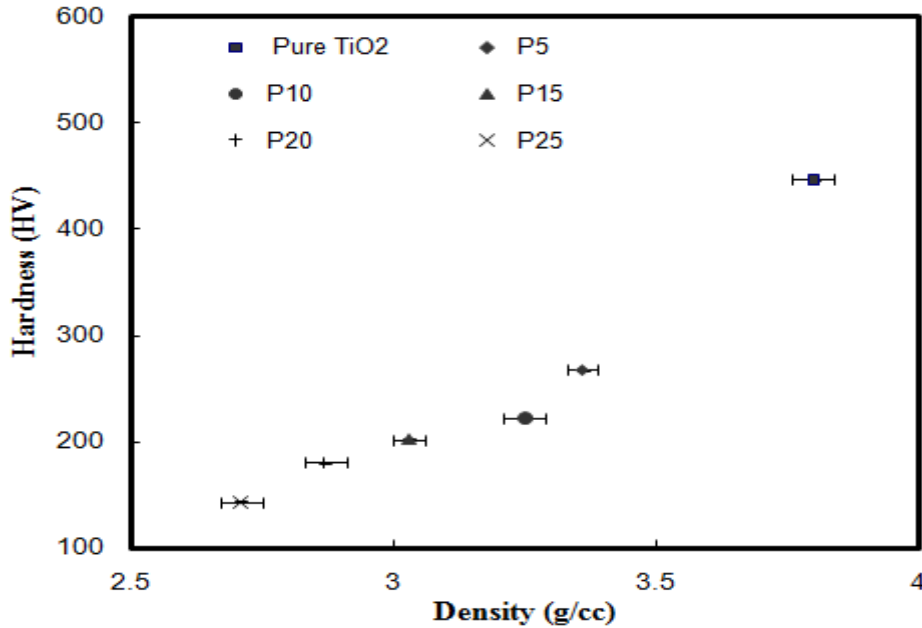


Figure 33 : Variation of hardness with sintered density for phase-pure porous scaffolds.

4.5.1.3 Metal-ion doped porous scaffolds

Results of Vickers hardness testing showed that addition of sintering additives led to an increase in the surface hardness of all the porous TiO₂ structures used in this study. The sintering was carried out at 1500°C for 3 h. The average hardness of all the structures was plotted as shown in Figure 34. Among the doped porous structures, A10 structures recorded the maximum hardness of 289.5(±2.3) HV, which represents 30% increase in hardness over P10 structures (without sintering additive). The minimum hardness of 237.66(±4.5) HV was recorded for B15 structures, which represents 18% increase in hardness over P15 structures. The hardness results

conjugate well with the density calculations. The structures (A10) which recorded the highest hardness also recorded the highest sintered density. The structures (B15) which recorded the least hardness also recorded the least sintered density.

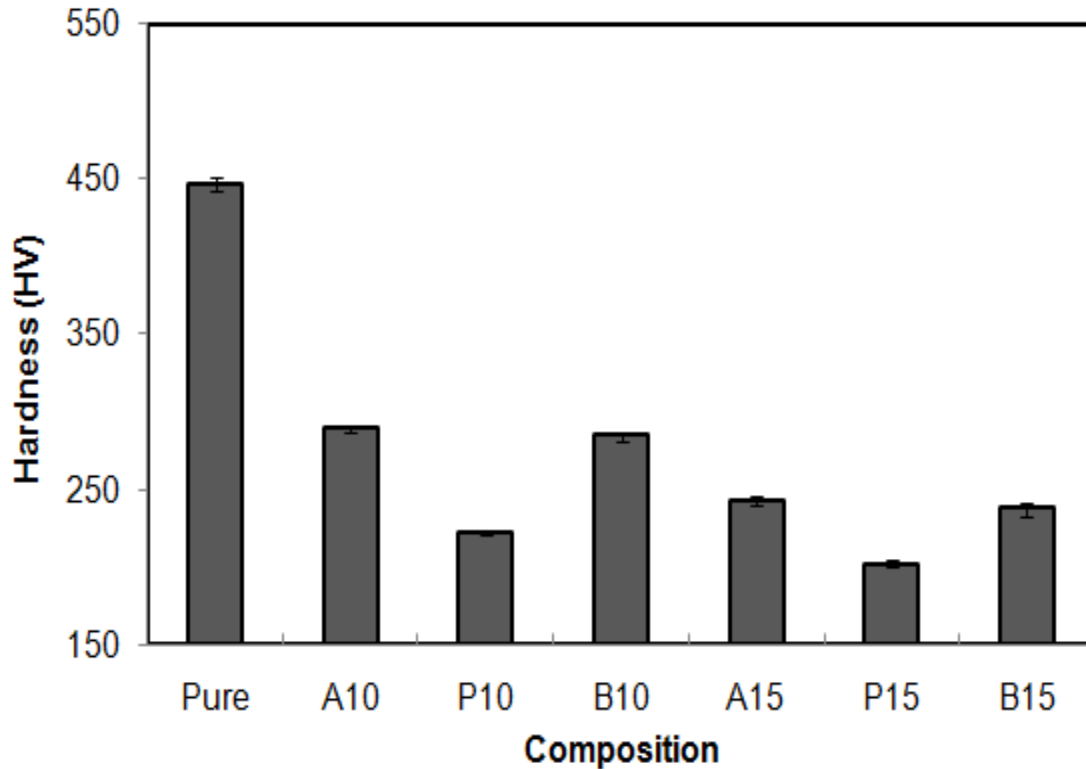


Figure 34: Variation of hardness with composition for pure, porous and porous scaffolds doped with sintering additives. (A – 2 wt% MgO, B – 2 wt% ZnO).

The variation of hardness with sintered density for all the metal-ion doped porous scaffolds is as shown in Figure 35. The hardness increases with the increase in the sintered density.

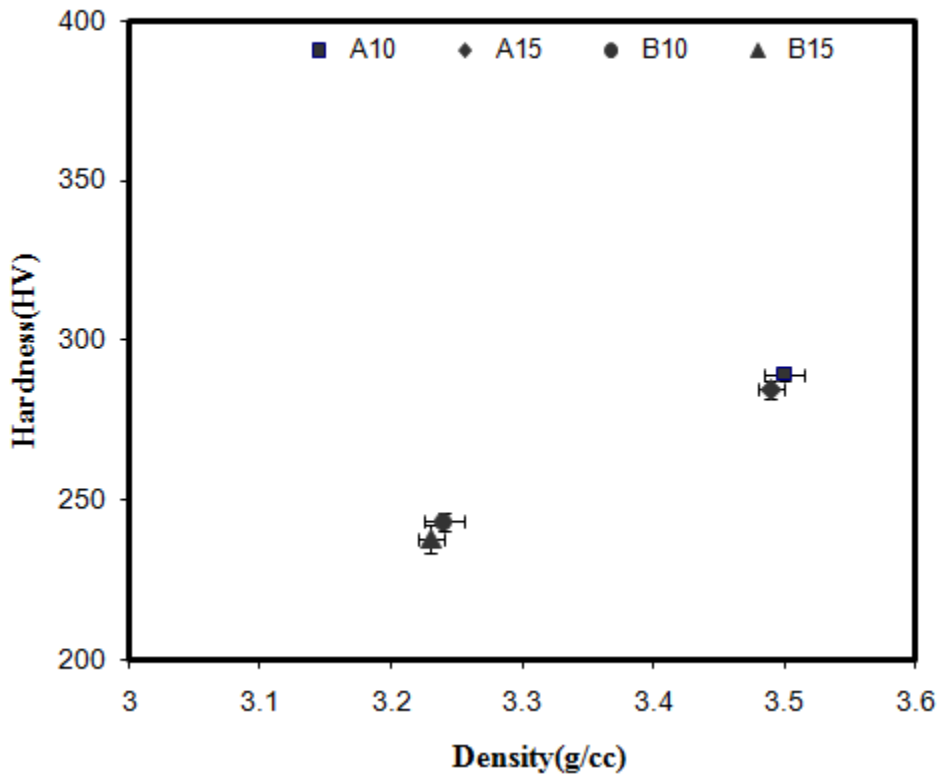


Figure 35: Variation of hardness with sintered density for metal-ion doped porous scaffolds.

4.5.2 Biaxial flexural testing

4.5.2.1 Metal-ion doped titania structures

Sintered TiO₂ structures of all compositions were subjected to biaxial flexural strength test. Structures 1.6 mm thick and 10.2 mm in diameter were used for the evaluation of biaxial flexural strength. The test was done on an Instron tensile tester. Initially the structures sintered using Cycle A were tested. Average biaxial flexural strengths of all the different compositions were evaluated and were compared to that of pure TiO₂ structures processed under same conditions. Pure TiO₂ structures recorded a biaxial flexural strength of 116.18(±1.30) MPa. The results are presented in Figure 36. It is also evident that the addition of dopants has a positive influence on biaxial flexural strength of TiO₂. In case of MgO and ZnO addition, biaxial flexural

strength increased with the increase in dopant addition till 2 wt%, after which the strength decreased, but in case of SiO₂ addition, the highest biaxial flexural strength of 136.7(±1.3) MPa was recorded for the 3 wt% addition (i.e. for composition C3). The compositions B2 and A2 showed biaxial strengths of 132.84 (±1.50) MPa and 124.64 (±1.35) MPa, respectively. Overall, there was 18% improvement for composition C3, 14% increase for the composition B2 and 7% increase for composition A2, in biaxial flexural strength when compared to the pure TiO₂ structures processed under same conditions. The results of hardness and biaxial flexural strength also conjugate well with our densification results. Though, doped structures possessed increased grain size, the mechanical properties of these compositions were superior to that of pure TiO₂ as we believe that additives possibly improved the grain boundary properties thereby providing improved sintered density and other mechanical properties. However, an in-depth understanding on how each additive influences TiO₂ may be possible through extensive TEM investigation of grain boundaries; which could not be accomplished in this work. Some variations in mechanical properties of TiO₂ ceramics doped with additives, can be better explained using the results from our SEM examination. As seen from Figure 24 b, d, grain boundaries are distinct and each grain is clearly visible, hence these structures possessed better mechanical properties in terms of hardness and biaxial flexural strength.

For sintering Cycle A, compositions A2, B2 and C3 showed significantly improved biaxial flexural strength. Accordingly, these compositions were selected to study the influence of sintering parameters using Cycle B. The biaxial strengths were low for structures sintered using Cycle B. Biaxial strengths of 102.19 (±1.31) MPa was recorded for pure TiO₂ structures.

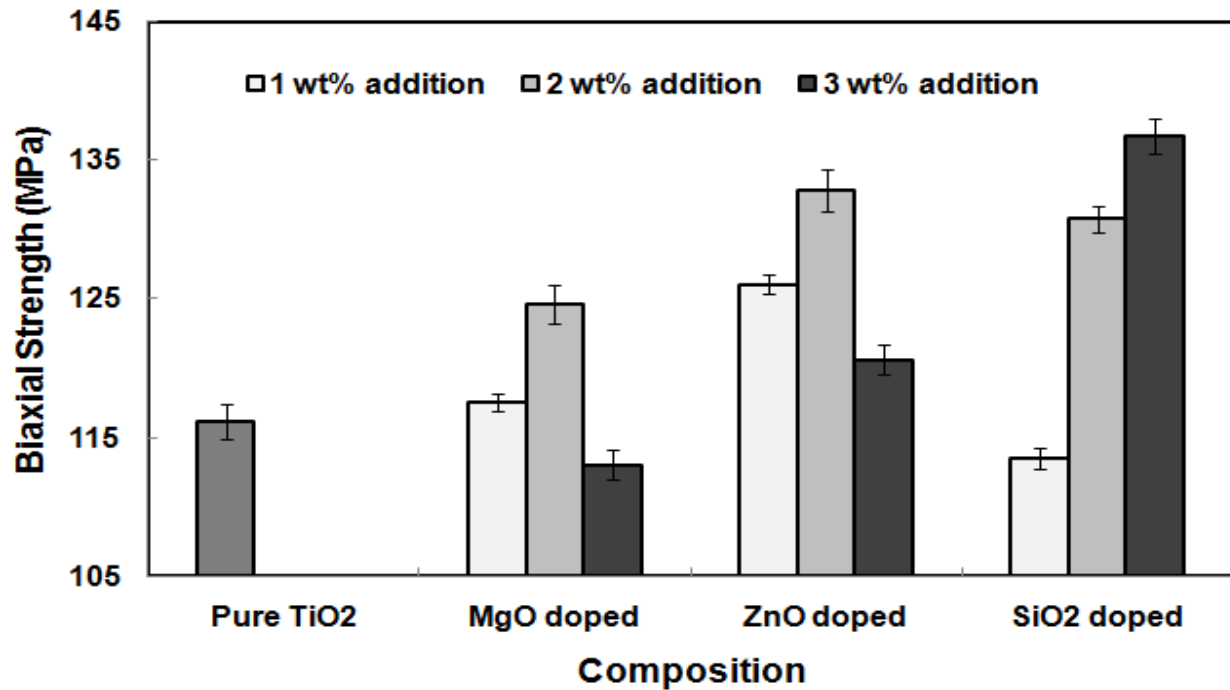


Figure 36: Effect of doping on biaxial flexural strength of nanocrystalline TiO₂ structures sintered using Cycle A.

The biaxial flexural strength also followed the same trend as that of hardness. The compositions A2, B2 and C3 possessed biaxial flexural strengths of 103.2 (± 0.66) MPa, 108.69 (± 1.35) MPa and 108.06 (± 1.07) MPa, respectively. Figure 37 shows the variation of biaxial flexural strength with composition. The results indicate that the sintering temperature has an effect on the biaxial flexural strength. The biaxial strength increases with increase in sintering temperature. It is also evident from the SEM micrographs that structures sintered using Cycle B had less distinct grain boundaries which led to the decrease in the biaxial flexural strength of these structures.

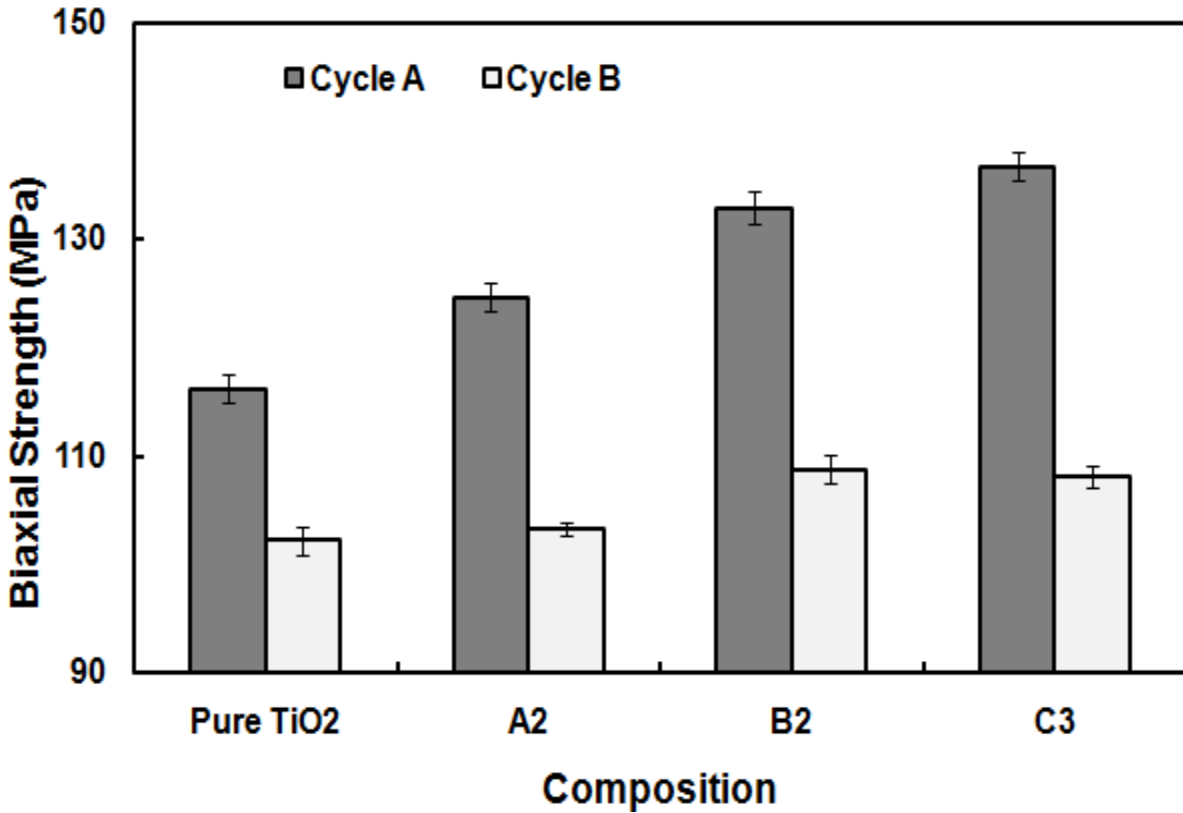


Figure 37: Effect of sintering parameters on biaxial flexural strength of pure and doped nanocrystalline titania. Cycle A represents sintering at 1500°C for 3 h and Cycle B represents sintering at 1500°C for 0.5 h and 1300°C for 3 h.

The variation of density with biaxial flexural strength is shown in Figure 38. The results show that the flexural strength increases with the increase in the sintered density for all the structures.

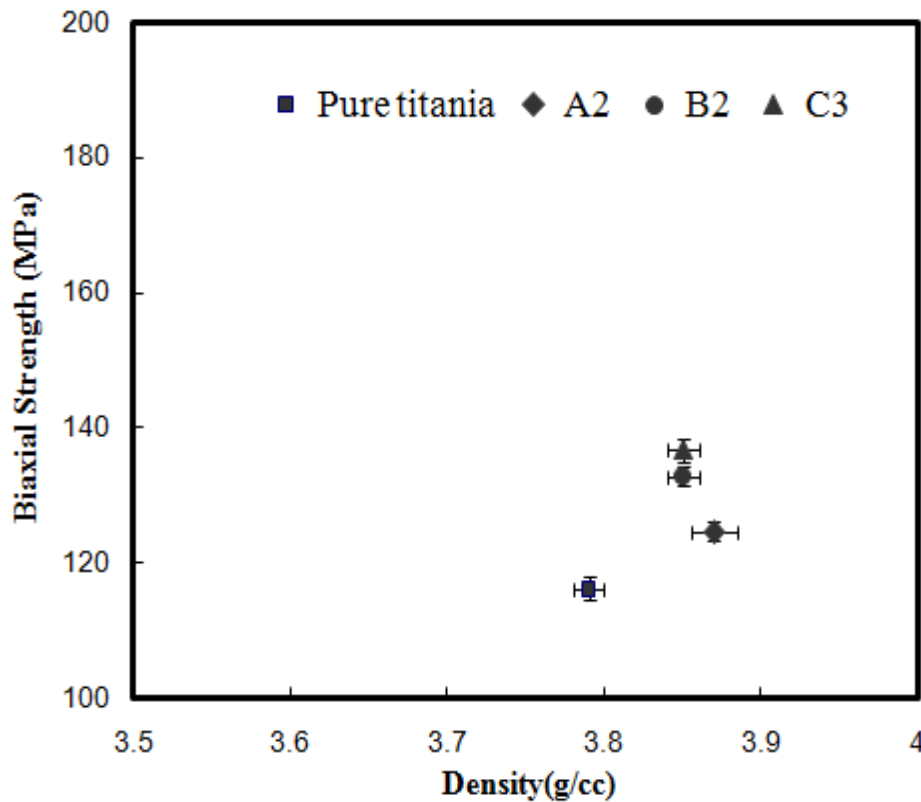


Figure 38 : Variation of density with biaxial strength for metal-ion doped structures.

From the results, it could be concluded that biaxial flexural strength can be increased by the addition of sintering additives, without sacrificing the phase purity of TiO_2 ceramics. This aspect could be useful to develop stronger materials for application in biomedical field. However, the use of high pressure processing routes such as cold and hot isostatic pressing, spark plasma sintering, etc yield still stronger structures with better mechanical properties.

4.5.2.2 Phase- pure porous scaffolds

Biaxial flexural testing was carried out on all the sintered porous structures. Sintered ceramic structures 1.6 mm thick and 9.8 mm in diameter were used for this test. Instron machine was used for testing the samples. The load at fracture was used to calculate the biaxial flexural strength. The results of the testing are as shown in Figure 39. Among the porous structures, the highest biaxial flexural strength of 114(\pm 5.8) MPa was recorded for P5 when sintering was carried out at 1500°C for 3 h. The minimum flexural strength of 62.27(\pm 2.08) MPa was recorded for P25 structures sintered at 1400°C. Both increase in amount of PEG and decrease in sintering temperature led to lower biaxial flexural strength. Increase in porosity also leads to decrease in biaxial flexural strength.

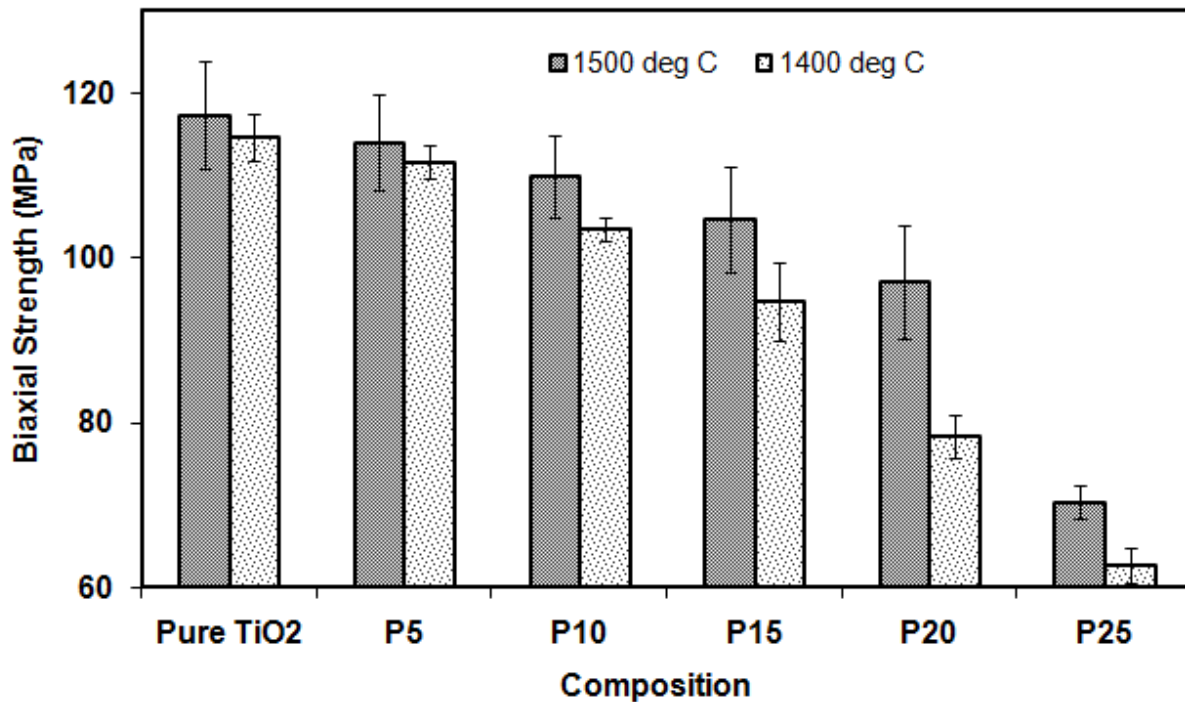


Figure 39: Variation of biaxial flexural strength for the pure and porous scaffolds

The variation of biaxial flexural strength with sintered density is as shown in Figure 40.

The flexural strength increases with the increase in the sintered density.

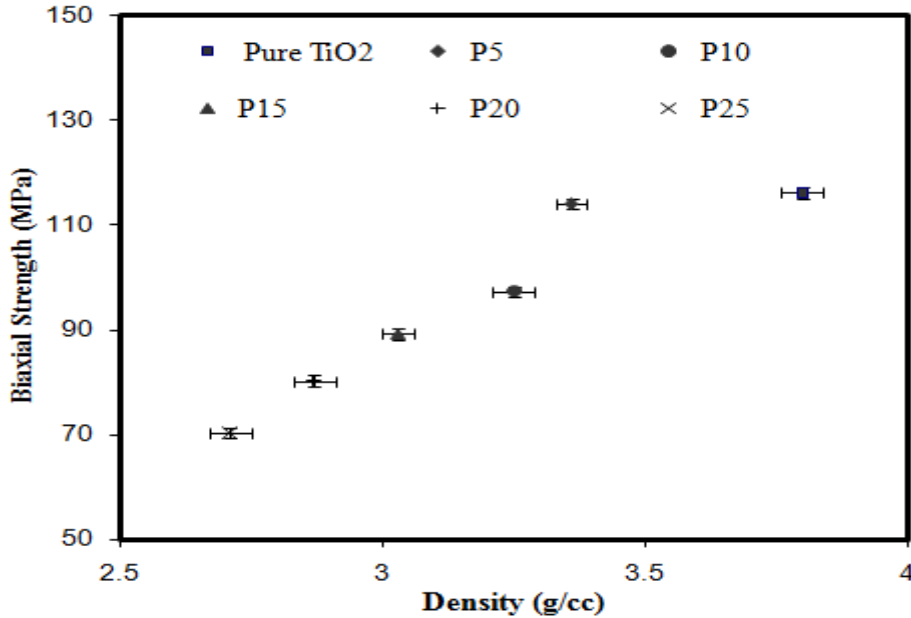


Figure 40: Variation of biaxial flexural with sintered density for phase-pure porous scaffolds

4.5.2.3 Metal-ion doped porous scaffolds

Biaxial flexural testing was done on all the doped porous structures sintered at 1500°C for 3 h. The average biaxial flexural strength was plotted as shown in Figure 41. Among all the doped porous structures the highest strength of 113.97 (± 2.8) MPa was shown for A10 structures, which represents 17% improvement over the composition P10 processed under same conditions. The minimum biaxial strength of 97.05 (± 2.8) MPa was shown for B15 structures. Overall the doped porous structures showed better mechanical strength when compared to undoped porous structures. The results are also in par with the densification and hardness values,

wherein highest density and hardness was recorded for A10 structures. The flexural strength decreased with an increase in the porosity of the samples.

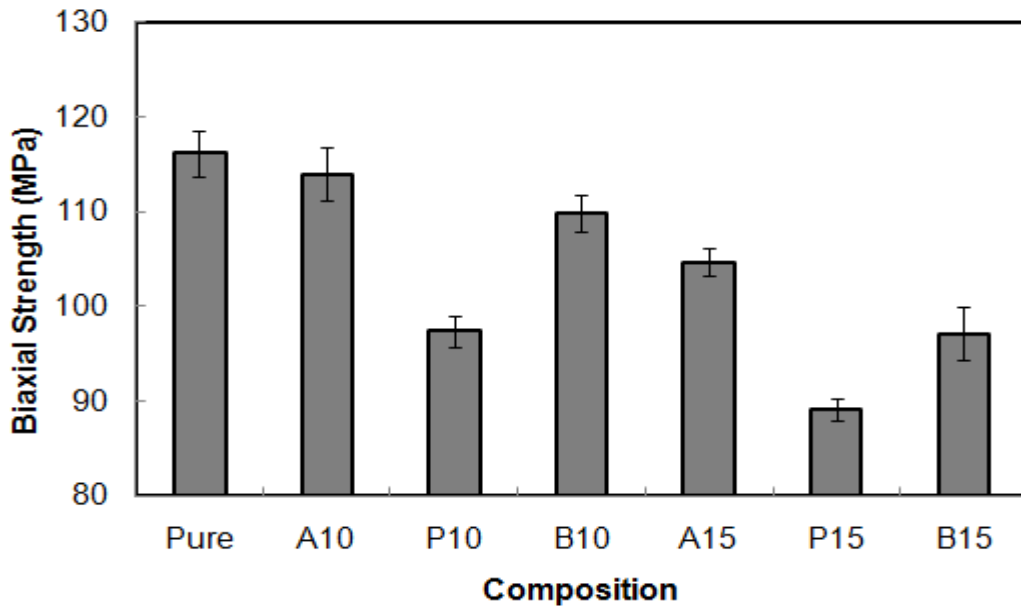


Figure 41: Variation of biaxial flexural strength with composition for pure, porous and porous scaffolds doped with sintering additives. (A – 2 wt% MgO, B – 2 wt% ZnO).

The variation of biaxial flexural strength for all the metal-ion doped porous scaffolds with sintered density is as shown in Figure 42. It is seen that the flexural strength increases with the addition of MgO and ZnO as dopants.

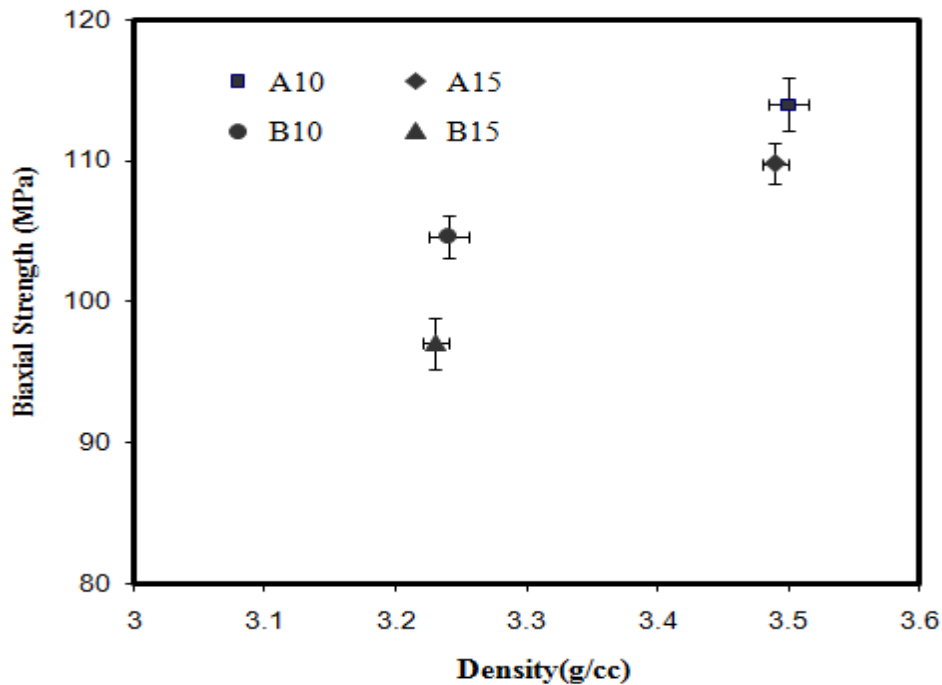


Figure 42: Variation of biaxial strength with sintered density for all metal-ion doped porous scaffolds.

Overall metal-ion doped porous structures were better as their hardness and biaxial flexural strengths were higher than the phase-pure porous structures.

The properties of MgO doped structures were superior as MgO:

- Lowers the grain boundary anisotropy and mobility.
- Increases surface diffusivity and pore mobility.
- Promotes lattice and grain boundary diffusions.
- Decrease the surface energy of the grains.

However, on further increasing the doping above 3 wt.% decrease the properties of the sintered structures as more intergranular pores and more transgranular fractured grains of titania were observed in the microstructures.

From the phase diagram of MgO—TiO₂ system it is evident that for 2 wt.% MgO at 1500°C there exists no solubility between MgO and TiO₂, hence no solid solution is formed. The eutectic reaction can be seen only at temperatures close to 1600°C where a series of eutectic compounds are formed at 7 wt.% MgO, 28 wt.% MgO and 39 wt.% MgO respectively. This is in correspondence with the SEM and XRD results, which did not show any phase impurities.

The phase diagram of ZnO – TiO₂ phase diagram shows a eutectic reaction occurring at 1418 °C leading to the formation of Zn₂TiO₄ at eutectic composition ~58 wt.% ZnO. The glassy brittle phase observed in the microstructures of ZnO doped titania ceramics has possibly formed as the sintering temperature exceeded the eutectic temperature.

SiO₂—TiO₂ phase diagram also shows complete insolubility between both the phases at temperatures below 1500°C. However, for higher weight percentages of SiO₂ (~82 wt.%), eutectic reaction is seen to occur. This is also in correspondence with the SEM and XRD results, where no brittle phases or impurities were present in the corresponding microstructures or diffraction patterns.

4.6 Biodegradation Studies

4.6.1 Metal-ion doped titania structures

Biodegradation study conducted in SBF, maintained at a constant temperature of 36.5°C, showed that the dopants or additives used altered or changed the rate of degradation (weight-loss) of TiO₂ ceramics. Pure, A2, B2 and C3 titania structures sintered using Cycle A were used for this study as these structures possessed better properties over the others. The results showed that for A2 structures, the percentage of weight-loss was 3.6% at the end of two weeks and 9.2% at the end of six weeks. Whereas in case of pure TiO₂ structures sintered under same conditions, weight loss was 5.0% at the end of two weeks and 11.2% at the end of six weeks. The composition A2 exhibited minimal weight-loss or degradation by the end of six weeks.

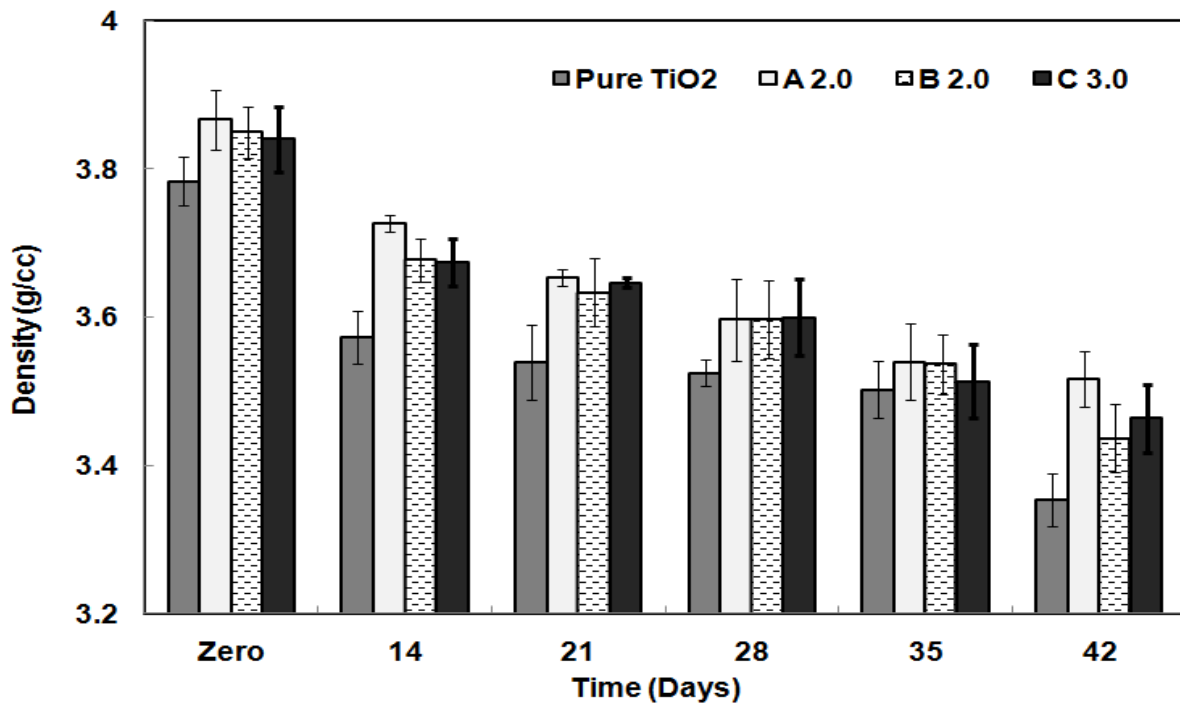


Figure 43: Variation in the density of the TiO₂ structures placed in SBF with time.

The decrease in density of sintered structures with time may be due to decrease in mass of the structures due to dissolution in SBF. Hence, the results indicate that rates of biodegradation are different for pure and doped TiO₂ structures. Figure 43 shows the change in density of the samples with time.

The influence of sintering additives on the biomechanical degradation of TiO₂ ceramics was studied. The surface hardness of the various compositions was measured. Figure 44 shows the change in hardness with time progression. It was noted that surface hardness of all structures degraded as time progressed. Pure TiO₂ showed a hardness of 449 HV at the beginning and showed a hardness of 202 HV at the end of the study. The lowest rate of degradation was seen in case of A2 structures, wherein a hardness of 495HV was recorded initially and 304 HV was recorded at the end of the study. For other compositions, the degradation in hardness over the entire period of time was comparatively higher.

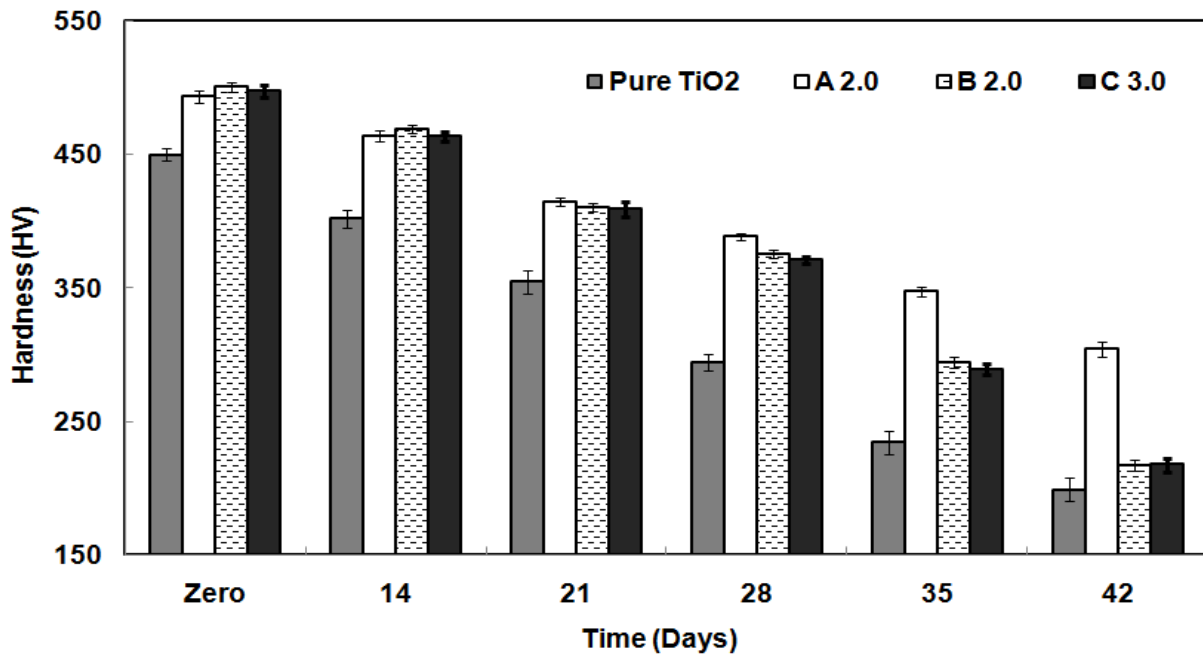


Figure 44: Variation in the hardness of the TiO₂ structures placed in SBF with time.

In the similar manner biaxial or flexural strength were evaluated for all the structures. Two to three specimens of each composition was tested for biaxial strength and the average value was evaluated. The variation of biaxial strength with time is shown in Figure 45. The results indicate that mechanical properties of sintered structures decreased as time progressed. Pure TiO₂ structures initially possessed a biaxial flexural strength of 116 MPa, but at the end of forty two days, biaxial flexural strength of 62.4 MPa was recorded. For the composition A2, biaxial flexural strength of 125 MPa was recorded initially and 100.2 MPa was recorded at the end of the experiment. Hence, the composition A2 degraded at a much lower rate when compared to all the other compositions used in this study.

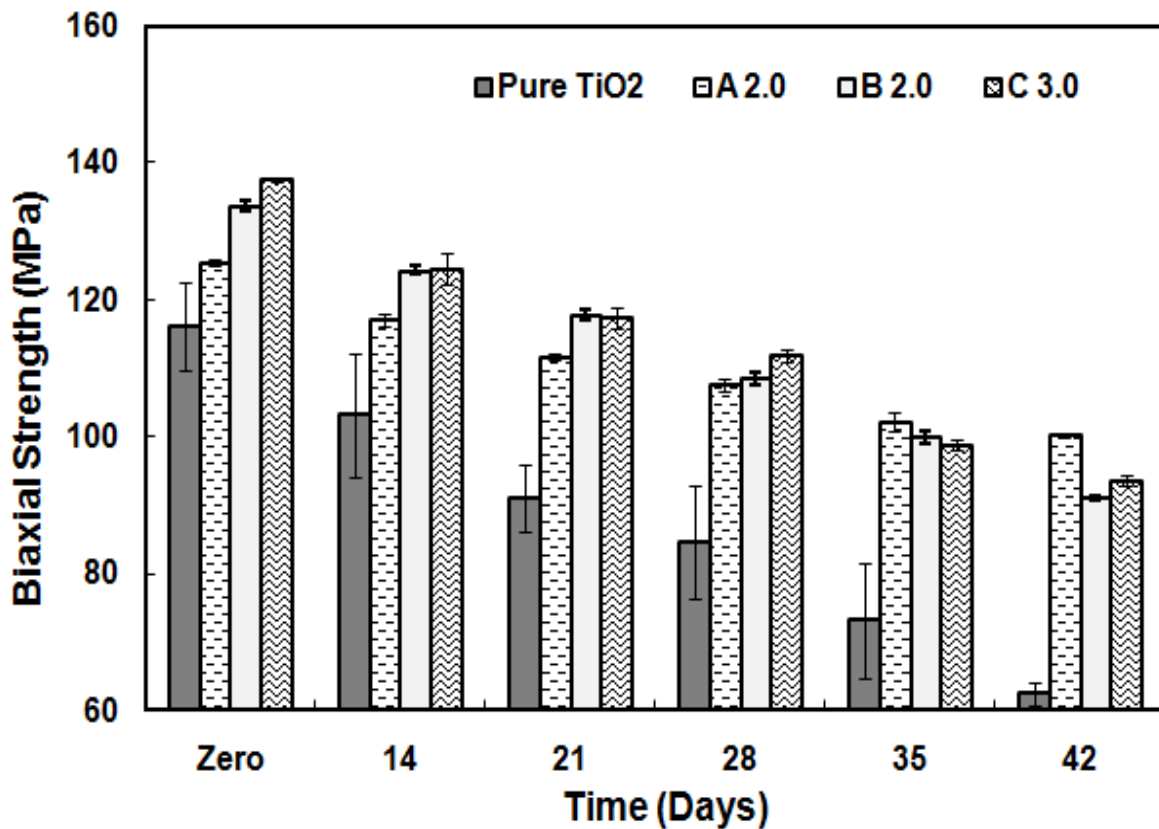


Figure 45: Variation in the biaxial flexural strength of the TiO₂ structures placed in SBF with time.

4.6.2 Phase-pure porous scaffolds

Biodegradation study of the porous TiO₂ samples were conducted in SBF, maintained at a constant temperature of 36.5°C. The porous structures P10, P15 and P20 were used for this study. It was seen that for the porous TiO₂ structures there was an increase in weight of the structures at the end of day 21 and day 42. The increase in the weight of the structures is due to the formation of apatite layer on the surface and sides of the structures. In case of pure TiO₂ structures, there was a decrease in the weight of the structures at the end of 42 days. This is possibly due to the degradation of the structures in SBF with time. The results state that resorption rates are vary for the different TiO₂ structures used in the study. The % change in weight of all the structures with time is shown in Figure 46.

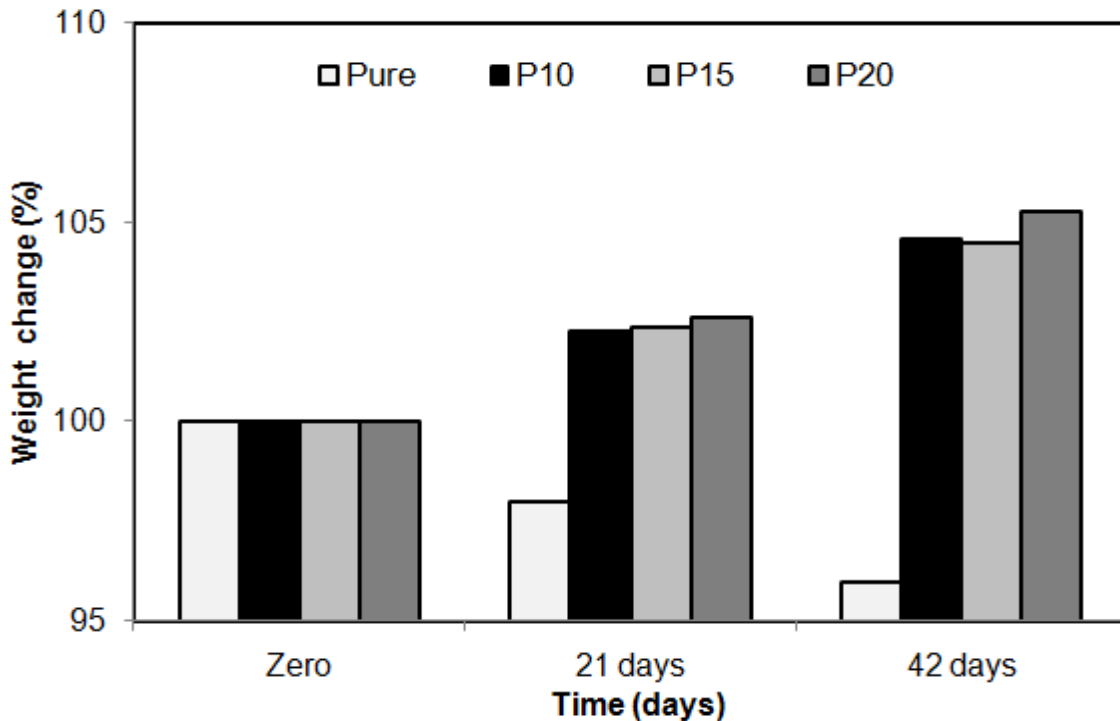


Figure 46: % Weight change Vs. time (days) for all the compositions.

The samples were dried in an oven for a day and were subjected to XRD analysis. The XRD pattern of the porous TiO₂ structures immersed in SBF for a period of 42 days is as shown in Figure 47. The pattern clearly shows the indication of peaks from hydroxyapatite (indicated on figure as HAp) in addition to the peaks from the rutile phase of TiO₂. By comparing the results with JCPDS standard files # 21-1276 and # 09-0432, the presence of rutile phase and hydroxyapatite were confirmed. The results thus proved the deposition of apatite layer on the surface of TiO₂ pellets placed in SBF. However in addition to these peaks, some additional peaks were observed which corresponded to Mg₂P₂O₇ phase. This result was confirmed by comparing with JCPDS standard file # 08-0038.

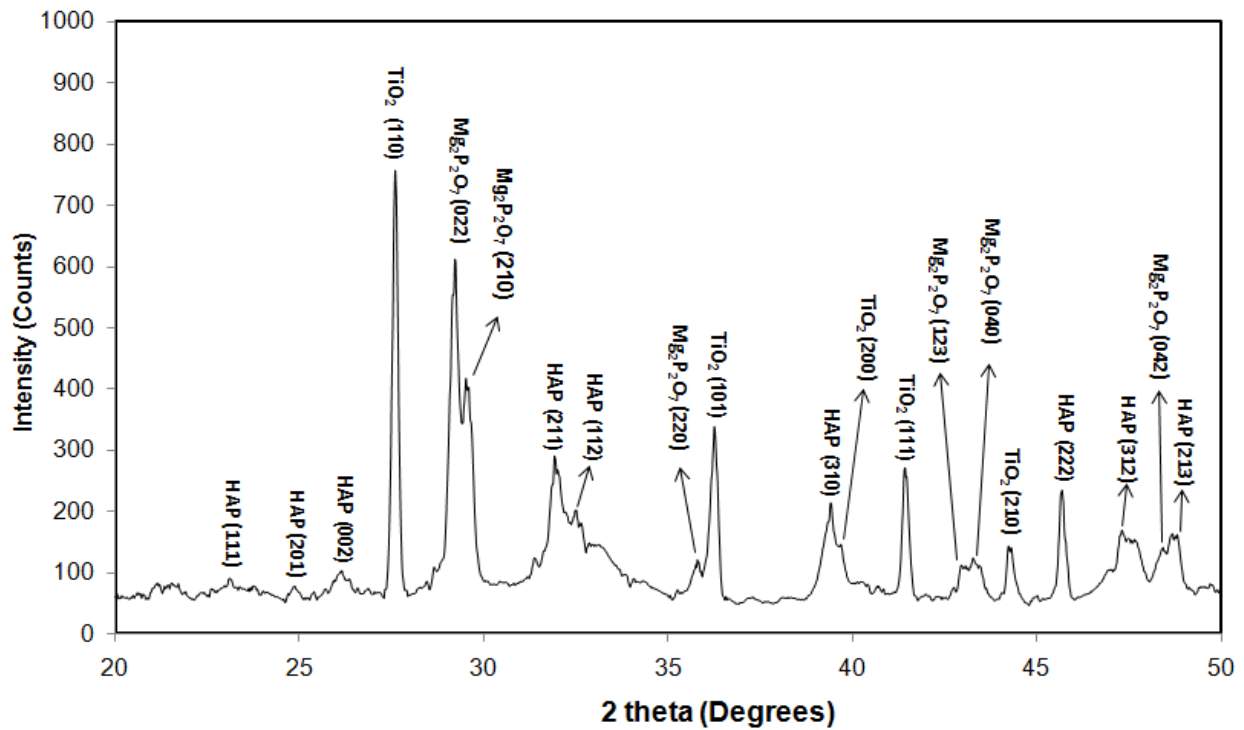


Figure 47: XRD pattern of porous scaffold placed in SBF for 42 days

The structures immersed in SBF were observed for the microstructural analysis under a scanning electron microscope. The microstructures confirmed the presence of apatite layer, as seen in Figure 48. The apatite deposited in the form of crystals on the surface of titania structures.

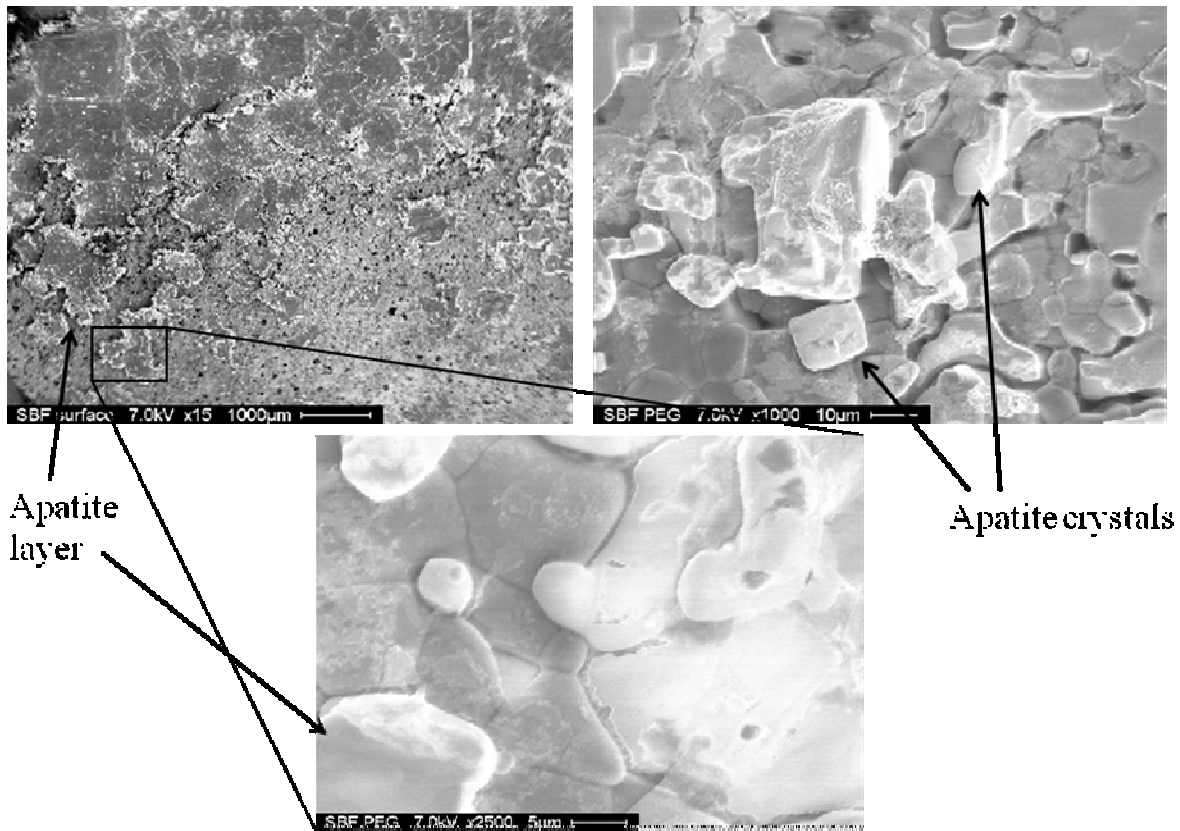


Figure 48: SEM micrographs showing formation of apatite crystals on the surface of titania

The hardness of the porous structures immersed in SBF was measured. The hardness was taken on one sample corresponding to each composition at five different locations and the average hardness was calculated. The hardness was measured for all the structures at the end of 21 days and 42 days respectively. It was observed that hardness decreased as time progressed. The variation in the hardness of the structures with time is plotted as shown in Figure 49. It was observed that the surface hardness of porous TiO_2 structures degraded at a much lower rate when

compared to pure TiO₂ structures. There was 22% degradation in hardness for all the porous TiO₂ structures used in this study. However, the pure TiO₂ structures, exhibited 55% degradation in hardness at the end of 42 days.

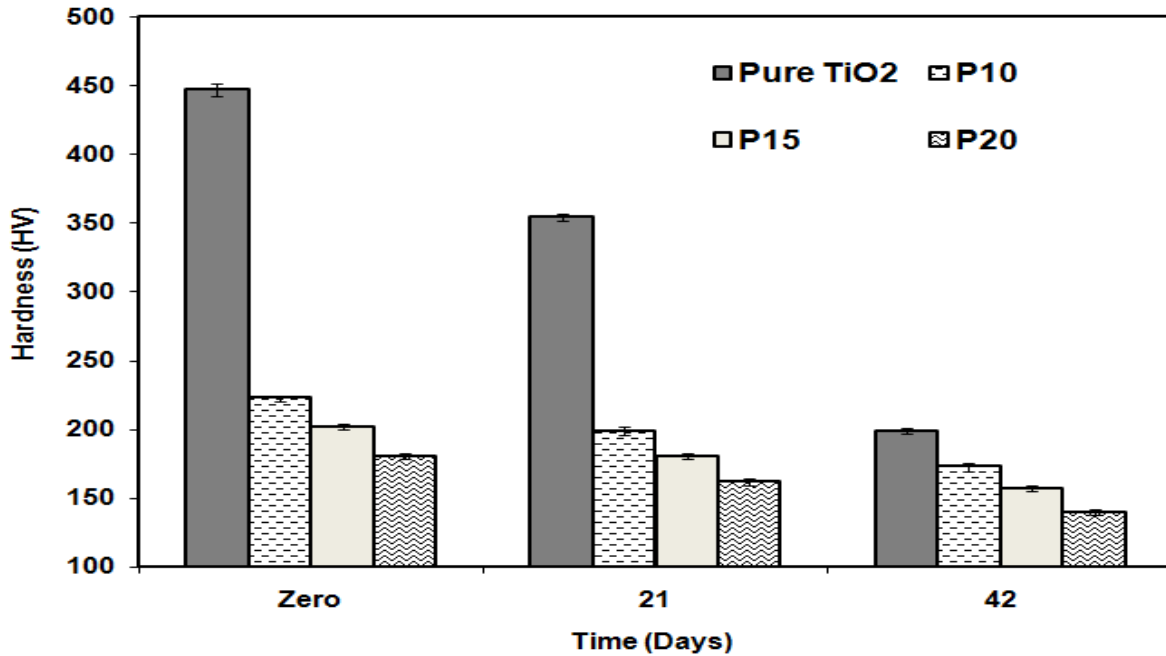


Figure 49: Variation in hardness of pure and porous scaffolds placed in SBF with time

The mechanical behavior of the porous TiO₂ structures was studied by evaluating the biaxial or flexural strength of all the structures. The biaxial flexural strength was measured at the end of 21 days and 42 days. The variation of the biaxial strength with time is shown in Figure 50. The results indicate that mechanical properties of the sintered structures decreased as time progressed. It was observed that at the end of 42 days, the minimum degradation of 30% in biaxial flexural strength was seen for P10 and P20 structures, whereas, 26% degradation in the flexural strength values was recorded for P15 structures. On the contrary, the pure TiO₂ structures showed 41% degradation in flexural strength at the end of 42 days.

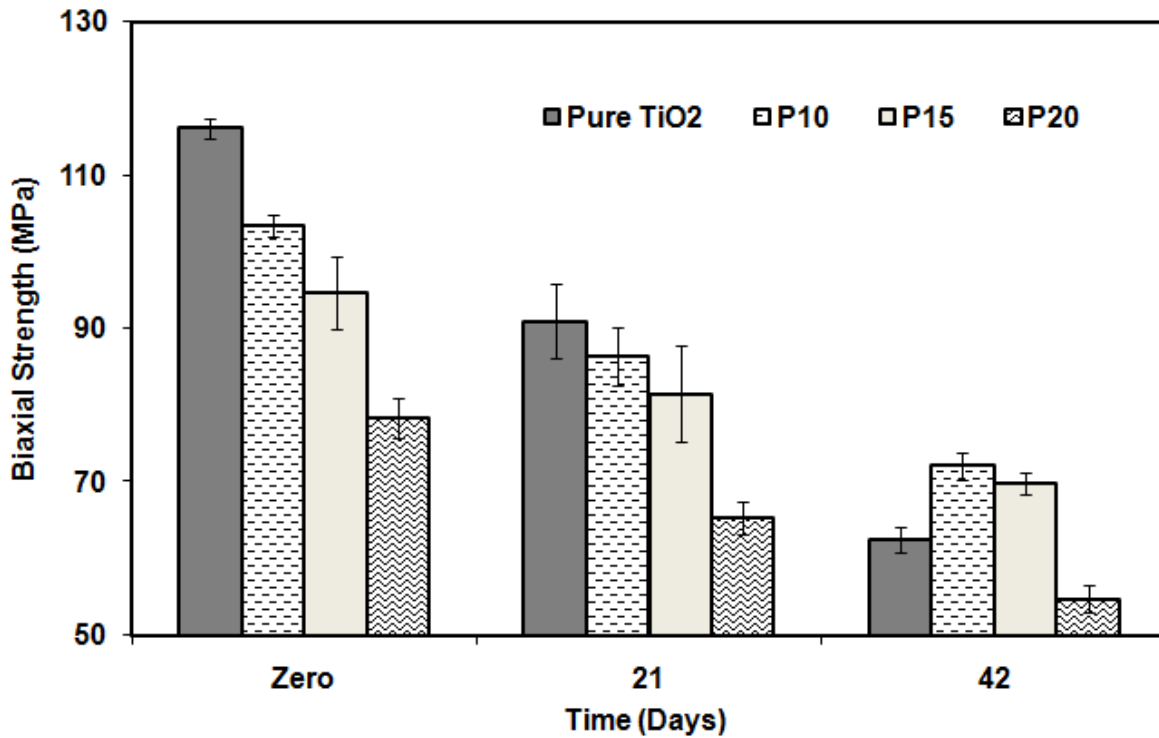


Figure 50 : Variation in biaxial flexural strength of pure and porous scaffolds placed in SBF with time

Therefore, the results of this study indicate that the porous TiO₂ structures were superior to the pure TiO₂ structures in all aspects for the biodegradation study. The results also conclude that the porous TiO₂ structures degraded at a slower rate when compared to the pure TiO₂ structures. The study also showed that the porous TiO₂ structures had more deposition of apatite on the surface as well as inside the pores which led to the increase in the weight of these structures during the entire process, whereas, the pure TiO₂ structures did not attract much apatite deposition on the surface, on the contrary it dissolved in SBF with time.

4.6.3 Metal-ion doped porous scaffolds

Biodegradation study of metal-ion doped porous scaffolds was conducted in SBF, maintained at a constant temperature of 36.5°C. All the structures namely A10, A15, B10, B15 were used for this study. It was seen that for all these structures there was about 2% increase in weight at the end of day 21. The increase in the weight of the structures is due to the formation of apatite layer on the surface and sides of the specimens. The apatite possibly seeped through the pores present on the surface of these samples thereby increasing the weight of the structures. The % change in weight for all the structures used in this study is shown in Figure 51.

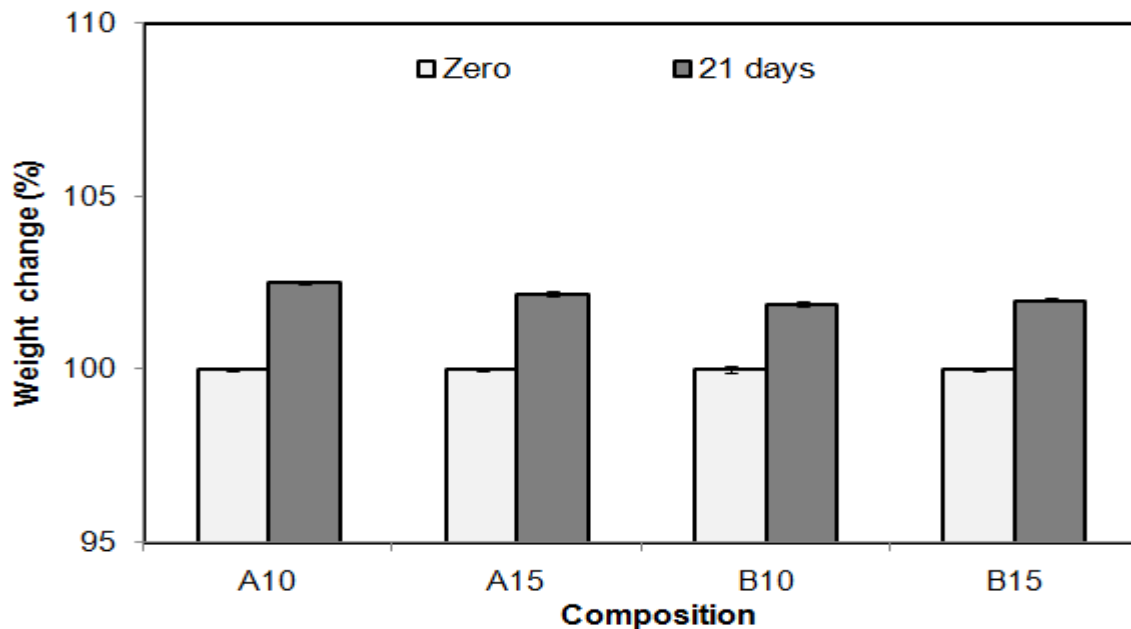


Figure 51: % Weight change Vs Composition for all metal-ion doped porous scaffolds

The average hardness of the all the metal-ion doped porous scaffolds immersed in SBF was measured. The hardness was taken on one sample of each composition at five different locations and the average hardness was then calculated. The hardness was measured for all the structures at the end of 21 days. It was seen that hardness decreased as time progressed. Figure

52 shows the hardness variation of the structures with time. It was observed that metal-ion doped porous scaffolds hardly showed any degradation of surface hardness with time. These structures showed better results than the phase-pure porous scaffolds which did not contain any additives. The rate of surface hardness degradation was almost negligible, whereas for porous scaffolds without any additive there was 11% degradation in hardness at the end of 21 days.

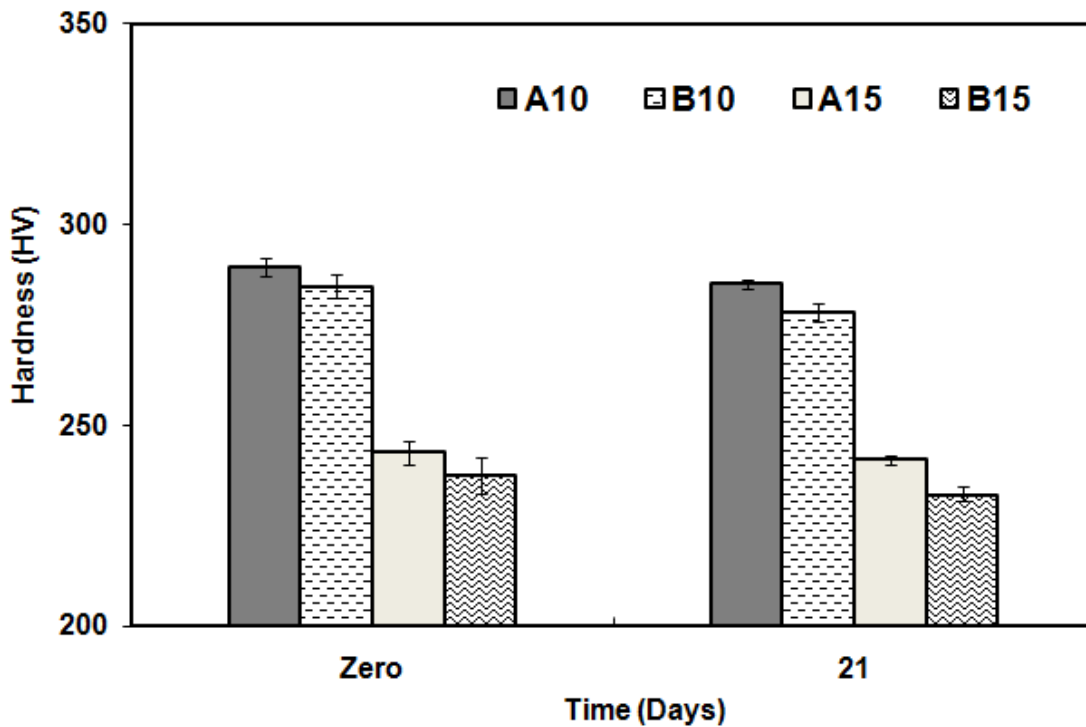


Figure 52: Variation in surface hardness for metal-ion doped porous scaffolds

The biaxial flexural strength for all the metal-ion doped porous scaffolds were measured at the end of the experiment. Figure 53 gives the variation of the biaxial strength with time. The results indicate that mechanical properties of the sintered structures decreased as time progressed. It was observed that at the end of 21 days, there was just 1% degradation in flexural strength for the composition A10. The maximum degradation of 3% was seen in case of B10

structures sintered under same conditions. Therefore, porous scaffolds could retain their flexural strength in the presences of additives. The additives thus proved beneficial.

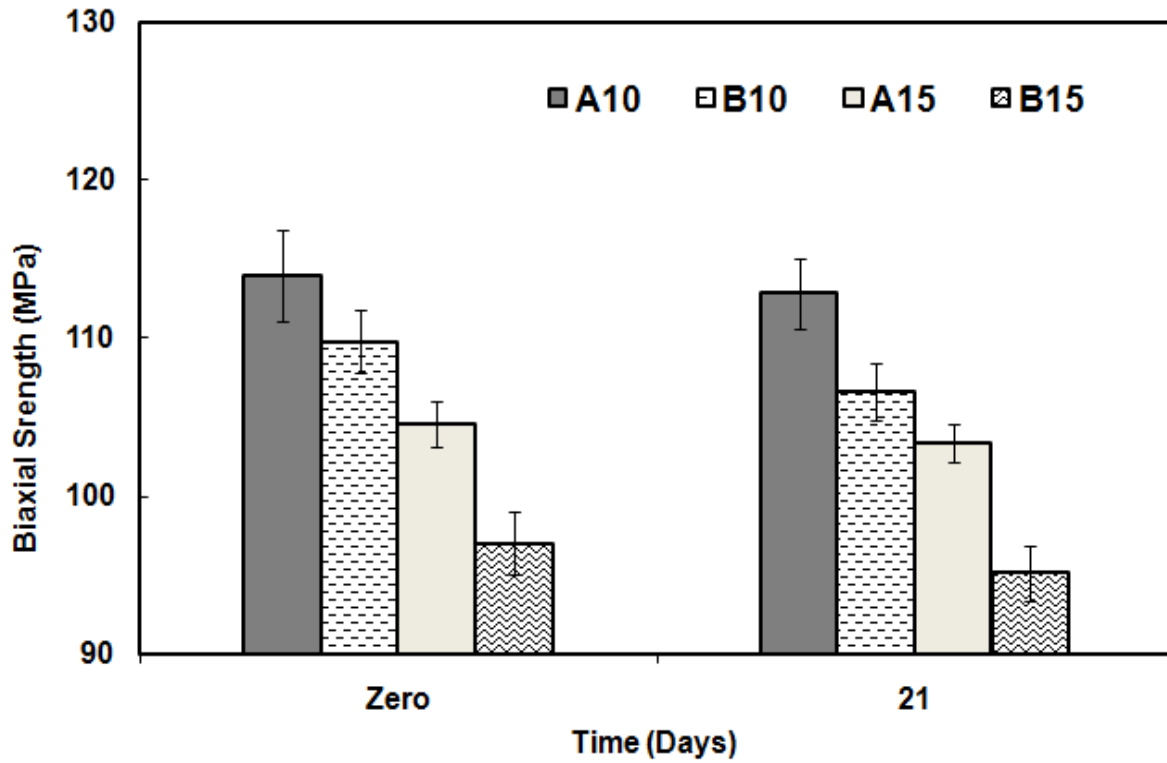


Figure 53: Variation in biaxial flexural strength for the metal-ion doped porous scaffolds

The results of bioactivity study conclude that metal-ion doped porous scaffolds retained the mechanical properties to a greater extent when compared to phase-pure porous scaffolds.

5. CONCLUSIONS

Sol-gel technique is a very efficient technique to synthesize nanocrystalline titania powder of particle size 5-15 nm. The effect of oxide-based sintering additives on physical, mechanical properties and biological properties of TiO₂ ceramics has been successfully studied. From my results, I conclude that the addition of dopants – MgO, ZnO and SiO₂ improved the mechanical properties of bulk TiO₂ structures without altering its phase purity. Densification results also proved that the sintered density of TiO₂ ceramics could be improved by the incorporation of sintering additives in small quantities. A maximum sintered density of 3.87g.cm⁻³ was achieved for A2 structures sintered at 1500°C (Cycle A) which was about 8.5% improvement in sintered density when compared to pure TiO₂ structures sintered under same conditions. SEM results indicated that dopant addition led to an increase in grain size for the structures sintered using Cycle A; a maximum grain growth of 12% was observed in case of 2 wt. % ZnO addition. The structures sintered at 1500°C (Cycle A) possessed better mechanical properties in terms of hardness and biaxial strength. There was a maximum of 12% improvement in hardness and 18% improve in the biaxial flexural strength for the compositions B2 and C3, respectively processed under same conditions. From this study, I conclude that Cycle A is the best suited sintering cycle for achieving good mechanical properties. The compositions A2, B2 and C3 possessed better densification and mechanical properties. The biodegradation studies of structures in SBF showed that presence of dopants changes the resorption rate and controls the surface mechanical degradation rate of TiO₂ ceramics. The composition A2 showed the minimal deterioration in hardness and biaxial flexural strength values with time.

Porous titania structures were successfully processed using polyethylene glycol as the pore-former. It was observed from the SEM micrographs that addition of pore-former inhibited the grain growth of titania ceramics. The % porosity increased with an increase in quantity of pore-former added. The maximum porosity of 48% was obtained for P25 structures sintered at 1400°C for 3 h. Results of bioactivity and SEM showed the deposition of apatite layer on the surface of the structures immersed in simulated body fluid, which was later confirmed by XRD analysis.

The properties of metal-ion doped porous titania scaffolds were also studied. For these structures, the porosity decreased with the addition of dopants (MgO, ZnO). Results of this study showed that, for MgO doped porous scaffolds, there was 30% increase in hardness and 17% increase in biaxial flexural strength over the other porous structures which contained the same amount of pore-former before sintering. For ZnO doped porous scaffolds, there was 28% improvement in hardness and 17% improvement in biaxial flexural strength over the other porous structures which contained the same amount of pore-former before sintering. The results of bioactivity studies conclude that metal-ion doped porous scaffolds could retain their mechanical strength to greater extent when compared to all other structures used in this study. However, in detailed *invitro* and *invivo* studies are essential to make these materials useful for many biomedical applications in the future.

6. FUTURE DIRECTIONS AND SUGGESTIONS

Mechanical properties of any material depend on its grain size. Nanostructured or nano-grained materials have superior properties when compared to their coarse-grained counterparts. From the results of our SEM studies, we see that the grain size obtained was in micron range, thus indicating that nano-features are lost during sintering. Hence, there is a need to control the grain growth, which can be done by Spark plasma sintering (SPS), high pressure – low temperature sintering, etc. Hence, I would recommend these techniques to control the grain growth and obtain better densification for all the sintered structures.

Another problem is the compaction method employed. Uniaxial compaction technique was used to prepare the green samples for this work. The green structures produced in this case might contain minor un-noticeable cracks or flaws which adversely affects the densification and mechanical properties of the sintered structures. Hence, improved powder compaction techniques should be adopted for better densification and improved mechanical properties of the sintered structures. I would recommend any automated compaction process for uniform pressing of all the green structures. Hot isostatic pressing (HIP) and cold isostatic pressing (CIP) could also be used for the pressing of samples as well.

Single oxide was used as an additive to improve the properties of the sintered structures in this work. Future study can be aimed at using a combination of sintering additives to improve the densification and other mechanical properties of titania structures.

Processing of porous titania structures with uniform pore size and uniform pore distribution is essential to meet the requirements of a scaffold with superior properties and applications. I would recommend Rapid prototyping technique to achieve the same.

Further *invitro* studies of titania structures in SBF for still longer period of time is essential to determine whether these materials could be used *invivo* for various biomedical applications.

LIST OF REFERENCES

- [1] Z. Li, B. Hou, Y. Xu, D. Wu and Y. Sun, *Journal of Colloid and Interface Science* 288 (2005) 149.
- [2] A. Bendavid, P. J. Martin, Å. Jamting and H. Takikawa, *Thin Solid Films* 355-356 (1999) 6.
- [3] L. Zhang, T. Kanki, N. Sano and A. Toyoda, *Separation and Purification Technology* 31 (2003) 105.
- [4] C.-M. Lin and S.-K. Yen, *Materials Science and Engineering: C* 26 (2006) 54.
- [5] J.-X. Liu, D.-Z. Yang, F. Shi and Y.-J. Cai, *Thin Solid Films* 429 (2003) 225.
- [6] X. Liu, X. Zhao, R. K. Y. Fu, J. P. Y. Ho, C. Ding and P. K. Chu, *Biomaterials* 26 (2005) 6143.
- [7] W.-H. Song, Y.-K. Jun, Y. Han and S.-H. Hong, *Biomaterials* 25 (2004) 3341.
- [8] S. J. Hwang, C. Petucci and D. Raftery, *J. Am. Chem. Soc.* 120 (1998) 4388.
- [9] W. Zhou, S. Tang, L. Wan, K. Wei and D. Li, *Journal of Materials Science* 39 (2004) 1139.
- [10] I. Hayakawa, Y. Iwamoto, K. Kikuta and S. Hirano, *Sensors and Actuators B: Chemical* 62 (2000) 55.
- [11] P.-T. Hsiao, K.-P. Wang, C.-W. Cheng and H. Teng, *Journal of Photochemistry and Photobiology A: Chemistry* 188 (2007) 19.
- [12] M. T. Taschuk, J. J. Steele, A. C. van Popta and M. J. Brett, *Sensors and Actuators B: Chemical* In Press, Corrected Proof.
- [13] T. J. Webster, R. W. Siegel and R. Bizios, *Biomaterials* 20 (1999) 1221.
- [14] C.-S. Kim, B. K. Moon, J.-H. Park, S. Tae Chung and S.-M. Son, *Journal of Crystal Growth* 254 (2003) 405.
- [15] S. W. Oh, S.-H. Park and Y.-K. Sun, *Journal of Power Sources* 161 (2006) 1314.

- [16] J. L. Guimarães, M. Abbate, S. B. Betim and M. C. M. Alves, *Journal of Alloys and Compounds* 352 (2003) 16.
- [17] D. H. Kim, H. S. Hong, S. J. Kim, J. S. Song and K. S. Lee, *Journal of Alloys and Compounds* 375 (2004) 259.
- [18] Y. Su, J. Yu and J. Lin, *Journal of Solid State Chemistry* 180 (2007) 2080.
- [19] K. L. Choy, *Progress in Materials Science* 48 (2003) 57.
- [20] S. Qiu and S. J. Kalita, *Materials Science and Engineering: A* 435-436 (2006) 327.
- [21] N. Masahashi, *Materials Science and Engineering: A* 452-453 (2007) 721.
- [22] Y. I. Lee, J.-H. Lee, S.-H. Hong and D.-Y. Kim, *Materials Research Bulletin* 38 (2003) 925.
- [23] A. Weibel, R. Bouchet, R. Denoyel and P. Knauth, *Journal of the European Ceramic Society* 27 (2007) 2641.
- [24] S.-C. Liao, K. D. Pae and W. E. Mayo, *Materials Science and Engineering A* 204 (1995) 152.
- [25] M. Mazaheri, Z. Razavi Hesabi and S. K. Sadrnezhad, *Scripta Materialia* 59 (2008) 139.
- [26] X. Fan, X. Chen, S. Zhu, Z. Li, T. Yu, J. Ye and Z. Zou, *Journal of Molecular Catalysis A: Chemical* 284 (2008) 155.
- [27] G. Liu, X. Zhang, Y. Xu, X. Niu, L. Zheng and X. Ding, *Chemosphere* 59 (2005) 1367.
- [28] J.-W. Shi, J.-T. Zheng, Y. Hu and Y.-C. Zhao, *Materials Chemistry and Physics* 106 (2007) 247.
- [29] Y.-h. Xu, H.-r. Chen, Z.-x. Zeng and B. Lei, *Applied Surface Science* 252 (2006) 8565.
- [30] Y.-h. Xu, D.-h. Liang, M.-l. Liu and D.-z. Liu, *Materials Research Bulletin* 43 (2008) 3474.
- [31] G. A. Crawford, N. Chawla, K. Das, S. Bose and A. Bandyopadhyay, *Acta Biomaterialia* 3 (2007) 359.
- [32] A. H., Tokyo: Takayama Press System Centre, *JAAS* (1991) 165.

- [33] H. L. L., J. Am. Ceram. Soc. 74 (1991) 1487.
- [34] L. Hench, L. Ethridge, E. C., (1982).
- [35] L. Hench, Ceramics and glasses. Metals Park, OH: ASM international 4 (1991) 1007.
- [36] C. Rey, Biomaterials 89 (1990) 13.
- [37] A. Akoa M, H, Kato, K., J.Mater Sci 16 (1981) 809.
- [38] D. P. ASchepers EJJG, Bioceramics, Oxford: Butterworth-Heinemann Ltd. 6 (1993) 401.
- [39] Y.-M. Kong, C.-J. Bae, S.-H. Lee, H.-W. Kim and H.-E. Kim, Biomaterials 26 (2005) 509.
- [40] B. W. Best S., J. Mater. Sci., Mater. Med. 5 (1994) 516.
- [41] S. Kalita, J. , Rokusek. D, Bose S., Hosick, H., L., Bandyopadhyay A., J.Biomed. Mater. Res. A 71 (2004) 35.
- [42] S. J. Kalita, S. Bose, H. L. Hosick and A. Bandyopadhyay, Biomaterials 25 (2004) 2331.
- [43] A. Lopes M., Santos J., D., Monteiro F., J., Knowles J., C, J Biomed Mater Res 39 (1998) 244.
- [44] E. Ahn, S., Gleason, N., J., Ying J., Y., , J Am. Ceram.Soc. 88 (2005) 3374
- [45] C. Knowles J., Bonfield, W.,, J. Biomed. Mater. Res. 27 (1993) 1591.
- [46] A. Lopes M., Santos J., D., Monteiro F., J., J Biomed Mater Res 48 (1999) 734.
- [47] A. Lopes M., Santos J., D., Monteiro F., J., J. Biomed. Mater. Res. 20 (1999) 2085.
- [48] J. Santos, D., Silva, P., L., Knowles, J.,C., Talal, S., Monteiro, F., J.,, Mater. Med. 7 (1996) 187.
- [49] J. L. Xu, K. A. Khor, Y. W. Gu, R. Kumar and P. Cheang, Biomaterials 26 (2005) 2197.
- [50] J. Karch, Birringer, R., Gleiter, H, Nature 330 (1987) 556.
- [51] Z. Yang, S. Si and Y. Fung, Thin Solid Films 515 (2007) 3344.

- [52] S. Cosnier, A. Senillou, M. Grätzel, P. Comte, N. Vlachopoulos, N. Jaffrezic Renault and C. Martelet, *Journal of Electroanalytical Chemistry* 469 (1999) 176.
- [53] F. Y. Oliva, L. B. Avalle, O. R. Cámara and C. P. De Pauli, *Journal of Colloid and Interface Science* 261 (2003) 299.
- [54] C. Cui, H. Liu, Y. Li, J. Sun, R. Wang, S. Liu and A. Lindsay Greer, *Materials Letters* 59 (2005) 3144.
- [55] M. Keshmiri and T. Troczynski, *Journal of Non-Crystalline Solids* 324 (2003) 289.
- [56] X.-X. Wang, W. Yan, S. Hayakawa, K. Tsuru and A. Osaka, *Biomaterials* 24 (2003) 4631.
- [57] W. Wu and G. H. Nancollas, *Colloids and Surfaces B: Biointerfaces* 10 (1997) 87.
- [58] Z. Yang, S. Si, X. Zeng, C. Zhang and H. Dai, *Acta Biomaterialia* 4 (2008) 560.
- [59] J. Forsgren, F. Svahn, T. Jarmar and H. Engqvist, *Acta Biomaterialia* 3 (2007) 980.
- [60] T. Kokubo, T. Matsushita and H. Takadama, *Journal of the European Ceramic Society* 27 (2007) 1553.
- [61] L. Jonášová, F. A. Müller, A. Helebrant, J. Strnad and P. Greil, *Biomaterials* 25 (2004) 1187.
- [62] X.-X. Wang, S. Hayakawa, K. Tsuru and A. Osaka, *Biomaterials* 23 (2002) 1353.
- [63] B. Yang, M. Uchida, H.-M. Kim, X. Zhang and T. Kokubo, *Biomaterials* 25 (2004) 1003.
- [64] X. Zhu, K.-H. Kim and Y. Jeong, *Biomaterials* 22 (2001) 2199.
- [65] T. Hanawa, *Materials Science and Engineering A* 267 (1999) 260.
- [66] J. J. B. Aldo R Boccaccini, *Expert Rev. Med. Devices* 2 (2005) 303.
- [67] S. Hulbert, (1993) 25.
- [68] S. F. Hulbert, Bokros, J., C., Hench, L., L., Wilson, J., Heimke, *High Tech Ceramics* (1987) 189.
- [69] L. L. Hench, *J Am. Ceram.Soc.* 74 (1991) 1487.
- [70] E. Schors, C., Holmes, R., E., (1993) 181.

- [71] A. Monnier A., J., J. Electrochem. Soc. 127 (1980) 1576.
- [72] N. N. Itakura M., Toyoda A., Iwasaki H., J. Appl. Phys. 6 (1967) 311.
- [73] A. Bally, R., Korobeinikova, E., N., Shmid, P., E., Levy, F., Bussy, F., J Phys. D: Appl. Phys. 31 (1998) 1149.
- [74] G. U., Solid state Ionics 101-103 (1997) 1171.
- [75] K. Akiyama, Toyama, N., Muraoka, K., Tsunashima, M., J Am. Ceram. Soc. 81 (1998) 1071.
- [76] H. A., Tokyo, JAAS (1991) 165.
- [77] C. Carter Barry, Norton Grant, M., (2007).
- [78] A. Sheinkman, I., Sheinkman, F., P., Dobrovolskii, I., P., Zvygina, *Izv. Akad. Nauk SSSR Neorg. Mater* 13 (1977) 1447.
- [79] R. Datta, K., (1993).
- [80] J. Yang, Swisher J., H., Materials Characterization 37 (1996) 153.
- [81] J. Jiao, Q. Xu and L. Li, Journal of Colloid and Interface Science 316 (2007) 596.
- [82] N. K. Miki Takeshi, Suzuki Kazuyuki, Kato. Kazumi, Reports of the National industrial research; Institute of Nagoya, 49 (2001) 271.
- [83] S. C. Bu, Chunxiang; Liu, Xiaoxin; Bai, Ling, Journal of Sol-Gel Science and Technology 43 (2007) 151.
- [84] S. Bu, Z. Jin, X. Liu, L. Yang and Z. Cheng, Materials Chemistry and Physics 88 (2004) 273.
- [85] M. Shaheer Akhtar, J.-M. Chun and O. B. Yang, Electrochemistry Communications 9 (2007) 2833.
- [86] S. J. Kalita, S. Qiu and S. Verma, Materials Chemistry and Physics 109 (2008) 392.
- [87] A. P. D. S. M.M. Akiyoshi, M.G. Da Silva, Am. Ceram. Soc. Bull 81 (2002) 39.
- [88] T. Kokubo, J Non-Cryst Solids 120 (1990) 138.

- [89] T. Kokubo, S. Ito, Z. T. Huang, T. Hayashi, S. Sakka, T. Kitsugi and T. Yamamuro, J. Biomed. Mater. Res. 24 (1990) 331.